MMNSA

Mathematical Modelling and Numerical Simulation with Applications

ISSN Online : 2791-8564

Year : 2022

Volume : 2

Issue : 3

www.mmnsa.org

VOLUME: 2 ISSUE: 3
ISSN ONLINE: 2791-8564

September 2022
https://www.mmnsa.org

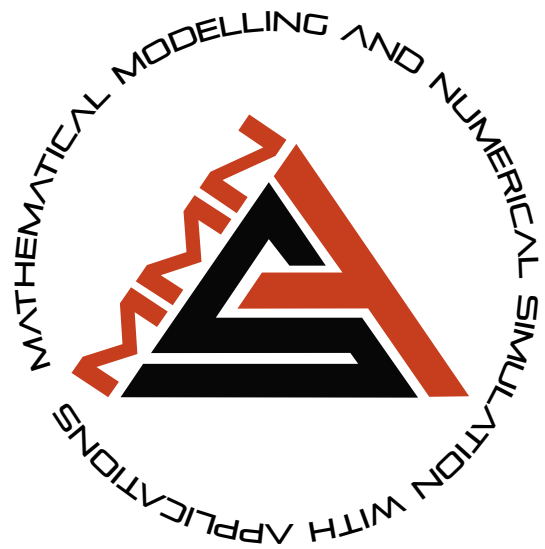

MATHEMATICAL MODELLING AND NUMERICAL SIMULATION WITH APPLICATIONS

Technical Editor

Halil İbrahim Özer
Department of Computer and Instructional Technologies
Education, Ahmet Keleşoğlu Faculty of Education,
Necmettin Erbakan University, Meram Yeniyol, 42090
Meram, Konya / TÜRKİYE
hiozer@gmail.com

English Editor

Abdulkadir Ünal
School of Foreign Languages, Foreign Languages, Alanya
Alaaddin Keykubat University, Antalya / TÜRKİYE
abdulkadir.unal@alanya.edu.tr

Editorial Secretariat

Fatma Özlem Coşar
Department of Mathematics and Computer Sciences,
Faculty of Science, Necmettin Erbakan University,
Meram Yeniyol, 42090 Meram, Konya / TÜRKİYE

Müzeyyen Akman
Department of Mathematics and Computer Sciences,
Faculty of Science, Necmettin Erbakan University,
Meram Yeniyol, 42090 Meram, Konya / TÜRKİYE

Contents

Research Articles

Mathematical Modelling and Numerical Simulation with Applications, 2022, 2(3), 127–146

https://www.mmnsa.org
ISSN Online: 2791-8564 / Open Access
https://doi.org/10.53391/mmnsa.2022.011

RESEARCH PAPER

An efficient application of scrambled response approach to estimate the population mean of the sensitive variables

Atiqa Zahid [1,†], Saadia Masood [1,*,†], Sumaira Mubarik [2,†] and Anwarud Din [3,*,†]

[1]Department of Mathematics and Statistics, Pir Mehr Ali Shah Arid Agriculture University, Rawalpindi, Punjab, Pakistan, [2]Department of Epidemiology and Biostatistics, School of Health Sciences, Wuhan University, 185 Donghu Road, Wuhan, Hubei, 430071 China, [3]Department of Mathematics, Sun Yat-Sen University Guangzhou, 510275 P.R. China

*Corresponding Author
† atiqazahid92@gmail.com (Atiqa Zahid); saadia.masood@uaar.edu.pk (Saadia Masood); sumairaawan86@gmail.com (Sumaira Mubarik); anwarud@mail.sysu.edu.cn (Anwarud Din)

Abstract

In the presence of one auxiliary variable and two auxiliary variables, we analyze various exponential estimators. The ranks of the auxiliary variables are also connected with the study variables, and there is a linkage between the study variables and the auxiliary variables. These ranks can be used to improve an estimator's accuracy. The Optional Randomized Response Technique (ORRT) and the Quantitative Randomized Response Technique are two techniques we utilize to estimate the sensitive variables from the population mean (QRRT). We used the scrambled response technique and checked the proposed estimators up to the first-order of approximation. The mean square error (MSE) equations are obtained for all the proposed ratio exponential estimators and show that our proposed exponential type estimator is more efficient than ratio estimators. The expression of mean square error is obtained up to the first degree of approximation. The empirical and theoretical comparison of the proposed estimators with existing estimators is also be carried out. We have shown that the proposed optional randomized response technique and quantitative randomized response model are always better than existing estimators. The simulation study is also carried out to determine the performance of the estimators. Few real-life data sets are also be applied in support of proposed estimators. It is observed that our suggested estimator is more efficient as compared to an existing estimator.

Key words: Randomized response technique; simple random sampling; scrambling response; sensitive and non-sensitive variables; exponential-type estimators
AMS 2020 Classification: 62D05; 62D10; 62E10; 62E17

1 Introduction

In the optional randomized response technique, while collecting data, sometimes the interviewer faces the problem of non-response. The interviewee hesitates to respond to sensitive questions regarding their private life, abortion, drug addiction, HIV infection status, duration of suffering from AIDS, sexual behavior, the incidence of domestic violence, and tax evasion, for example,

➤ **Received:** 25.05.2022 ➤ **Revised:** 18.07.2022 ➤ **Accepted:** 27.07.2022 ➤ **Published:** 10.08.2022

any sensitive query. In general, people do not feel comfortable when asked about their past medication use status relative to medical problems, sexual activity, premature births, etc. [1] proposed an optional randomized response model to manage those cases. This model elaborates that one query can be delicate and may not be sensitive to another. In this technique, the interviewee can choose whether to provide the answer or scramble the answer. Under this model, the mean and sensitivity level of parameters are estimated. We cannot trace the reaction provided by the interviewee through investigation. The story of sensitivity of the question is the proportion of individuals who give the scrambled answers. Ratio-type estimators are developed when a variable of concern is sensitive and auxiliary variables are non-sensitive information. Additional information is used to increase the estimator's precision at designing and at the estimation stages. We use ratio, product, and regression estimators more frequently when there is a connection between the dependent and independent variables. In a similar expression, the variables of independent ranks are also correlated with the relating upsides of the study variables [2]. Along these lines, the ranked auxiliary variable (that contains the ranks of the auxiliary variable) can be treated as another additional variable. This data may help us expand the proficiency of an estimator. In ORRT, most of the respondents assumed that the aspects of inquiry are sensitive, but some are more willing to answer directly. In ORT, respondents are given an option either to supply RR using a specified randomized device or to respond directly according to the extent to which the respondent feels that the question is sensitive or not. Most of the methods developed for ORT are limited to SRSWR sampling only. A few of the ORT techniques are available for complex surveys.

We are investigating a multiplicative randomized response strategy for providing quantitative randomized responses (QRRT) to sensitive queries. The respondent multiplies his sensitive response by a random number from a known distribution and gives the product to the interviewer, who has no idea what the random number is valuable and consequently receives a scrambled response. The respondent generates S using some specified method and multiplies his sensitive answer Y by S.

The interviewer receives the scrambled answer Z = YS. The particular values S are unknown to the interviewer, but its distribution is known, Let Scrambling variable is denoted by S with E(S) = θ_1 and their variance is V(S) = σ_1^2. Some specific distributions for random scrambling numbers are proposed and investigated, as well as methods for creating scrambling numbers.

The application of the proposed Quantitative randomized response technique (QRRT) has also been discussed. A new composite class of estimators is defined using scrambled response to estimate the population means of a sensitive variable. Methods for studying sensitive behavior include randomized response techniques, which provide anonymity to interviewees who answer sensitive questions. The quantitative randomized response technique (QRRT) variation on this approach allows researchers to estimate the frequency or quantity of sensitive behaviors. The application of the proposed optional Randomized Response Technique has been discussed. The randomized response technique in a survey reduces potential bias due to nonresponse and social desirability when asking questions about sensitive behaviors and beliefs [3]. Use of randomization device (outcome unobserved by the interviewer) conceals individual responses and protects respondent privacy Auxiliary variables are first used in a ratio-type estimator by [4]. The use of more than one auxiliary characteristic improves the Estimation. To know about the variability present in a finite population variance may be required, which is also essential for future predictions and studies. Therefore, we review different estimators in the literature and propose a new class of estimators. We have some auxiliary information that is used in variance estimation. We are interested in comparing the different variance estimators. We sought to recommend a variance estimator for use in the analysis of the content evaluation survey. There are various ways and examples of the use of assisting (auxiliary) variables like

- A hospital survey may identify insufficient quantity in a specific hospital.
- In Socioeconomic surveys, in advance, may well know the availability of food, educational status, and medical facilities of a region.
- The entirely cultivated area in the agriculture production survey may well be known in advance.

In this paper, generalized two-stage optional randomized response technique (ORRT) and Quantitative randomized response technique are derived for a finite population mean of a delicate variable based on Randomized Response technique using non-sensitivity additional information.

2 Few existing estimators in simple random sampling

Now we discuss MSE estimators which exist in the literature. Firstly, note the simple sample MSE estimator.

i) The unbiased usual estimator of the population mean of Z is given

$$MSE(\hat{\mu}_{YS}) = \left(\frac{1-f}{n}\right)\bar{Z}^2[\sigma_y^2 + \sigma_s^2]. \tag{1}$$

ii) [5] proposed a ratio estimator, which is given as

$$MSE(\hat{\mu}_{RS}) = \left(\frac{1-f}{n}\right)\bar{Z}^2[C_y^2 + \frac{\sigma_s^2}{\mu_y^2} + C_x^2 - 2C_xC_y\rho_{yx}]. \tag{2}$$

iii) [6] suggested a ratio estimator, which is given as

$$MSE(\hat{\mu}_{RG}) = \bar{Z}^2\left(\frac{1-f}{n}\right)[C_y^2 + \frac{W\sigma_s^2}{\mu_y^2} + C_x^2 - 2C_xC_y\rho_{yx}]. \tag{3}$$

iv) [7] suggested a ratio estimator.

$$MSE\left(\hat{\mu}_{RN}\right) = \bar{Z}^2\left(\frac{1-f}{n}\right)\left[C_y^2 + \frac{WK^2\sigma_s^2}{\mu_y^2} + C_x^2 - 2C_xC_y\rho_{yx}\right]. \tag{4}$$

v) [8] proposed the exponential-type estimator created on generalized two-stage optional-scrambled reply method which is given as

$$MSE(\hat{t}_{GRR}) = \bar{Z}^2\left(\frac{1-f}{n}\right)\left[C_y^2 + \frac{K^2W(1-T)^2\sigma_s^2}{\mu_y^2} - C_y^2\rho^2{}_{yx}\right]. \tag{5}$$

3 Proposed model I

Mean estimator for generalized two-stage optional scramble response

Let the set proportion of the population is denoted by $T(0 \leq T \leq 1)$, for which we can assume to give the true responses along with $W(0 \leq W \leq 1)$ to be the Sensitivity level related to that sensitive question. Here we have a scrambling variable S with zero (0) mean and variance σ_s^2 and let $K(-1 \leq K \leq 1)$ is suitably chosen scalar. [8] proposed the ORRT for the estimation of population mean in the case of sensitive study variables. Their suggested scenario states: Let the sensitive study variable be denoted by Y having the population mean μ_y and unknown population variance σ_y^2. The ORRT can be written as

$$Z = \left\{\begin{array}{ll} Y & \text{with probability T + (1 − W)(1 − T)} \\ Y + KS & \textit{with probability } W(1-T) \end{array}\right\}, \tag{6}$$

$$E(Z) = [T + (1-W)(1-T)E(Y) + [W(1-T)E(Y+KS)],$$
$$E(Z) = \mu_{YM}.$$

Generalized exponential-ratio-type estimator using one-auxiliary variable for generalized two stages optional scramble response

Let a simple random sample without replacement of size n be drawn from the population consisting of N units. Let Z, Y and X be the optional randomized response variable, the study variable, and the auxiliary variable respectively. Let the population (sample) means of Z, Y and X are μ_Z, μ_Y and μ_X ($\bar{z}$, $\bar{y}$ and $\bar{x}$) symbols, respectively, and notations to be used are:

$$E(Z) = \mu_Z, \mu_Z, \mu_Y \text{ and } \mu_X, E(U) = \mu_U, E(X) = \mu_X, E(S) = \mu_S = 0,$$
$$E(e_0) = E(e_1) = E(e_2) = E(e_3) = 0, \bar{r}_x = \bar{R}_x(1+e_2), \bar{x} = \bar{X}(1+e_1), \bar{y} = \bar{Y}(1+e_0),$$
$$E(e_3^2) = \lambda C_z^2, E(e_0e_1) = \lambda\rho_{yx}C_yC_x,\ E(e_0e_2) = \lambda\rho_{yr_x}C_yC_r,\ E(e_0e_3) = \lambda\rho_{yz}C_yC_z,$$
$$E(e_0e_3) = \lambda\rho_{yz}C_yC_z,\ E(e_1e_2) = \lambda\rho_{xr_x}C_xC_r,\ ]E(e_1e_3) = \lambda\rho_{xz}C_xC_z,\ E(e_3e_2) = \lambda\rho_{rx_z}C_xC_r,$$
$$C_z^2 = C_y^2 + \frac{K^2W(1-T)\sigma_s^2}{\mu_y^2},\ \rho_{zx} = \frac{\rho_{yx}}{\sqrt{1+\frac{K^2W(1-T)\sigma_s^2}{\sigma_y^2}}},\ \rho_{zr_x} = \frac{cov(x,y)}{C_{rx}C_y\sqrt{1+\frac{K^2W(1-T)\sigma_s^2}{\mu_y^2\sigma_y^2}}},\ \theta = \frac{a\bar{X}}{a\bar{X}+b}.$$

Table 1. Special case for the proposed estimator

Estimator	a	b
$\hat{\bar{Z}}_{pr}^{(1)}$	1	C_x
$\hat{\bar{Z}}_{pr}^{(2)}$	1	$\beta_2(x)$
$\hat{\bar{Z}}_{pr}^{(3)}$	$\beta_2(x)$	C_x
$\hat{\bar{Z}}_{pr}^{(4)}$	C_x	$\beta_2(x)$
$\hat{\bar{Z}}_{pr}^{(5)}$	1	ρ_{xy}
$\hat{\bar{Z}}_{pr}^{(6)}$	C_x	ρ_{xy}
$\hat{\bar{Z}}_{pr}^{(7)}$	ρ_{xy}	C_x
$\hat{\bar{Z}}_{pr}^{(8)}$	$\beta_2(x)$	ρ_{xy}
$\hat{\bar{Z}}_{pr}^{(9)}$	ρ_{xy}	$\beta_2(x)$

Motivated by [9], [10], and [11] proposed a difference- ratio-type exponential an estimator $\hat{\bar{Z}}_{pr}$ that is given by

$$\hat{\bar{Z}}_{pr} = \{\omega_1\bar{z} + \omega_2(\bar{X}-\bar{x}) + \omega_3(\bar{R}_x - \bar{r}_x)\}\exp\left(\frac{a(\bar{X}-\bar{x})}{a(\bar{X}-\bar{x})+2b)}\right). \tag{7}$$

By taking expectation, we can find the bias $\hat{\bar{Z}}_{pr}$ under first approximation, which is given as

$$Bias(\hat{\bar{Z}}_{pr}) = \frac{1}{8}\left[-8\bar{Z} + 4\lambda\theta C_x(\bar{X}C_x\omega_2 + \bar{R}_x\rho_{xr_x}C_r\omega_3\rho_{xr_x}) + \bar{Z}\omega_1(8 + \theta\lambda C_x (3\theta C_x - 4C_y\rho_{yx}))\right]. \tag{8}$$

The MSE of $\hat{\bar{Z}}_{pr}$under the first order of approximation are respectively given

$$\begin{aligned} MSE(\hat{\bar{Z}}_{pr}) = {} & \bar{Z}^2 + \lambda\bar{X}C_x^2\omega_2(-\bar{Z} + \bar{X}\omega_2) + \lambda\bar{R}_x^2C_r^2\omega_3^2 + \lambda\bar{R}_xC_xC_r(-\bar{Z} + 2\bar{X}\omega_2)\omega_3\rho_{xr_x} \\ & + \bar{Z}^2\omega_1^2\left[1 + \lambda\left\{C_y^2 + C_x - 2C_y\rho_{yx})\right\}\right] + \frac{1}{4}\bar{Z}\omega_1\left[-8\bar{Z} + \lambda C_x\left\{C_x(-3\bar{Z}\theta + 8\bar{X}\omega_2) + \right.\right. \\ & \left.\left. 8\bar{R}_xC_r\omega_3\rho_{xr_x} + 4C_y(\bar{Z} - 2\bar{X}\omega_2)\rho_{xy}\right\} - 8\bar{R}_x\lambda C_yC_r\omega_3\rho_{yr_x}\right]. \end{aligned} \tag{9}$$

The optimum values of ω_1, ω_2, and ω_3, obtained by minimizing equation (9) respectively, given by

$$\omega_{1(opt)} = \frac{8 - \lambda\theta^2 2C_x^2}{8\left(1 + \lambda C_z^2\left(1 - Q_{z.xrx}^2\right)\right)},$$

$$\omega_{2(opt)} = \frac{\bar{Z}\left[\lambda\theta^3C_x^3\left(-1 + \rho_{xr_x}^2\right) + \left(-8C_z + \lambda\theta^2 2C_x^2C_z\right)\left(\rho_{zx} - \rho_{xr_x}\rho_{zr_x}\right) + 4\theta C_x\left(-1 + \rho_{xr_x}^2\right)\left(-1 + \lambda C_z^2\left(1 - Q_{z.xr_x}^2\right)\right)\right]}{8\bar{X}C_x\left(-1 + \rho_{xr_x}^2\right)\left(1 + \lambda C_z^2\left(1 - Q_{z.xr_x}^2\right)\right)},$$

and

$$\omega_{3(opt)} = \frac{\bar{Z}\left(8 - \lambda\theta^2C_x^2\right)C_z\left(\rho_{xr_x}\rho_{zx} - \rho_{zr_x}\right)}{8\bar{R}_xC_r\left(-1 + \rho_{xr_x}^2\right)\left(1 + \lambda C_z^2\left(1 - Q_{z.xr_x}^2\right)\right)},$$

$$Q_{z.xr_x}^2 = \frac{\rho_{zx}^2 + \rho_{zr_x}^2 - 2\rho_{zx}\rho_{zr_x}\rho_{xr_x}}{1 - \rho_{xr_x}^2}.$$

Substitute the value of $\omega_1, \omega_2, \omega_3$ in equation (9), and we get the minimum MSE given by

$$MSE_{\min}(\hat{\bar{Z}}_{pr}) = \frac{\lambda\bar{Z}^2\left\{64C_y^2(1 - Q_{z.xr_x}^2) - \lambda\theta^4C_x^4C - 16\lambda\theta^2C_x^2C_y^2(1 - Q_{z.xr_x}^2)\right\}}{64\left\{1 + \lambda C_y^2(1 - Q_{z.xr_x}^2)\right\}}. \tag{10}$$

Efficiency comparison

We present the mathematical comparison of the proposed estimator with existing estimators under Model-I as

i) By equations (5) and (10)

$$MSE_{\min}(\hat{\bar{Z}}_{pr}) \leq MSE(\hat{t}_{GRR}).$$

ii) By equations (2) and (10)

$$MSE_{\min}(\hat{\bar{Z}}_{pr}) \leq MSE(\hat{\mu}_{RS}).$$

iii) By equations (4) and (10)

$$MSE_{\min}(\hat{\bar{Z}}_{pr}) \leq MSE(\hat{\mu}_{RN}).$$

iv) By equations (3) and (10)

$$MSE_{\min}(\hat{\bar{Z}}_{pr}) \leq MSE(\hat{\mu}_{RG}).$$

Real-life conifer tree data set 1

Real-life data set is used for numerical comparison. Detail is given as: Population Source: [12]. Let z be our study variable used in our estimator and model. We study the total height of the conifer tree. x is our auxiliary variable which is non-sensitive. We measure the circumference of the conifer tree at breast height. We assume three samples in our simulation study, n = 100, n = 200, and n = 300.

z: Total height of a conifer tree in feet;
x: Circumference of a conifer tree at breast height in cm
N=399, ρ_{XY} = 0.914981, ρ_{zr_x} = 0.983609, ρ_{xr_x} = 0.890219, μ_X = 285.125, μ_Y = 5182.64, σ_X = 310.1403, σ_Z = 3250.5050, C_z = 0.354194, C_x = 0.948459, C_r = 0.573765

Table 2. The MSE and PRE values of estimators for real-life data set 1

n	W	T	Estimator	Theoretical	PRE
50	0.3	0.3	$\hat{\mu}_{YS}$	55.909	100.00
			$\hat{\mu}_{RS}$	54.303	102.95
			$\hat{\mu}_{RG}$	10.708	522.11
			$\hat{\mu}_{RN}$	55.258	101.17
			$\hat{t}_{GRR}$	9.7486	573.51
			$\hat{\bar{Z}}_{pr}^{(1)}$	5.8744	951.74
			$\hat{\bar{Z}}_{pr}^{(2)}$	5.8344	958.275
			$\hat{\bar{Z}}_{pr}^{(3)}$	5.781	967.11
			$\hat{\bar{Z}}_{pr}^{(4)}$	5.8344	958.27
			$\hat{\bar{Z}}_{pr}^{(5)}$	5.8135	961.72
			$\hat{\bar{Z}}_{pr}^{(6)}$	5.8135	961.72
			$\hat{\bar{Z}}_{pr}^{(7)}$	5.7810	967.11
			$\hat{\bar{Z}}_{pr}^{(8)}$	5.8135	961.72
			$\hat{\bar{Z}}_{pr}^{(9)}$	5.8344	958.27
	0.5	0.5	$\hat{\mu}_{YS}$	56.033	100.00
			$\hat{\mu}_{RS}$	54.303	103.18
			$\hat{\mu}_{RG}$	10.718	522.75
			$\hat{\mu}_{RN}$	55.259	101.40
			$\hat{t}_{GRR}$	9.7507	574.66
			$\hat{\bar{Z}}_{pr}^{(k)*}$	5.8744	953.85
	0.7	0.7	$\hat{\mu}_{YS}$	55.909	100.00
			$\hat{\mu}_{RS}$	54.303	102.95
			$\hat{\mu}_{RG}$	10.729	521.08
			$\hat{\mu}_{RN}$	55.259	101.17
			$\hat{t}_{GRR}$	9.7486	573.51
			$\hat{\bar{Z}}_{pr}^{(k)*}$	5.8744	951.74
100	0.3	0.3	$\hat{\mu}_{YS}$	23.404	100.00
			$\hat{\mu}_{RS}$	21.798	107.36
			$\hat{\mu}_{RG}$	24.409	95.88
			$\hat{\mu}_{RN}$	22.7538	102.86
			$\hat{t}_{GRR}$	24.0141	97.459
			$\hat{\bar{Z}}_{pr}^{(1)}$	20.516	114.07
			$\hat{\bar{Z}}_{pr}^{(2)}$	21.841	107.15
			$\hat{\bar{Z}}_{pr}^{(3)}$	20.943	111.75
			$\hat{\bar{Z}}_{pr}^{(4)}$	21.811	107.15
			$\hat{\bar{Z}}_{pr}^{(5)}$	21.49	108.81
			$\hat{\bar{Z}}_{pr}^{(6)}$	21.48	108.91
			$\hat{\bar{Z}}_{pr}^{(7)}$	20.43	111.75
			$\hat{\bar{Z}}_{pr}^{(8)}$	21.89	108.91
			$\hat{\bar{Z}}_{pr}^{(9)}$	21.841	107.15
	0.5	0.5	$\hat{\mu}_{YS}$	23.528	100.00
			$\hat{\mu}_{RS}$	21.798	107.93
			$\hat{\mu}_{RG}$	22.754	103.41
			$\hat{\mu}_{RN}$	21.754	108.41
			$\hat{t}_{GRR}$	25.015	94.072
			$\hat{\bar{Z}}_{pr}^{(k)*}$	20.516	114.68
	0.7	0.7	$\hat{\mu}_{YS}$	23.528	100.00
			$\hat{\mu}_{RS}$	21.7984	107.93
			$\hat{\mu}_{RG}$	22.7540	103.41
			$\hat{\mu}_{RN}$	22.754	103.41
			$\hat{t}_{GRR}$	24.015	97.972
			$\hat{\bar{Z}}_{pr}^{(k)*}$	20.516	114.68
150	0.3	0.3	$\hat{\mu}_{YS}$	13.853	100.00
			$\hat{\mu}_{RS}$	12.046	113.33
			$\hat{\mu}_{RG}$	2.5196	541.88

		$\hat{\mu}_{RN}$	13.002	105.00
		$\hat{t}_{GRR}$	13.779	99.082
		$\hat{Z}_{pr}^{(1)}$	2.2938	595.22
		$\hat{Z}_{pr}^{(2)}$	2.1938	631.22
		$\hat{Z}_{pr}^{(3)}$	2.3938	578.70
		$\hat{Z}_{pr}^{(4)}$	2.4938	555.22
		$\hat{Z}_{pr}^{(5)}$	2.4938	595.22
		$\hat{Z}_{pr}^{(6)}$	1.4938	595.22
		$\hat{Z}_{pr}^{(7)}$	4.4938	312.22
		$\hat{Z}_{pr}^{(8)}$	3.4938	396.22
		$\hat{Z}_{pr}^{(9)}$	2.0938	595.22
0.5	0.5	$\hat{\mu}_{YS}$	13.777	100.00
		$\hat{\mu}_{RS}$	12.046	114.36
		$\hat{\mu}_{RG}$	2.5220	546.26
		$\hat{\mu}_{RN}$	13.002	105.95
		$\hat{t}_{GRR}$	13.778	99.98
		$\hat{Z}_{pr}^{(k)*}$	2.2942	600.50
0.7	0.7	$\hat{\mu}_{YS}$	13.777	100.00
		$\hat{\mu}_{RS}$	13.046	105.60
		$\hat{\mu}_{RG}$	2.5220	546.26
		$\hat{\mu}_{RN}$	13.002	105.95
		$\hat{t}_{GRR}$	13.278	103.75
		$\hat{Z}_{pr}^{(k)*}$	2.2942	600.50

Using Table 2, we find the percentage relative efficiency of existing and proposed estimators, shown in the graph. Black boxes indicate the existing estimator, and red boxes indicate the proposed estimator. This graph shows our proposed estimator is more efficient compared to the existing estimator.

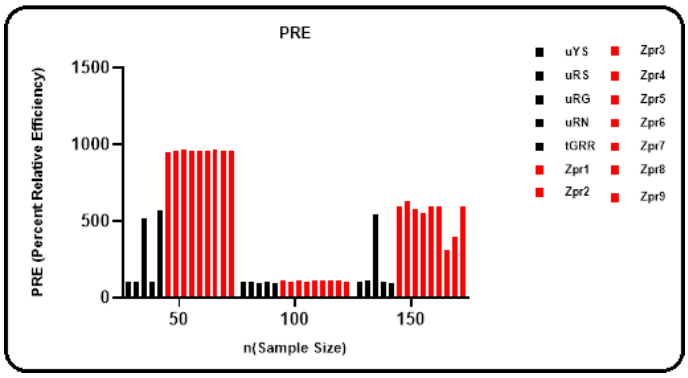

Figure 1. PRE of Real-Life data set 1

Percentage relative efficiency

We have computed the percentage relative efficiency of proposed estimators at different combinations of existing estimators. We used the following expression to obtain the percentage relative performance. Results are presented above tables.

$$PRE = \frac{MSE(\hat{\mu}_{YS})}{MSE(\hat{\mu}_{Q})} * 100, \tag{11}$$

where $Q = RS, RG, NR, GRR$.

Simulation study

We consider a multivariate normal population with multiple covariance matrices to represent (Y, X) distribution. The normal distribution is followed by scrambling variables. The standard deviation is equal to 100 percent of the standard deviation of X when the mean is 0. We generate two populations. For population 1, N is 1000 and mean is 2. For population 2, N is 1000 and mean is 3. Correlation is always positive for both populations. After Simulation, we standardize the study variable and auxiliary variable and rank of the auxiliary variable. The Simulation is conducted to evaluate the performance of the proposed estimator. For this study, we have generated the population size N=1000 from a standard normal distribution using the MVRNORM package in

software R, where study and auxiliary variables are correlated with a correlation given below. The whole simulation process starting from the drawing sample from variable Y and auxiliary variable X from the normal population and calculating the estimates, was repeated 10000 times. The reported generalized response is calculated using the formula $Z = Y + KS$. The covariance matrices are given by

Table 3. Data Summary I

Population 1	**Population 2**
N = 1000	N = 1000
μ= [2,2]	μ= [3,3]
$\Sigma = \begin{pmatrix} 2 & 1 \\ 1 & 4 \end{pmatrix}$	$\Sigma = \begin{pmatrix} 2 & 1 \\ 1 & 4 \end{pmatrix}$
ρ_{yx}=0.37144	ρ_{yx}=0.388517

Table 4. The MSE and PRE values of estimators for Population 1&2

				Population 1			**Population 2**		
n	*W*	*T*	Estimator	Theoretical	Empirical	PRE	Theoretical	Empirical	PRE
200	0.3	0.3	$\hat{\mu}_{YS}$	0.01600	0.01697	100.00	0.03194	0.01425	100.00
			$\hat{\mu}_{RS}$	0.05133	0.01770	31.17	0.03160	0.01425	175.60
			$\hat{\mu}_{RG}$	0.01610	0.01679	101.28	0.02347	0.01527	136.07
			$\hat{\mu}_{RN}$	0.05065	0.01787	31.58	0.09302	0.01439	210.07
			$\hat{t}_{GRR}$	0.00700	0.02390	233.44	0.01988	0.16697	160.68
			$\hat{\bar{Z}}_{pr}^{(1)}$	0.00470	0.00018	340.4	0.01815	0.01130	242.60
			$\hat{\bar{Z}}_{pr}^{(2)}$	0.00446	0.00058	366.78	0.0178	0.01190	179.07
			$\hat{\bar{Z}}_{pr}^{(3)}$	0.00400	0.00020	409.17	0.018	0.00720	190.02
			$\hat{\bar{Z}}_{pr}^{(4)}$	0.00447	0.00089	366.78	0.01425	0.00570	224.14
			$\hat{\bar{Z}}_{pr}^{(5)}$	0.00429	0.00039	381.63	0.01418	0.01000	225.24
			$\hat{\bar{Z}}_{pr}^{(6)}$	0.00429	0.00105	381.63	0.01425	0.00470	224.91
			$\hat{\bar{Z}}_{pr}^{(7)}$	0.00400	0.00110	409.17	0.01381	0.00023	231.04
			$\hat{\bar{Z}}_{pr}^{(8)}$	0.00429	0.00065	381.63	0.01417	0.01010	225.45
			$\hat{\bar{Z}}_{pr}^{(9)}$	0.00447	0.00066	366.78	0.01426	0.00070	223.91
	0.5	0.5	$\hat{\mu}_{YS}$	0.01700	0.01697	100.00	0.03346	0.01425	100.00
			$\hat{\mu}_{RS}$	0.05133	0.01770	31.49	0.01317	0.01425	107.98
			$\hat{\mu}_{RG}$	0.01610	0.01679	111.07	0.02112	0.01527	142.34
			$\hat{\mu}_{RN}$	0.05084	0.01787	31.53	0.02350	0.01439	200.88
			$\hat{t}_{GRR}$	0.03240	0.02390	233.44	0.01988	0.16697	168.25
			$\hat{\bar{Z}}_{pr}^{(k)*}$	0.00700	0.00067	255.44	0.01815	0.00980	242.60
	0.7	0.7	$\hat{\mu}_{YS}$	0.01600	0.01697	100.00	0.03194	0.01425	100.00
			$\hat{\mu}_{RS}$	0.05133	0.01770	31.91	0.01317	0.01425	107.98
			$\hat{\mu}_{RG}$	0.01620	0.01679	101.28	0.02354	0.01527	135.72
			$\hat{\mu}_{RN}$	0.05103	0.01787	31.23	0.02112	0.01439	142.34
			$\hat{t}_{GRR}$	0.00700	0.02390	233.44	0.01988	0.16697	160.68
			$\hat{\bar{Z}}_{pr}^{(k)*}$	0.00470	0.00046	340.4	0.01815	0.00136	242.60
500	0.3	0.3	$\hat{\mu}_{YS}$	0.01030	0.00209	100.00	0.01395	0.00615	100.00
			$\hat{\mu}_{RS}$	0.50725	0.00419	2.036	0.00482	0.00378	289.56
			$\hat{\mu}_{RG}$	0.00404	0.00427	255.19	0.00586	0.00420	237.81
			$\hat{\mu}_{RN}$	0.05004	0.00406	20.64	0.00768	0.00377	181.61
			$\hat{t}_{GRR}$	0.00175	0.02391	588.90	0.00497	0.16688	280.82
			$\hat{\bar{Z}}_{pr}^{(1)}$	0.00112	0.00021	925.80	0.00455	0.00029	306.99
			$\hat{\bar{Z}}_{pr}^{(2)}$	0.00117	0.00023	885.61	0.00427	0.00050	326.51
			$\hat{\bar{Z}}_{pr}^{(3)}$	0.00116	0.00014	885.61	0.00430	0.00094	324.41
			$\hat{\bar{Z}}_{pr}^{(4)}$	0.00115	0.00047	893.95	0.00427	0.00017	326.51
			$\hat{\bar{Z}}_{pr}^{(5)}$	0.00115	0.00011	893.95	0.00430	0.00650	324.41
			$\hat{\bar{Z}}_{pr}^{(6)}$	0.00114	0.00018	908.15	0.00430	0.00017	324.78
			$\hat{\bar{Z}}_{pr}^{(7)}$	0.00115	0.00047	893.95	0.00427	0.00371	326.51
			$\hat{\bar{Z}}_{pr}^{(8)}$	0.00114	0.00013	881.63	0.00430	0.00022	324.78
			$\hat{\bar{Z}}_{pr}^{(9)}$	0.00116	0.00016	885.61	0.00430	0.00530	324.41
	0.5	0.5	$\hat{\mu}_{YS}$	0.01191	0.00209	100.00	0.01547	0.00615	100.00
			$\hat{\mu}_{RS}$	0.05072	0.00419	20.30	0.00482	0.00378	321.03

			$\hat{\mu}_{RG}$	0.00406	0.00427	293.74	0.00588	0.00420	263.30
			$\hat{\mu}_{RN}$	0.05024	0.00406	20.71	0.00687	0.00377	225.35
			$\hat{t}_{GRR}$	0.00176	0.02391	678.57	0.00497	0.16688	311.23
			$\hat{Z}_{pr}^{(k)*}$	0.00112	0.00017	1067.7	0.00455	0.00047	340.35
	0.7	0.7	$\hat{\mu}_{YS}$	0.01033	0.00209	100.00	0.01395	0.00615	100.00
			$\hat{\mu}_{RS}$	0.50725	0.00419	2.0365	0.00482	0.00378	289.56
			$\hat{\mu}_{RG}$	0.00406	0.00427	254.20	0.00588	0.00420	237.19
			$\hat{\mu}_{RN}$	0.05043	0.00406	20.48	0.00604	0.00377	230.77
			$\hat{t}_{GRR}$	0.00175	0.02391	588.90	0.00497	0.16688	280.82
			$\hat{Z}_{pr}^{(k)*}$	0.00112	0.00047	925.80	0.00454	0.00064	306.99
700	0.3	0.3	$\hat{\mu}_{YS}$	0.00912	0.00086	100.00	0.01395	0.00239	100.00
			$\hat{\mu}_{RS}$	0.00206	0.00175	442.02	0.00842	0.00164	165.81
			$\hat{\mu}_{RG}$	0.00162	0.00178	563.27	0.00235	0.00170	594.52
			$\hat{\mu}_{RN}$	0.00499	0.00166	182.26	0.01128	0.00171	123.70
			$\hat{t}_{GRR}$	0.00070	0.02388	1299.83	0.00298	0.16685	468.05
			$\hat{Z}_{pr}^{(1)}$	0.00047	0.00013	1957.36	0.00181	0.00050	767.23
			$\hat{Z}_{pr}^{(2)}$	0.00047	0.00017	1938.1	0.00178	0.00044	583.42
			$\hat{Z}_{pr}^{(3)}$	0.00046	0.00010	1957.36	0.00178	0.00030	581.97
			$\hat{Z}_{pr}^{(4)}$	0.00047	0.00060	1938.1	0.00178	0.00038	583.42
			$\hat{Z}_{pr}^{(5)}$	0.00047	0.00014	1945.2	0.00178	0.00022	581.97
			$\hat{Z}_{pr}^{(6)}$	0.00046	0.00067	1945.29	0.00178	0.00350	582.23
			$\hat{Z}_{pr}^{(7)}$	0.00046	0.00021	1957.36	0.00177	0.00062	582.23
			$\hat{Z}_{pr}^{(8)}$	0.00046	0.00031	1945.29	0.00178	0.00120	583.42
			$\hat{Z}_{pr}^{(9)}$	0.00047	0.00032	1938.1	0.00178	0.00010	581.97
	0.5	0.5	$\hat{\mu}_{YS}$	0.01070	0.00086	100.00	0.01547	0.00239	100.00
			$\hat{\mu}_{RS}$	0.00506	0.00175	214.15	0.00842	0.00164	183.82
			$\hat{\mu}_{RG}$	0.00162	0.00178	659.78	0.00235	0.00170	658.27
			$\hat{\mu}_{RN}$	0.00501	0.00166	213.35	0.01046	0.00171	147.87
			$\hat{t}_{GRR}$	0.00070	0.02388	1524.14	0.00199	0.16685	778.09
			$\hat{Z}_{pr}^{(k)*}$	0.00047	0.00016	2297.22	0.00182	0.00085	850.59
	0.7	0.7	$\hat{\mu}_{YS}$	0.00912	0.00086	100.00	0.01395	0.00239	100.00
			$\hat{\mu}_{RS}$	0.00506	0.00175	180.23	0.00841	0.00164	165.81
			$\hat{\mu}_{RG}$	0.00163	0.00178	561.07	0.00235	0.00170	592.99
			$\hat{\mu}_{RN}$	0.00503	0.00166	180.12	0.00964	0.00171	144.70
			$\hat{t}_{GRR}$	0.00070	0.02388	1299.83	0.00199	0.16685	702.05
			$\hat{Z}_{pr}^{(k)*}$	0.00047	0.00022	1957.36	0.00182	0.00052	767.23

*where assumes the values from 1 to 9.

In Table 4, according to population 1 we make a graph of PRE in which red boxes show the proposed estimator, and black boxes show the existing estimator. Percentage Relative Efficiency of Proposed and Existing estimator through simulation is given in that graph which shows that our proposed estimator is efficient compared to another estimator. By using population 2 we make a graph. Percentage Relative Efficiency of Proposed and Existing estimator through simulation is given in that graph which shows that our proposed estimator is efficient compared to another estimator. N shows sample size. Black boxes show the existing estimator, and Red boxes show the proposed estimator.

(a) Population 1 **(b)** Population 2

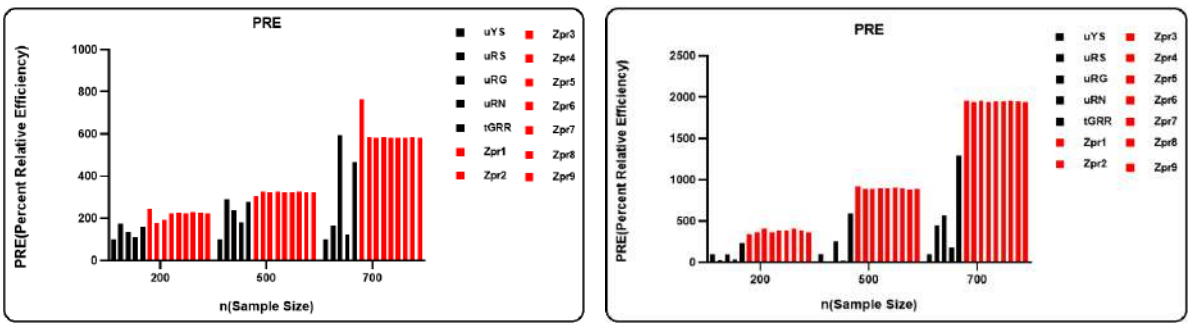

Figure 2. PRE of simulated data summary I

Generalized exponential-type estimator using two auxiliary variables for generalized two-stages optional scrambled response

Motivated by [13], we suggest a generalized exponential-type estimator for population mean using Model I, as

$$\hat{t}_{GRE} = \bar{z}\exp\left[\alpha\left(\frac{\bar{X}^{1/h} - \bar{x}^{1/h}}{\bar{X}^{1/h} + (a-1)\bar{x}^{1/h}} + \frac{\bar{U}^{1/h} - \bar{u}^{1/h}}{\bar{U}^{1/h} + (b-1)\bar{u}^{1/h}}\right)\right]. \tag{12}$$

According to a first-order approximation, the bias and mean square error (MSE) $\hat{t}_{GRE}$ are given

$$Bias(\hat{t}_{GRE}) = \lambda\bar{Z}\left[\frac{\alpha C_x^2}{ah^2}\left(1-\frac{1}{a}\right) + \frac{\alpha C_u^2}{bh^2}\left(1-\frac{1}{b}\right) - \frac{\alpha}{h}\left(\frac{C_{zx}}{a} + \frac{C_{zx}}{b}\right) + \frac{\alpha^2}{2h^2}\left(\frac{C_u^2}{b^2} + \frac{C_x^2}{a^2} + \frac{2C_{xu}}{ab}\right)\right]. \tag{13}$$

By taking a square and applying expectation from equation (13), we obtained

$$MSE(\hat{t}_{GRE}) = \lambda\bar{Z}^2\left[C_z^2 + \frac{\alpha C_x^2}{a^2b^2} + \frac{\alpha C_u^2}{b^2h^2} - \frac{2\alpha C_{zx}}{ah} - \frac{2\alpha C_{zx}}{bh} + \frac{2\alpha^2 C_{xu}}{abh^2}\right]. \tag{14}$$

To obtain the minimum MSE, we need to estimate the value of a and b. By equation (14), we obtain $\hat{a}_{(opt)} = \frac{\alpha}{h}\left[\frac{C_{xu}^2 - C_u^2C_x^2}{C_{xu}C_{zu} - C_u^2C_{zu}}\right]$ and $\hat{b}_{(opt)} = \frac{\alpha}{h}\left[\frac{C_{xu}^2 - C_u^2C_x^2}{C_{xu}C_{zx} - C_{zu}^2C_x^2}\right]$.

Using $\hat{a}_{(opt)}$ and $\hat{b}_{(opt)}$, we get a minimum MSE of $(\hat{t}_{GRE})$ as

$$MSE(\hat{t}_{GRE}) = \lambda\bar{Z}^2\left[C_z^2 + \frac{C_x^2C_{zu}^2 + C_u^2C_{zu}^2 - 2C_{xu}^2C_{zx}C_{zu}}{C_{xu}^2 - C_u^2C_x^2}\right]. \tag{15}$$

Efficiency comparison

We present the mathematical comparison of the proposed estimator using two auxiliary variables with the existing estimators under Model-I as

i) By equation (5) and (15)

$$MSE_{\min}(\hat{t}_{GRE}) \leq MSE(\hat{t}_{GRR}).$$

ii) By equation (2) and (15)

$$MSE_{\min}(\hat{t}_{GRE}) \leq MSE(\hat{\mu}_{RS}).$$

iii) By equation (4) and (15)

$$MSE_{\min}(\hat{t}_{GRE}) \leq MSE(\hat{\mu}_{RN}).$$

iv) By equation (3) and (15)

$$MSE_{\min}(\hat{t}_{GRE}) \leq MSE(\hat{\mu}_{RG}).$$

Real-life apple tree data set 2

We used data from 204 villages in Turkey's Black Sea Region, including apple production amount in 1999 (as the main variety), number of apple trees in 1999 (as the first auxiliary variety), and apple income and sales in 1998, to estimate the standard and new estimators (as the second auxiliary variety) (Source: Republic of Turkey's National Bureau of statistics)]. The MSE and PRE are calculated and simulated by the proposed model's generalized exponential type ratio estimator compared to the RRT ratio estimator for population 3.

We assume three samples in our simulation study, n= 50, 100, and 120.

N=204, ρ_{XZ} = 0.71, ρ_{xu} = 0.83, ρ_{zu} = 0.94, σ_{zx} = 77372777, σ_{zu} = 5684276, σ_{xu} = 94636084, μ_X = 26441, μ_Z = 966, μ_U = 1014, σ_X = 45402.78, σ_Z = 2389.76 and σ_U = 2521.40.

Table 5. The MSE and PRE values of estimators for Real-life dataset 2

n	W	T	**Estimator**	**Theoretical**	**PRE**
50	0.3	0.3	$\hat{\mu}_{YS}$	86278.68	100.00
			$\hat{\mu}_{RS}$	86234.28	100.05
			$\hat{\mu}_{RG}$	42787.88	201.64
			$\hat{\mu}_{RN}$	86234.28	100.05
			$\hat{t}_{GRR}$	42765.76	201.74
			$\hat{t}_{GRE}$	22350.49	386.02
	0.5	0.5	$\hat{\mu}_{YS}$	86286.93	100.00
			$\hat{\mu}_{RS}$	86234.28	100.06
			$\hat{\mu}_{RG}$	42788.51	201.65
			$\hat{\mu}_{RN}$	86234.28	100.06
			$\hat{t}_{GRR}$	42765.89	201.76
			$\hat{t}_{GRE}$	22350.49	386.06
	0.7	0.7	$\hat{\mu}_{YS}$	86278.68	100.00
			$\hat{\mu}_{RS}$	86234.28	100.05
			$\hat{\mu}_{RG}$	42789.13	201.63
			$\hat{\mu}_{RN}$	86234.28	100.05
			$\hat{t}_{GRR}$	42765.76	201.74
			$\hat{t}_{GRE}$	22350.49	386.02
100	0.3	$\hat{\mu}_{YS}$	42875.44	100.00	
			$\hat{\mu}_{RS}$	42830.05	100.10
			$\hat{\mu}_{RG}$	21252.26	201.74
			$\hat{\mu}_{RN}$	42830.05	100.10
			$\hat{t}_{GRR}$	21241.27	201.84
			$\hat{t}_{GRE}$	17351.62	247.09
	0.5	0.5	$\hat{\mu}_{YS}$	42883.68	100.00
			$\hat{\mu}_{RS}$	42830.05	100.12
			$\hat{\mu}_{RG}$	21252.57	201.78
			$\hat{\mu}_{RN}$	42830.05	100.12
			$\hat{t}_{GRR}$	21241.33	201.88
			$\hat{t}_{GRE}$	17351.62	247.14
	0.7	0.7	$\hat{\mu}_{YS}$	42875.44	100.00
			$\hat{\mu}_{RS}$	42830.05	100.10
			$\hat{\mu}_{RG}$	21252.88	201.73
			$\hat{\mu}_{RN}$	42830.05	100.10
			$\hat{t}_{GRR}$	21241.27	201.84
			$\hat{t}_{GRE}$	17351.62	247.097
120	0.3	0.3	$\hat{\mu}_{YS}$	19460.53	100.00
			$\hat{\mu}_{RS}$	19414.6	100.23
			$\hat{\mu}_{RG}$	19634.35	100.81
			$\hat{\mu}_{RN}$	19414.6	100.23
			$\hat{t}_{GRR}$	19629.37	116.93
			$\hat{t}_{GRE}$	14654.87	132.79
	0.5	0.5	$\hat{\mu}_{YS}$	19468.78	100.00
			$\hat{\mu}_{RS}$	19414.6	100.27
			$\hat{\mu}_{RG}$	19634.49	102.07
			$\hat{\mu}_{RN}$	19414.6	100.27
			$\hat{t}_{GRR}$	19629.40	102.18
			$\hat{t}_{GRE}$	14654.87	132.84
	0.7	0.7	$\hat{\mu}_{YS}$	19460.53	100.00
			$\hat{\mu}_{RS}$	19414.6	100.23
			$\hat{\mu}_{RG}$	19634.63	100.12
			$\hat{\mu}_{RN}$	19414.6	100.23
			$\hat{t}_{GRR}$	19629.37	102.09
			$\hat{t}_{GRE}$	14654.87	132.79

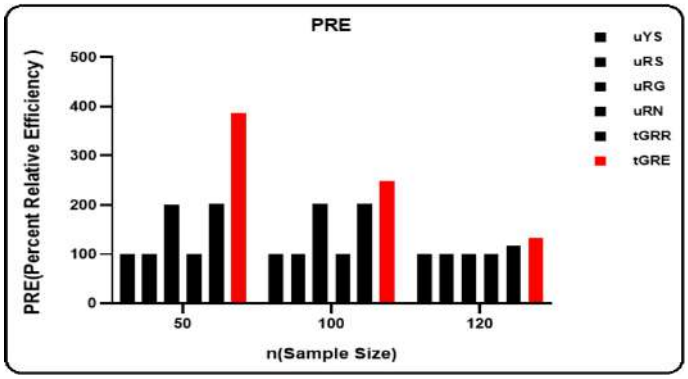

Figure 3. PRE of Real-life data set 2

Simulation study

We used R studio Version 1.3.1093 for the coding and simulation study. To describe the (Y, X) distribution, we assume a multivariate normal population with distinct covariance matrices. We generate random variables by following a multivariate normal distribution. The normal distribution is followed by scrambling variables. With a mean of 0 and an SD equal to 100% of the standard deviation of variable X. The reported generalized response is calculated using the formula Z = Y+ KS. The covariance matrices are given as:

Table 6. Data summary II

Population 1	**Population-2**
N =1000	N =1000
μ= [2,2,2]	μ= [3,3,3]
$\sum = \begin{pmatrix} 8 & 1 & 2.5 \\ 1 & 2 & 1.5 \\ 2.5 & 1.5 & 2 \end{pmatrix}$	$\sum = \begin{pmatrix} 2 & 1 & 2.2 \\ 1 & 3 & 1.2 \\ 2.2 & 1.2 & 3 \end{pmatrix}$
ρ_{xy}=0.27451	ρ_{xy}=0.40759
ρ_{xy}= 0.721011	ρ_{xy}= 0.39536

Table 7. The MSE and PRE values of estimators for Population 1&2

				Population 1			Population 2		
n	*W*	*T*	Estimator	Theoretical	Empirical	PRE	Theoretical	Empirical	PRE
200	0.3	0.3	$\hat{\mu}_{YS}$	0.03519	0.03140	100.00	0.01358	0.07440	100
			$\hat{\mu}_{RS}$	0.01755	0.00843	200.51	0.13800	0.02654	93.792
			$\hat{\mu}_{RG}$	0.03083	0.00866	114.13	9.79250	0.01910	112.69
			$\hat{\mu}_{RN}$	0.01438	0.00810	244.71	0.13640	0.01118	99.95
			$\hat{t}_{GRR}$	0.02892	0.02628	121.66	0.06609	0.14720	20.52
			$\hat{t}_{GRE}$	0.00523	0.00135	672.87	0.01135	0.01098	119.64
	0.5	0.5	$\hat{\mu}_{YS}$	0.03111	0.03140	100.00	0.01472	0.07440	100.00
			$\hat{\mu}_{RS}$	0.01754	0.00843	177.32	0.13870	0.02654	67.61
			$\hat{\mu}_{RG}$	0.03081	0.00866	101.00	0.01207	0.01910	121.89
			$\hat{\mu}_{RN}$	0.01302	0.00810	238.98	0.13706	0.01118	10.73
			$\hat{t}_{GRR}$	0.02890	0.02628	107.65	0.06613	0.14720	20.32
			$\hat{t}_{GRE}$	0.00523	0.00135	595.04	0.01135	0.01098	129.66
	0.7	0.7	$\hat{\mu}_{YS}$	0.03519	0.03140	100.00	0.01358	0.07440	100.00
			$\hat{\mu}_{RS}$	0.01754	0.00843	200.51	0.13870	0.02654	94.792
			$\hat{\mu}_{RG}$	0.03086	0.00866	114.01	0.01209	0.01910	112.27
			$\hat{\mu}_{RN}$	0.01619	0.00810	217.34	0.13772	0.01118	9.862
			$\hat{t}_{GRR}$	0.02892	0.02628	121.66	0.06600	0.14720	20.57
			$\hat{t}_{GRE}$	0.00523	0.00135	672.87	0.01135	0.01098	119.64
500	0.3	0.3	$\hat{\mu}_{YS}$	0.01185	0.00788	100.00	0.00787	0.00175	100.00
			$\hat{\mu}_{RS}$	0.00579	0.00216	204.65	0.13300	0.00641	59.918
			$\hat{\mu}_{RG}$	0.00771	0.00204	153.73	0.00301	0.00273	261.24
			$\hat{\mu}_{RN}$	0.00895	0.02631	132.25	0.13069	0.00274	69.023
			$\hat{t}_{GRR}$	0.00723	0.00213	163.88	0.01652	0.14720	43.75
			$\hat{t}_{GRE}$	0.00131	0.00037	906.36	0.00284	0.00025	277.35
	0.5	0.5	$\hat{\mu}_{YS}$	0.01262	0.00788	100.00	0.00900	0.00175	100.00
			$\hat{\mu}_{RS}$	0.00579	0.00216	218.04	0.13300	0.00641	69.773
			$\hat{\mu}_{RG}$	0.00771	0.00204	163.70	0.00301	0.00273	298.40
			$\hat{\mu}_{RN}$	0.00805	0.02631	156.75	0.13135	0.00274	68.586

			$\hat{t}_{GRR}$	0.00723	0.00213	174.59	0.01653	0.14720	54.545
			$\hat{t}_{GRE}$	0.00130	0.00037	965.66	0.00283	0.00025	317.41
	0.7	0.7	$\hat{\mu}_{YS}$	0.01185	0.00788	100.00	0.00787	0.00175	100.00
			$\hat{\mu}_{RS}$	0.00579	0.00216	204.65	0.13300	0.00641	59.188
			$\hat{\mu}_{RG}$	0.00771	0.00204	153.57	0.00302	0.00273	260.26
			$\hat{\mu}_{RN}$	0.00714	0.02631	165.76	0.13201	0.00274	59.63
			$\hat{t}_{GRR}$	0.00723	0.00213	163.88	0.01652	0.14720	54.545
			$\hat{t}_{GRE}$	0.00131	0.00037	906.36	0.00284	0.00025	277.35
700	0.3	0.3	$\hat{\mu}_{YS}$	0.01185	0.00328	100.00	0.00673	0.00090	100.00
			$\hat{\mu}_{RS}$	0.00579	0.00088	204.65	0.13186	0.00277	51.037
			$\hat{\mu}_{RG}$	0.00771	0.00094	153.73	0.00120	0.00114	558.34
			$\hat{\mu}_{RN}$	0.00895	0.00083	132.25	0.12955	0.00121	51.947
			$\hat{t}_{GRR}$	0.00723	0.02629	163.88	0.00661	0.14728	101.96
			$\hat{t}_{GRE}$	0.00131	0.00010	906.36	0.00114	0.00014	592.78
	0.5	0.5	$\hat{\mu}_{YS}$	0.01262	0.00328	100.00	0.00786	0.00090	100.00
			$\hat{\mu}_{RS}$	0.00579	0.00088	218.04	0.13186	0.00277	59.65
			$\hat{\mu}_{RG}$	0.00771	0.00094	163.70	0.00120	0.00114	651.43
			$\hat{\mu}_{RN}$	0.00805	0.00083	156.75	0.13021	0.00121	60.41
			$\hat{t}_{GRR}$	0.00723	0.02629	174.59	0.00661	0.14728	121.21
			$\hat{t}_{GRE}$	0.00130	0.00010	965.66	0.00114	0.00014	692.91
	0.7	0.7	$\hat{\mu}_{YS}$	0.01185	0.00328	100.00	0.00673	0.00090	100.00
			$\hat{\mu}_{RS}$	0.00579	0.00088	204.65	0.13180	0.00277	51.03
			$\hat{\mu}_{RG}$	0.00772	0.00094	153.57	0.00120	0.00114	556.24
			$\hat{\mu}_{RN}$	0.00714	0.00083	165.76	0.13087	0.00121	51.423
			$\hat{t}_{GRR}$	0.00723	0.02629	163.88	0.00660	0.14728	101.51
			$\hat{t}_{GRE}$	0.00131	0.00010	906.36	0.00114	0.00014	592.78

The results are represented in Tables 2, 4, 5, and 7. Tables 2 and 5 are used for real-life data sets in which we find theoretical values and percentage relative efficiency. It observed that the percentage relative efficiency of the proposed estimators ($\hat{\bar{Z}}_{pr}^{(k)*}$, $\hat{t}_{GRE}$) according to the model I is better as compared to the existing estimator ($\hat{\mu}_{YS}$,$\hat{\mu}_{RS}$,$\hat{\mu}_{RG}$,$\hat{\mu}_{RN}$,$\hat{t}_{GRR}$). Tables 4 and 8 are used for artificial data. It also shows higher PRE as compared to other ratio estimators. Graphical representation also shows that our proposed estimator's percentage relative efficiency is greater than existing estimators. We used table 7 (population 1) for PRE representations. Red boxes show the proposed estimator, and Black boxes show existing estimators. N shows sample size. Percentage Relative Efficiency of Proposed and Existing estimator through simulation is given in that graph which shows that our proposed estimator is efficient compared to another estimator. We follow population 2 and make a graph for percentage relative efficiency. Red boxes show the proposed estimator, and Black boxes show existing estimators. N shows sample size. Percentage Relative Efficiency of Proposed and Existing estimator through simulation is given in that graph which shows that our proposed estimator PRE values are efficient compared to another estimator.

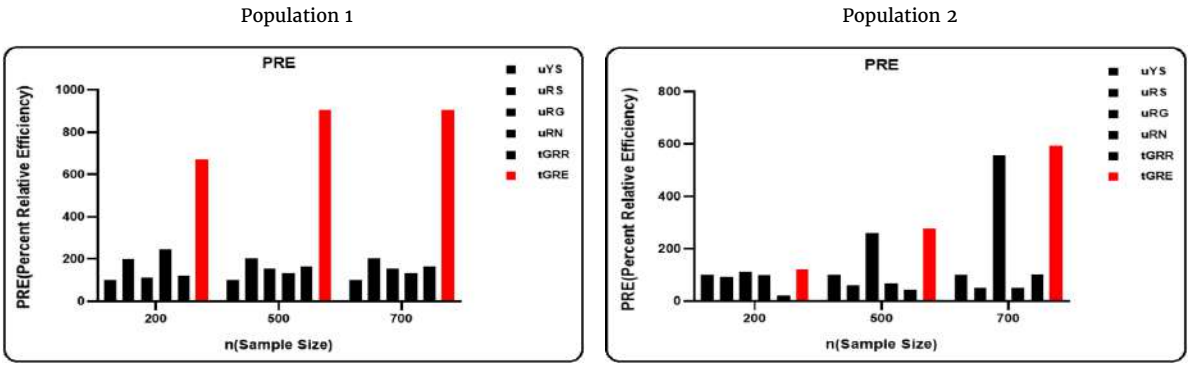

Figure 4. PRE of simulated data summary II

4 Proposed model II

Mean estimator for generalized quantitative randomized response

[14] proposed a quantitative randomized response model. In this study, the study variable Y_i is represented by a mean μ_Y and unknown variance σ_y^2. We assumed that $\theta_1 = E(S)$ variance is equal to $\sigma_1^2 = V(S)$ and their probability lies between $0 \leq p \leq 1$.

$$Z_{\alpha i} = \left\{ \begin{array}{ll} Y_i & \text{with probability p} \\ Y_i S & \text{with probability (1 – p)} \end{array} \right\}. \tag{16}$$

We get

$$\hat{\mu}_y^* = \frac{\bar{Z}^*}{p + (1-p)\theta_1},$$

where

$$\bar{Z}_\alpha = \sum_{i=1}^{n} Z_{\alpha i}/n\ ,\ V(\hat{\mu}_x^*) = \frac{\sigma_Z^2}{n(p + (1-p)\theta_1)^2},$$

where

$$\sigma_{Z^*}^2 = \mu_y^2(1 + C_x^2)(p + (1-p)\theta_1^2(1 + C_1^2)) - \mu_x^2(p + (1-P)\theta_1)^2,$$

with

$$C_x = \frac{\sigma y}{\mu_Y} \text{ and } C_1 = \frac{\sigma_1}{\theta_1}.$$

Generalized exponential ratio type estimator using one auxiliary variable for quantitative randomized response

Motivated by [9], [10], and [11], proposed a difference- ratio-type-exponential estimator $\hat{\bar{Z}}_{\alpha i}$ that is given by

$$\hat{\bar{Z}}_{\alpha i} = \{\omega_1 \bar{z} + \omega_2(\bar{X} - \bar{x}) + \omega_3(\bar{R}_x - \bar{r}_x)\} \exp\left(\frac{a(\bar{X} - \bar{x})}{a(\bar{X} - \bar{x}) + 2b)}\right), \tag{17}$$

$$\hat{\bar{Z}}_{\alpha i} = \omega_1 \bar{Z} S_1 - \omega_1 \bar{Z} S_1 e_3 - \omega_2 \bar{X} e_1 - \omega_3 \bar{R}_x e_2 \left\{1 - \frac{e_1}{2} + \frac{3e_1^2}{8} + ...\right\}. \tag{18}$$

By expanding the equation (10) and keeping terms only up to order two $e_1 s$ we can write

$$\begin{aligned}(\hat{\bar{Z}}_{pr} - \bar{Z}) = &- \bar{Z} + \bar{Z} S_1 \omega_1 + \omega_1 \bar{Z} S_1 e_0 - 1/2\theta \bar{Z} e_1 S_1 \omega_1 - \bar{X}\omega_2 e_1 - \bar{R}_x e_2 \omega_3 - 1/2\theta \bar{Z} e_1 e_0 S_1 \omega_1 \\ &+ 3/8\theta^2 \bar{Z} S_1 e_1^2 \omega_1 + 1/2\bar{X}\theta e_1^2 \omega_2 + 1/2\bar{R}_x e_2 e_1 \omega_3.\end{aligned} \tag{19}$$

By taking expectation, we can find the bias $\hat{\bar{Z}}_{\alpha i}$ under first approximation, which is given as

$$\begin{aligned}Bias(\hat{\bar{Z}}_{\alpha i}) = &\frac{1}{8}[-8\bar{Z} + 4\lambda\theta C_x(\bar{X} C_x \omega_2 + \bar{R}_x \rho_{xr_x} C_r \omega_3 + \bar{Z}\theta_1 \omega_1\{(8 + \lambda\theta C_x \\ &(3\theta C_x - 4C_y \rho_{yx})\}].\end{aligned} \tag{20}$$

The MSE of $\hat{\bar{Z}}_{\alpha i}$ under the first order of approximation are respectively given by

$$\begin{aligned}MSE(\hat{\bar{Z}}_{\alpha i}) = &\bar{Z}^2 + \lambda \bar{X} C_x^2 \omega_2(-\bar{Z}\theta_1 + \bar{X}\omega_2) + \lambda \bar{R}_x^2 C_r^2 \omega_3^2 + \lambda \bar{R}_x C_x C_r(-\bar{Z}\theta_1 + 2\bar{X}\omega_2)\omega_3 \rho_{xr_x} + \\ &\bar{Z}^2 \theta_1 \omega_1^2[1 + \lambda\{C_y^2 + C_x - 2C_y \rho_{yx})\}] + \frac{1}{4}\omega_1\theta_1[-8\omega_1\alpha\theta_2 + \lambda C_x \\ &\{C_x(-3\omega_1 \bar{Z}\theta + 8\bar{X}\omega_2) + 8\bar{R}_x C_r \omega_3 \rho_{xr_x} + 4C_y(\bar{Z}\theta_1 - 2\bar{X}\omega_2)\rho_{xy}\} - 8\bar{R}_x \lambda C_y C_r \omega_3 \rho_{yr_x}].\end{aligned} \tag{21}$$

The optimum value of $\omega_1\ \omega_2\ \omega_3$, obtained by minimizing above equation respectively, given by $\omega_{1(opt)} = \frac{8 - \lambda\theta^2 C_x^2}{8(1 + \lambda C_z^2(1 - Q_{z.xrx}^2))}$,

$$\omega_{2(opt)} = \frac{\bar{Z}\left[\lambda\theta^3 C_x^3\left(-1 + \rho_{xr_x}^2\right) + \left(-8C_z + \lambda 2\theta^2 C_x^2 C_z\right)(\rho_{zx} - \rho_{xr_x}\rho_{zr_x}) + 4C_x\left(-1 + \rho_{xr_x}^2\right)\left(-1 + \lambda C_z^2\left(1 - Q_{z.xr_x}^2\right)\right)\right]}{8\bar{X}C_x\left(-1 + \rho_{xr_x}^2\right)\left(1 + \lambda C_z^2\left(1 - Q_{z.xr_x}^2\right)\right)},$$

and

$$\omega_{3(opt)} = \frac{\bar{Z}\left(8 - \lambda\theta^2 C_x^2\right) C_z\left(\rho_{xr_x}\rho_{zx} - \rho_{zr_x}\right)}{8\bar{R}_x C_r\left(-1 + \rho_{xr_x}^2\right)\left(1 + \lambda C_z^2\left(1 - Q_{z.xr_x}^2\right)\right)},$$

where

$$Q^2_{z.xr_x} = \frac{\rho^2_{zx} + \rho^2_{zr_x} - 2\rho_{zx}\rho_{zr_x}\rho_{xr_x}}{1 - \rho^2_{xr_x}}.$$

Substitute the value ω_1 ω_2, ω_3 in equation (21), and we get the minimum MSE $\bar{x} = \bar{X}(1 + e_1)$given by

$$MSE_{\min}(\hat{\bar{Z}}_{\alpha i}) = \frac{\lambda \bar{Z}\theta_1 \left[64C^2_y(1 - Q^2_{z.xr_x}) - \lambda\theta^4 C^4_x C - 16\lambda\theta^2 C^2_x C^2_y(1 - Q^2_{z.xr_x})\right]}{64\left\{1 + \lambda C^2_y(1 - Q^2_{z.xr_x})\right\}}. \tag{22}$$

Efficiency comparison

We present the mathematical comparison of the proposed estimator with existing estimators under Model-II

v) By equations (5) and (22)

$$MSE_{\min}(\hat{\bar{Z}}_{\alpha i}) \leq MSE(\hat{t}_{GRR}).$$

vi) By equations (2) and (22)

$$MSE_{\min}(\hat{\bar{Z}}_{\alpha i}) \leq MSE(\hat{\mu}_{RS}).$$

vii) By equations (4) and (22)

$$MSE_{\min}(\hat{\bar{Z}}_{\alpha i}) \leq MSE(\hat{\mu}_{RN}).$$

viii) By equations (3) and (22)

$$MSE_{\min}(\hat{\bar{Z}}_{\alpha i}) \leq MSE(\hat{\mu}_{RG}).$$

Simulation study

We generate the correlated scrambling variables S with parameters θ_1 and σ_1. The discrete uniform distribution is followed by scrambling variable, where $S = U(a_1, b_1)$. Scrambling variables followed uniform distribution. In other words, Stakes integer values between a_1 and b_1. The reported generalized response is calculated using the formula $Z = YS$. Z is our auxiliary variable. And Y is the study variable and S is the scramble variable.

Table 8. Data summary III

Population 1	**Population 2**
N = 1000	N = 1000
μ= [2,2]	μ= [3,3]
$\sum = \begin{pmatrix} 2 & 1 \\ 1 & 4 \end{pmatrix}$	$\sum = \begin{pmatrix} 6 & 2 \\ 2 & 4 \end{pmatrix}$
ρ_{yx}=0.37144	ρ_{yx}=0.388517
$S_{\min}$ = 0, $S_{\max}$ = 3	$S_{\min}$ = 0, $S_{\max}$ = 5

Table 9. The MSE and PRE values of estimators for Population 1

				Population 1			Population 2		
n	W	T	Estimator	Theoretical	Empirical	PRE	Theoretical	Empirical	PRE
200	0.3	0.3	$\hat{\mu}_{YS}$	0.04768	0.00702	100.00	0.2981	0.0012	100.00
			$\hat{\mu}_{RS}$	0.57105	0.0085	115.01	0.2840	0.0096	104.97
			$\hat{\mu}_{RG}$	0.07370	0.0096	64.69	0.4047	0.0010	73.65
			$\hat{\mu}_{RN}$	0.05688	0.0078	83.82	0.2894	0.0095	103.06
			$\hat{t}_{GRR}$	0.04509	0.0062	105.95	0.2618	0.0029	113.85
			$\hat{\bar{Z}}^{(1)}_{pr}$	0.0414	0.00042	115.74	0.1686	0.00028	176.81
			$\hat{\bar{Z}}^{(2)}_{pr}$	0.04016	0.00035	118.72	0.1647	0.00011	177.79
			$\hat{\bar{Z}}^{(3)}_{pr}$	0.03810	0.0002	125.10	0.1639	0.00039	178.51
			$\hat{\bar{Z}}^{(4)}_{pr}$	0.04016	0.00014	118.72	0.1668	0.00029	177.72
			$\hat{\bar{Z}}^{(5)}_{pr}$	0.03930	0.00024	121.08	0.1683	0.00022	178.13

			$\hat{\bar{Z}}_{pr}^{(6)}$	0.03938	0.00041	121.08	0.1676	0.00041	178.33
			$\hat{\bar{Z}}_{pr}^{(7)}$	0.03811	0.00060	125.10	0.1659	0.00070	178.47
			$\hat{\bar{Z}}_{pr}^{(8)}$	0.03937	0.00132	121.08	0.1623	0.00034	178.53
			$\hat{\bar{Z}}_{pr}^{(9)}$	0.04016	0.0027	118.72	0.1616	0.00105	177.76
	0.5	0.5	$\hat{\mu}_{YS}$	0.04926	0.0010	100.00	0.2996	0.0029	100.00
			$\hat{\mu}_{RS}$	0.05710	0.0036	64.69	0.2894	0.0094	103.76
			$\hat{\mu}_{RG}$	0.07375	0.0031	66.799	0.2840	0.0098	105.49
			$\hat{\mu}_{RN}$	0.05694	0.0034	83.82	0.3718	0.0045	84.70
			$\hat{t}_{GRR}$	0.04509	0.0062	109.23	0.2618	0.0032	114.43
			$\hat{\bar{Z}}_{pr}^{(k)*}$	0.04145	0.00049	118.83	0.1686	0.00234	177.71
	0.7	0.7	$\hat{\mu}_{YS}$	0.04760	0.0010	100.00	0.2981	0.0028	100.00
			$\hat{\mu}_{RS}$	0.05710	0.0042	64.69	6.2890	0.0014	4.74
			$\hat{\mu}_{RG}$	0.07370	0.0035	64.62	0.2840	0.0098	104.95
			$\hat{\mu}_{RN}$	0.05701	0.0042	83.82	6.3388	0.0025	4.70
			$\hat{t}_{GRR}$	0.04509	0.0063	105.74	0.2618	0.0032	113.85
			$\hat{\bar{Z}}_{pr}^{(k)*}$	0.04145	0.00011	115.01	0.1686	0.00043	176.81
500	0.3	0.3	$\hat{\mu}_{YS}$	0.01810	0.00090	100.00	0.0805	0.0038	100.00
			$\hat{\mu}_{RS}$	0.05354	0.00089	33.83	0.5070	0.0034	15.87
			$\hat{\mu}_{RG}$	0.01840	0.00072	98.53	0.0710	0.0098	113.38
			$\hat{\mu}_{RN}$	0.05332	0.00061	33.95	0.3224	0.0035	24.96
			$\hat{t}_{GRR}$	0.01120	0.00051	161.08	0.0754	0.0032	120.97
			$\hat{\bar{Z}}_{pr}^{(1)}$	0.01038	0.000028	174.87	0.0665	0.000421	122.97
			$\hat{\bar{Z}}_{pr}^{(2)}$	0.01026	0.000035	176.41	0.1647	0.00017	107.79
			$\hat{\bar{Z}}_{pr}^{(3)}$	0.01010	0.00045	179.20	0.1639	0.00019	108.51
			$\hat{\bar{Z}}_{pr}^{(4)}$	0.01036	0.00009	174.71	0.1668	0.00032	107.72
			$\hat{\bar{Z}}_{pr}^{(5)}$	0.01030	0.00042	175.08	0.1683	0.00079	108.13
			$\hat{\bar{Z}}_{pr}^{(6)}$	0.03938	0.00029	141.08	0.1676	0.00017	108.33
			$\hat{\bar{Z}}_{pr}^{(7)}$	0.03811	0.000027	142.10	0.1659	0.00029	108.47
			$\hat{\bar{Z}}_{pr}^{(8)}$	0.03937	0.00036	132.08	0.1623	0.00053	108.53
			$\hat{\bar{Z}}_{pr}^{(9)}$	0.04016	0.00099	119.72	0.1616	0.00062	107.76
	0.5	0.5	$\hat{\mu}_{YS}$	0.01970	0.0010	100.00	0.0620	0.0048	132.26
			$\hat{\mu}_{RS}$	0.02354	0.00087	83.68	6.5070	0.0014	115.50
			$\hat{\mu}_{RG}$	0.01840	0.0089	107.08	0.0720	0.0098	113.88
			$\hat{\mu}_{RN}$	0.02339	0.00076	84.69	6.5894	0.0015	122.29
			$\hat{t}_{GRR}$	0.01120	0.00063	175.11	0.0665	0.0032	123.25
			$\hat{\bar{Z}}_{pr}^{(k)*}$	0.01038	0.00057	190.13	0.0805	0.0024	100.00
	0.7	0.7	$\hat{\mu}_{YS}$	0.01810	0.00010	100.00	0.5070	0.0022	15.87
			$\hat{\mu}_{RS}$	0.02354	0.00071	84.391	0.0710	0.0098	113.35
			$\hat{\mu}_{RG}$	0.01840	0.00091	98.44	0.5560	0.0035	14.22
			$\hat{\mu}_{RN}$	0.02345	0.00092	83.397	0.0654	0.0032	122.98
			$\hat{t}_{GRR}$	0.01120	0.00063	161.08	0.0565	0.0018	143.75
			$\hat{\bar{Z}}_{pr}^{(k)*}$	0.01030	0.00005	174.87	0.0620	0.0048	132.26
700	0.3	0.3	$\hat{\mu}_{YS}$	0.01220	0.000201	100.00	0.0369	0.0034	100.00
			$\hat{\mu}_{RS}$	0.02283	0.0089	83.10	0.0550	0.0042	67.01
			$\hat{\mu}_{RG}$	0.00737	0.0086	166.24	0.0284	0.0018	130.17
			$\hat{\mu}_{RN}$	0.02260	0.0092	84.21	6.6000	0.0035	56.02
			$\hat{t}_{GRR}$	0.00450	0.0063	271.78	0.0261	0.0071	141.22
			$\hat{\bar{Z}}_{pr}^{(1)}$	0.00415	0.00042	294.92	0.0201	0.000962	184.50
			$\hat{\bar{Z}}_{pr}^{(2)}$	0.00401	0.00086	218.72	0.1247	0.0001	177.79
			$\hat{\bar{Z}}_{pr}^{(3)}$	0.04810	0.00040	225.10	0.1339	0.00014	178.51
			$\hat{\bar{Z}}_{pr}^{(4)}$	0.04016	0.00021	218.72	0.1368	0.0011	177.72
			$\hat{\bar{Z}}_{pr}^{(5)}$	0.03930	0.00073	221.08	0.1483	0.00168	178.13
			$\hat{\bar{Z}}_{pr}^{(6)}$	0.03938	0.00081	221.08	0.1676	0.0012	178.33
			$\hat{\bar{Z}}_{pr}^{(7)}$	0.03811	0.00029	225.10	0.1559	0.0020	178.47
			$\hat{\bar{Z}}_{pr}^{(8)}$	0.03937	0.00059	221.08	0.1623	0.0011	178.53
			$\hat{\bar{Z}}_{pr}^{(9)}$	0.04016	0.00070	218.72	0.1616	0.0003	177.76
	0.5	0.5	$\hat{\mu}_{YS}$	0.01380	0.00102	100.00	6.5506	0.0014	100.00
			$\hat{\mu}_{RS}$	0.05283	0.0092	6.5506	6.5506	0.0014	58.78
			$\hat{\mu}_{RG}$	0.00737	0.0082	0.0284	0.0284	0.0042	135.5
			$\hat{\mu}_{RN}$	0.05260	0.0094	6.6329	6.6329	0.0028	58.0
			$\hat{t}_{GRR}$	0.00450	0.0063	0.0301	0.0301	0.0035	127.88

		$\hat{Z}_{pr}^{(k)*}$	0.00416	0.00038	0.0262	0.0262	0.0071	147.01
0.7	0.7	$\hat{\mu}_{YS}$	0.01220	0.0010	100.00	6.6000	0.0034	100.00
		$\hat{\mu}_{RS}$	0.05283	0.0087	23.19	0.0262	0.0042	130.17
		$\hat{\mu}_{RG}$	0.00737	0.0088	166.09	0.0262	0.0018	130.17
		$\hat{\mu}_{RN}$	0.05274	0.0087	23.14	0.0201	0.0045	56.08
		$\hat{t}_{GRR}$	0.00450	0.0049	271.78	0.0262	0.0061	122.84
		$\hat{\hat{Z}}_{pr}^{(k)*}$	0.00416	0.00043	294.92	0.0201	0.00051	184.50

In Table 9 PRE for population 1 is given. Percentage Relative Efficiency of Proposed and Existing estimator through simulation is given in that graph which shows that our proposed estimator is efficient compared to another estimator. Black boxes show the existing estimator, and Red boxes show the proposed estimators. Using population I, we estimate PRE. In table 9 by using population 2 we find the percentage relative efficiency of estimators. Red boxes show the proposed estimator, and Black boxes show existing estimators. Percentage Relative Efficiency of Proposed and Existing estimator through simulation is given in that graph which shows that our proposed estimator is efficient compared to another estimator.

Population 1 Population 2

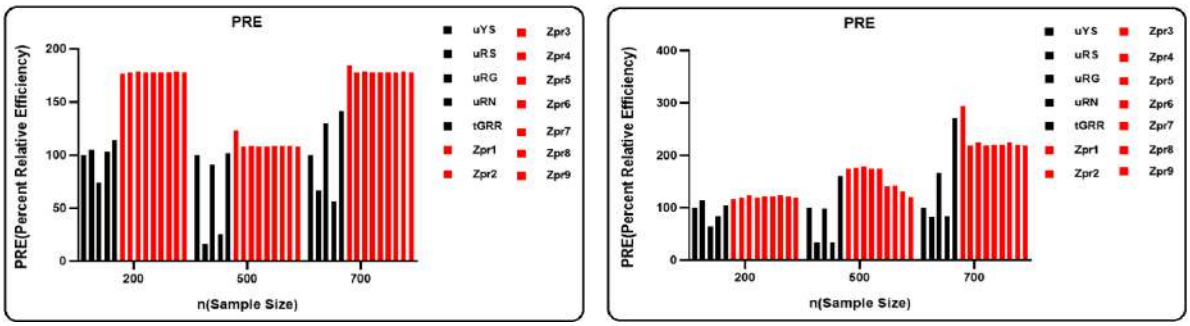

Figure 5. PRE of simulated data summary III

5 Generalized exponential-type estimator using two auxiliary variables for generalized quantitative randomize response

Motivated by [13], we suggest a generalized exponential-type estimator for population mean using Model II, as

$$\hat{t}_{GRE} = \bar{z}\exp\left[\alpha\left(\frac{\bar{X}^{1/h} - \bar{x}^{1/h}}{\bar{X}^{1/h} + (a-1)\bar{x}^{1/h}} + \frac{\bar{U}^{1/h} - \bar{u}^{1/h}}{\bar{U}^{1/h} + (b-1)\bar{u}^{1/h}}\right)\right] \tag{23}$$

$$\begin{aligned}(\hat{t}_{GRE} - \bar{Z}) = \bar{Z}S\Bigg[&\delta_z - \frac{\alpha\delta_z\delta_x}{ah} - \frac{\alpha\delta_x^2}{ah} - \frac{\alpha\delta_z\delta_u}{bh} + \frac{\alpha\delta_x}{ah} + \frac{\alpha\delta_x^2}{ah^2} - \frac{\alpha\delta_x^2}{a^2h^2} - \frac{\alpha\delta_u}{bh} + \frac{\alpha\delta_u^2}{bh^2} - \frac{\alpha\delta_u^2}{b^2h^2} \\ &+ \frac{\alpha^2\delta_x^2}{2a^2h^2} + \frac{\alpha^2\delta_u^2}{2b^2h^2} + \frac{\alpha^2\delta_x\delta_u}{abh^2}\Bigg].\end{aligned} \tag{24}$$

By taking expectations on both sides

$$Bias(\hat{t}_{GRE}) = \lambda\bar{Z}\theta_1\left[\frac{\alpha C_x^2}{ah^2}\left(1 - \frac{1}{a}\right) + \frac{\alpha C_u^2}{bh^2}\left(1 - \frac{1}{b}\right) - \frac{\alpha}{h}\left(\frac{C_{zx}}{a} + \frac{C_{zx}}{b}\right) + \frac{\alpha^2}{2h^2}\left(\frac{C_u^2}{b^2} + \frac{C_x^2}{a^2} + \frac{2C_{xu}}{ab}\right)\right]. \tag{25}$$

By taking a square and applying expectation from equation (20), we obtained

$$MSE(\hat{t}_{GRE}) = \lambda\bar{Z}^2\theta_1\left[C_z^2 + \frac{\alpha C_x^2}{a^2b^2} + \frac{\alpha C_u^2}{b^2h^2} - \frac{2\alpha C_{zx}}{ah} - \frac{2\alpha C_{zx}}{bh} + \frac{2\alpha^2 C_{xu}}{abh^2}\right]. \tag{26}$$

To obtain the minimum MSE, we need to estimate the value of a and b. By equation (22), we obtain

$$\hat{a}_{(opt)} = \frac{\alpha}{h}\left[\frac{C_{xu}^2 - C_u^2C_x^2}{C_{xu}C_{zu} - C_u^2C_{zu}}\right] \text{ and } \hat{b}_{(opt)} = \frac{\alpha}{h}\left[\frac{C_{xu}^2 - C_u^2C_x^2}{C_{xu}C_{zx} - C_{zu}^2C_x^2}\right].$$

Using $\hat{a}_{(opt)}$ and $\hat{b}_{(opt)}$, we get a minimum MSE of $(\hat{t}_{GRE})$ as

$$MSE(\hat{t}_{GRE}) = \lambda \bar{Z}^2 \theta_1 \left[C_z^2 + \frac{C_x^2 C_{zu}^2 + C_u^2 C_{zu}^2 - 2C_{xu}^2 C_{zx}^2 C_{zu}^2}{C_{xu}^2 - C_u^2 C_x^2} \right]. \tag{27}$$

Efficiency comparison

We present the mathematical comparison of the proposed estimator using two auxiliary variables with the existing estimators under Model-II as

I By equation (5) and (27)

$$MSE_{\min}(\hat{t}_{GRE}) \leq MSE(\hat{t}_{GRR}).$$

II By equation (2) and (27)

$$MSE_{\min}(\hat{t}_{GRE}) \leq MSE(\hat{\mu}_{RS}).$$

III By equation (4) and (27)

$$MSE_{\min}(\hat{t}_{GRE}) \leq MSE(\hat{\mu}_{RN}).$$

IV By equation (3) and (27)

$$MSE_{\min}(\hat{t}_{GRE}) \leq MSE(\hat{\mu}_{RG}).$$

Simulation study for proposed generalized exponential type estimator using two auxiliary variables by model-II

To describe the (Y, X) distribution, we assume a multivariate normal population with distinct covariance matrices. We can generate the correlated scrambling variable S. With the chosen parameters, θ_1 and σ_1. The discrete uniform distribution is followed by scrambling variables. Where $S = U(a_1, b_1)$, in other words, S takes integer values between a_1 and b_1. The reported generalized response is calculated using the formula $Z = YS$.

Table 10. Data summary IV

Population 1	**Population 2**
N =1000	N =1000
μ= [2,2,2]	μ= [3,3,3]
$\sum = \begin{pmatrix} 8 & 1 & 2.5 \\ 1 & 2 & 1.5 \\ 2.5 & 1.5 & 2 \end{pmatrix}$	$\sum = \begin{pmatrix} 2 & 1 & 2.2 \\ 1 & 3 & 1.2 \\ 2.2 & 1.2 & 3 \end{pmatrix}$
ρ_{xy}=0.27451	ρ_{xy}=0.40759
ρ_{xy}= 0.721011	ρ_{xy}= 0.39536
$S_{\min}$ = 0, $S_{\max}$ = 3	$S_{\min}$ = 0, $S_{\max}$ = 5

Table 11. The MSE and PRE values of estimators for Population 1

				Population 1			Population 2		
n	*W*	*T*	Estimator	Theoretical	Empirical	PRE	Theoretical	Empirical	PRE
200	0.3	0.3	$\hat{\mu}_{YS}$	0.0153	0.11143	100.00	0.08297	1.81129	100.00
			$\hat{\mu}_{RS}$	1.2377	0.03221	81.24	0.02340	1.7110	52.45
			$\hat{\mu}_{RG}$	0.0426	0.02870	36.02	0.02630	0.0514	314.65
			$\hat{\mu}_{RN}$	1.2419	0.03008	91.23	0.02940	0.0493	44.45
			$\hat{t}_{GRR}$	0.0410	0.05720	37.40	0.02630	0.9229	314.86
			$\hat{t}_{GRE}$	0.0054	0.00716	283.43	0.01130	0.0171	733.54
	0.5	0.5	$\hat{\mu}_{YS}$	0.0182	0.11143	100.00	0.08376	1.81129	100.00
			$\hat{\mu}_{RS}$	1.2377	0.03221	41.47	0.0750	1.7110	111.68
			$\hat{\mu}_{RG}$	0.0427	0.02870	42.83	0.02630	0.0514	317.46
			$\hat{\mu}_{RN}$	1.2407	0.03008	51.47	0.0900	0.0493	93.066
			$\hat{t}_{GRR}$	0.0411	0.05720	44.51	0.02630	0.9229	317.82
			$\hat{t}_{GRE}$	0.0054	0.00716	337.41	0.01131	0.0171	740.51
	0.7	0.7	$\hat{\mu}_{YS}$	0.0153	0.11143	100.00	0.08290	1.81129	100.00
			$\hat{\mu}_{RS}$	1.2377	0.03221	31.237	0.0750	1.7110	110.53
			$\hat{\mu}_{RG}$	0.0427	0.02870	35.93	0.02640	0.0514	314.28
			$\hat{\mu}_{RN}$	1.2390	0.03008	102.0	0.02340	0.0493	354.27

			$\hat{t}_{GRR}$	0.0410	0.05720	37.40	0.02630	0.9229	314.86
			$\hat{t}_{GRE}$	0.0054	0.00716	283.43	0.01131	0.0171	733.54
500	0.3	0.3	$\hat{\mu}_{YS}$	0.0154	0.03042	100.00	0.08290	1.7778	100.00
			$\hat{\mu}_{RS}$	1.3189	0.01270	51.12	0.06600	1.6565	125.60
			$\hat{\mu}_{RG}$	0.0107	0.01281	144.09	0.0659	0.1408	125.79
			$\hat{\mu}_{RN}$	1.3231	0.01267	81.160	0.02140	0.1476	387.45
			$\hat{t}_{GRR}$	0.0103	0.05715	149.58	0.00658	0.9229	1259.46
			$\hat{t}_{GRE}$	0.0014	0.00384	1133.57	0.00280	0.0212	2934.16
	0.5	0.5	$\hat{\mu}_{YS}$	0.0182	0.03042	100.00	0.08370	1.7778	100.00
			$\hat{\mu}_{RS}$	1.3189	0.01270	138.5	0.06700	1.6565	124.60
			$\hat{\mu}_{RG}$	0.0107	0.01281	171.30	0.0659	0.1408	125.79
			$\hat{\mu}_{RN}$	1.3219	0.01267	138.2	0.02240	0.1476	388.45
			$\hat{t}_{GRR}$	0.0103	0.05715	178.02	0.00650	0.9229	1271.28
			$\hat{t}_{GRE}$	0.0014	0.00384	1349.48	0.00280	0.0212	2962.06
	0.7	0.7	$\hat{\mu}_{YS}$	0.0153	0.03042	100.00	0.08290	1.7778	100.00
			$\hat{\mu}_{RS}$	1.3189	0.01270	116.42	0.02640	1.6565	144.51
			$\hat{\mu}_{RG}$	0.0106	0.01281	143.70	0.0660	0.1408	125.13
			$\hat{\mu}_{RN}$	1.3207	0.01267	116.2	0.02840	0.1476	145.45
			$\hat{t}_{GRR}$	0.0103	0.05715	149.58	0.00658	0.9229	1259.46
			$\hat{t}_{GRE}$	0.0014	0.00384	1133.57	0.00282	0.0212	2934.1
700	0.3	0.3	$\hat{\mu}_{YS}$	0.0153	0.01373	100.00	0.01202	1.76471	100.00
			$\hat{\mu}_{RS}$	1.3352	0.00966	115 .00	0.02640	1.6297	414.51
			$\hat{\mu}_{RG}$	0.0042	0.00961	360.23	0.00260	0.91076	456.00
			$\hat{\mu}_{RN}$	1.3394	0.01030	114.60	0.02840	0.92118	441.45
			$\hat{t}_{GRR}$	0.0041	0.05715	373.94	0.00260	0.92313	456.30
			$\hat{t}_{GRE}$	0.0005	0.00241	2833.85	0.00113	0.2073	1063.05
	0.5	0.5	$\hat{\mu}_{YS}$	0.0182	0.01373	100.00	0.01280	1.76471	100.00
			$\hat{\mu}_{RS}$	1.3352	0.00966	136.9	0.02740	1.6297	44.51
			$\hat{\mu}_{RG}$	0.0043	0.00961	428.26	0.00263	0.91076	485.63
			$\hat{\mu}_{RN}$	1.3382	0.01030	136.0	0.00294	0.92118	435.37
			$\hat{t}_{GRR}$	0.0041	0.05715	445.04	0.00263	0.92313	486.18
			$\hat{t}_{GRE}$	0.0005	0.00241	3373.6	0.00113	0.2073	1132.79
	0.7	0.7	$\hat{\mu}_{YS}$	0.0153	0.01373	100.00	0.01202	1.76471	100.00
			$\hat{\mu}_{RS}$	0.0567	0.00966	269.84	0.00274	1.6297	438.68
			$\hat{\mu}_{RG}$	1.3350	0.00961	21.15	0.00264	0.91076	455.46
			$\hat{\mu}_{RN}$	0.0043	0.01030	359.24	0.02940	0.92118	457.03
			$\hat{t}_{GRR}$	1.3370	0.05715	71.14	0.00263	0.92313	456.30
			$\hat{t}_{GRE}$	0.0005	0.00241	2833.85	0.00113	0.2073	1063.05

The results are represented in Tables 9, and 11. Tables 9 and 11 are used for artificial data. It observed that the percentage relative efficiency of the proposed estimators ($\hat{\bar{Z}}_{pr}^{(k)*}$, $\hat{t}_{GRE}$) according to model II is better as compared to the existing estimator ($\hat{\mu}_{YS}$, $\hat{\mu}_{RS}$, $\hat{\mu}_{RG}$, $\hat{\mu}_{RN}$, $\hat{t}_{GRR}$). It also shows higher PRE as compared to other ratio estimators. Graphical representation also shows that our proposed estimator's percentage relative efficiency is greater than existing estimators. By using table 11 (population 1) we make a graph to represent the PRE of estimators. Red boxes show the proposed estimator, and Black boxes show existing estimators. n shows sample size. Percentage Relative Efficiency of Proposed and Existing estimator through simulation is given in that graph which shows that our proposed estimator PRE values are efficient compared to another estimator. By using table 11 (population 2) we represent the PRE of estimators. Red boxes show the proposed estimator, and Black boxes show existing estimators. N shows sample size. Percentage Relative Efficiency of Proposed and Existing estimator through simulation is given in that graph which shows that our proposed estimator PRE values are efficient compared to another estimator.

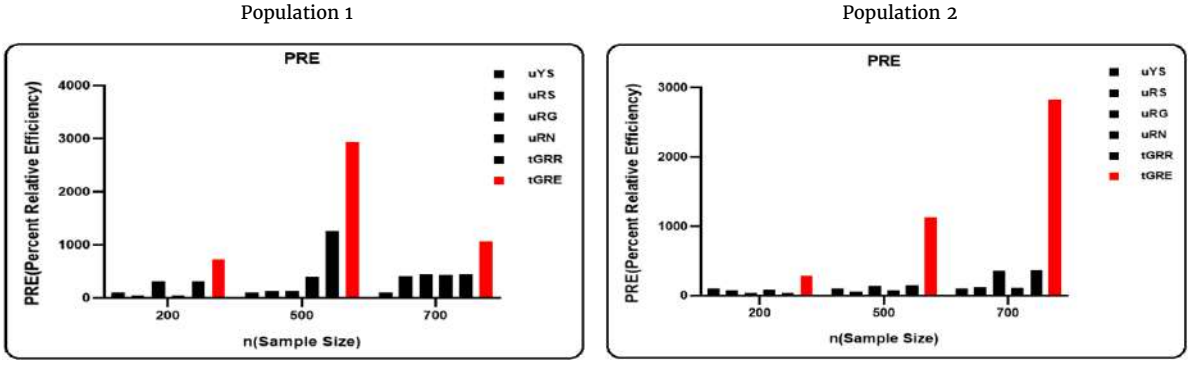

Figure 6. PRE of simulated data summary IV

6 Conclusion

For many scholars, figuring out the population means in a sample survey is important. However, more research on mean square error estimates using auxiliary data is required. In this study, the population mean is calculated using single or dual auxiliary variables and simple random sampling. For better results in the first estimator, we rank our auxiliary variable that is connected with the research variables. In comparison to an existing estimator, they provide efficient or better outcomes. They are also more efficient relative to the current estimator in terms of %.In the second proposed estimator; we use dual auxiliary variables to improve results. We compare a dual auxiliary variable with one auxiliary variable. Dual auxiliary variables show better results as compared to one auxiliary variable. The superiority of proposed MSE estimators over the usual MSE the expressions for least mean square errors using first-order approximation and the various unknown constant values. Using auxiliary data allows us to come up with more accurate population estimations. Using a single auxiliary variable, the performance of suggested estimators is compared to MSE estimators. The efficiency comparison makes estimators crucial. Other estimators that don't use auxiliary features are less effective than MSE estimators. The relative efficiency of the new estimators, which outperform the old estimators, is also calculated.

Declarations

Consent for publication

Not applicable.

Conflicts of interest

The authors declare that they have no conflict of interests.

Funding

No funding was used in this study.

Data Availability

The data used to support the findings of this study are included in the article.

Author's contributions

A.Z.: Conceptualization, Methodology, Software. S.M. (Saadia Masood): Data Curation, Writing-Original draft preparation. S.M. (Sumaira Mubarik): Visualization, Investigation. A.D.: Supervision, Software, Validation, Writing-Reviewing and Editing. All authors discussed the results and contributed to the final manuscript.

Acknowledgements

Not applicable.

References

[1] Gupta, S., Gupta, B., & Singh, S. Estimation of sensitivity level of personal interview survey questions. *Journal of Statistical Planning and Inference*, 100(2), 239-247, (2002). [CrossRef]
[2] Haq, A., & Shabbir, J. Improved family of ratio estimators in simple and stratified random sampling. *Communications in Statistics-Theory and Methods*, 42(5), 782-799, (2013). [CrossRef]
[3] Warner, S.L. Randomized response: A survey technique for eliminating evasive answer bias. *Journal of the American Statistical Association*, 60(309), 63-69, (1965). [CrossRef]
[4] Laplace, P.S. A philosophical essay on probabilities, 1819. *English translation, Dover*, (1951).
[5] Sousa, R., Shabbir, J., Corte Real, P., & Gupta, S. Ratio estimation of the mean of a sensitive variable in the presence of auxiliary information. *Journal of Statistical Theory and Practice*, 4(3), 495-507, (2010). [CrossRef]
[6] Gupta, S., Kalucha, G., Shabbir, J., & Dass, B.K. Estimation of finite population mean using optional RRT models in the presence of nonsensitive auxiliary information. *American Journal of Mathematical and Management Sciences*, 33(2), 147-159, (2014). [CrossRef]
[7] Noor-Ul-Amin, M., Mushtaq, N., & Hanif, M. Estimation of mean using generalized optional scrambled responses in the presence of non-sensitive auxiliary variable. *Journal of Statistics and Management Systems*, 21(2), 287-304, (2018). [CrossRef]
[8] Waseem, Z., Khan, H., & Shabbir, J. Generalized exponential type estimator for the mean of sensitive variable in the presence of non-sensitive auxiliary variable. *Communications in Statistics-Theory and Methods*, 50(14), 3477-3488, (2021). [CrossRef]
[9] Gupta, S., Shabbir, J., & Sehra, S. Mean and sensitivity estimation in optional randomized response models. *Journal of Statistical Planning and Inference*, 140(10), 2870-2874, (2010). [CrossRef]
[10] Grover, L.K., & Kaur, P. An improved estimator of the finite population mean in simple random sampling. *Model Assisted Statistics and Applications*, 6(1), 47-55, (2011). [CrossRef]

[11] Grover, L.K., & Kaur, P. A generalized class of ratio type exponential estimators of population mean under linear transformation of auxiliary variable. *Communications in Statistics-Simulation and Computation*, 43(7), 1552-1574, (2014). [CrossRef]
[12] Platt, W.J., Evans, G.W., & Rathbun, S.L. The population dynamics of a long-lived conifer (Pinus palustris). *The American Naturalist*, 131(4), 491-525, (1988). [CrossRef]
[13] Waseem, Z., Khan, H., Shabbir, J., & Fatima, S.E. A generalized class of exponential type estimators for estimating the mean of the sensitive variable when using optional randomized response model. *Communications in Statistics-Simulation and Computation*, 1-13, (2020). [CrossRef]
[14] Eichhorn, B.H., & Hayre, L.S. Scrambled randomized response methods for obtaining sensitive quantitative data. *Journal of Statistical Planning and inference*, 7(4), 307-316, (1983). [CrossRef]

Mathematical Modelling and Numerical Simulation with Applications (MMNSA) (https://www.mmnsa.org)

Mathematical Modelling and Numerical Simulation with Applications, 2022, 2(3), 147–163

https://www.mmnsa.org
ISSN Online: 2791-8564 / Open Access
https://doi.org/10.53391/mmnsa.2022.012

RESEARCH PAPER

The investigation of several soliton solutions to the complex Ginzburg–Landau model with Kerr law nonlinearity

Muhammad Abubakar Isah [1,*,†] and Asıf Yokus [1,†]

[1]Firat University, Faculty of Science, Department of Mathematics, 23200 Elazig, Türkiye

*Corresponding Author
† myphysics_09@hotmail.com (Muhammad Abubakar Isah); asfyokus@yahoo.com (Asıf Yokus)

Abstract

This work investigates the complex Ginzburg–Landau equation (CGLE) with Kerr law in nonlinear optics, which represents soliton propagation in the presence of a detuning factor. The φ^6-model expansion approach is used to find optical solitons such as dark, bright, singular, and periodic as well as the combined soliton solutions to the model. The results presented in this study are intended to improve the CGLE's nonlinear dynamical characteristics, it might also assist in comprehending some of the physical implications of various nonlinear physics models. The hyperbolic sine, for example, appears in the calculation of the Roche limit and gravitational potential of a cylinder, while the hyperbolic cotangent appears in the Langevin function for magnetic polarization. The current research is frequently used to report a variety of fascinating physical phenomena, such as the Kerr law of non-linearity, which results from the fact that an external electric field causes non-harmonic motion of electrons bound in molecules, which causes nonlinear responses in a light wave in an optical fiber. The obtained solutions' 2–dimensional, 3-dimensional, and contour plots are shown.

Key words: φ^6-model expansion method; complex Ginzburg-Landau equation; traveling wave solution; Kerr law nonlinearity
AMS 2020 Classification: 35Qxx; 35C07; 35Q51

1 Introduction

Partial differential equations were first employed for the study of surfaces in geometry [1, 2, 3, 4, 5] and a vast range of mechanical issues. Renowned mathematicians from throughout the world were keenly interested in studying a wide range of issues brought on by partial differential equations in the late 19th century [6]. Since optical solitons which are the solutions of the NPDEs can be used as information carriers for transmitting digital signals over long distances in optical fiber networks, the propagation of optical solitons in nonlinear optical fibers has received a lot of attention [7, 8, 9, 10, 11]. Maintaining a moderate balance between nonlinearity and group velocity dispersion is the fundamental concept for the presence of the optical solitons. The study of exact solutions of the nonlinear partial differential equations NLPDEs, as scientific methods of the concepts, will help one to clarify these phenomena. Many successful methods for obtaining exact solutions of NLPDEs, such as the Adomian's decomposition method [12], exponential rational function method [13], the F-expansion method [14], the $\left(\frac{1}{G'}\right)$-expansion method [15, 16], Jacobi elliptic function technique [17, 18], the modified sub-equation method [19], the $\left(\frac{G'}{G}\right)$-expansion method [20], the auto-Bäcklund transformation method [21], extended direct algebraic method [22], the homoclinic technique [23], reduction perturbation method [24],

➤ **Received:** 06.07.2022 ➤ **Revised:** 07.09.2022 ➤ **Accepted:** 14.09.2022 ➤ **Published:** 16.09.2022

the φ^6-model expansion method [25, 26, 27, 28], the nonstandard finite difference [29]. The recent developments in the field of mathematical modelling as well as its applications have been introduced in the last few decades [30, 31, 32].

Many researchers have recently solved the CGLE. Chu et al. [33] have solved this equation with the help of modified extended tanh technique and received different forms of solitons, such as, hyperbolic and trigonometric functions. The modified simple equation method is used to obtain some bright, dark and singular soliton solutions by Arnous and Ahmed [34]. Liu and Yu [35] used the modified Hirota bilinear method and obtained Kink waves and period waves. In [36, 37], first integral method and $\left(\frac{G'}{G}\right)$-expansion method is used to secure the hyperbolic, trigonometric as well as rational function solution. Several integration techniques are used to obtain multiple soliton solutions such as bright, dark and singular soliton by Mirzazadeh and Ekici [38]. The other methods include GRE method [39], ansatz functions technique [40], and so on.

The main idea about this paper is to derive new solitons such as dark, bright, singular, rational, combined periodic, combined singular and periodic solitary wave solutions to the CGLE model using Kerr law nonlinearity with the help of the newly developed φ^6-model expansion method [41] which has not been studied yet based on our knowledge. The nonlinear responses that an external electric field-induced nonharmonic motion of electrons trapped in molecules causes to a light wave in an optical fiber give rise to the Kerr law of nonlinearity. The authors achieve their aims by retrieving new solutions which are different from the previous work.

The following is the outline for this paper: In Section 2, the mathematical analysis of the model is studied. The new φ^6-model expansion approach is described in Section 3. Section 4 consists of application of the proposed method on the complex Ginzburg-Landau equation using Kerr law nonlinearity to retrieve solitons such as dark, bright, singular, periodic, combined singular and combined periodic soliton solutions. Some of the traveling wave solution's physical structures are graphically displayed in the related 3D, 2D, and contour graphs. In Section 5, the result of the derived solutions is discussed, while the whole work is concluded in Section 6.

2 Mathematical analysis of the model

Arnous, Ahmed H., et al. [34] gives the dimensionless shape of (GCLE) that will be investigated in this article.

$$iq_t + aq_{xx} + cF(|q|^2)q = \frac{1}{|q|^2 q^*}\left[\alpha |q|^2 (|q|^2)_{xx} - \beta \left\{(|q|^2)_x\right\}^2\right] + \gamma q, \tag{1}$$

where $q = q(x,t)$ is a complex function that describes the wave profile seen in a variety of phenomena such as nonlinear optics and plasma physics, x is the non-dimensional distance along the fibers, t is time in dimensionless form, q^* is a conjugate of q, a, c, α, β and γ are valued constants. The coefficients a and c are determined by the group velocity dispersion (GVD) and nonlinearity, respectively. The terms with α, β and γ result from perturbation effects, specifically detuning.

In Eq. (1), F is a real-valued algebraic function that must be smooth. $F(|q|^2)q$ is continuously differentiable k times, implying that

$$F(|q|^2)q \in \cup_{m,n=1}^{\infty} C^k\left((-n,n)\times(-m,m);R^2\right). \tag{2}$$

By setting up

$$\alpha = 2\beta, \tag{3}$$

Eq. (1) turns to

$$iq_t + aq_{xx} + cF(|q|^2)q = \frac{\beta}{|q|^2 q^*}\left[2|q|^2 (|q|^2)_{xx} - \left\{(|q|^2)_x\right\}^2\right] + \gamma q. \tag{4}$$

To solve Eq. (1), the standard decomposition into phase-amplitude components yields:

$$q(x,t) = P(\zeta)e^{i(-kx+wt+\theta)}, \tag{5}$$

and the wave variable ζ is given by

$$\zeta = \lambda(x - vt). \tag{6}$$

The function P represents the pulse shape here, v is the soliton's velocity. In the phase factor, k denotes the frequency of the soliton, ω the soliton wave number and the phase constant θ. Substituting the phase-amplitude decomposition into Eq. (4) results in the following couple of equations after breaking into real and imaginary parts [33, 34]:

$$-\left(ak^2 + \gamma + \omega\right)P + cF\left(P^2\right)P + (a - 4\beta)P'' = 0, \tag{7}$$

and

$$v = -2ka. \tag{8}$$

In the following part after the description of the method, Eq. (7) will be examined using Kerr's nonlinearity law.

3 Description of the method

According to Zayed et al. [28] the following are the key steps of a recent φ^6-model expansion method:

Step-1: Consider the following nonlinear evolution equation for $q = q(x,t)$

$$F(q, q_x, q_t, q_{xx}, q_{xt}, q_{tt}, \ldots) = 0, \tag{9}$$

there F is a polynomial of $q(x,t)$ and its highest order partial derivatives, including its nonlinear terms.

Step-2: Making use of the wave transformation

$$q(x,t) = q(\zeta), \quad \zeta = \lambda(x - vt), \tag{10}$$

where v represents wave speed, then, Eq. (9) can be converted into the nonlinear ordinary differential equation shown below

$$\Omega(q, q', qq', q'', \ldots) = 0, \tag{11}$$

where the derivatives with respect to ζ are represented by prime.

Step-3: Suppose that the formal solution to Eq. (11) exists:

$$q(\zeta) = \sum_{i=0}^{2N} \alpha_i U^i(\zeta), \tag{12}$$

where $\alpha_i (i = 0, 1, 2, \ldots, N)$ are to be determined constants, N can be obtained using the balancing rule and $U(\zeta)$ satisfies the auxiliary NLODE;

$$\begin{aligned} U'^2(\zeta) &= h_0 + h_2 U^2(\zeta) + h_4 U^4(\zeta) + h_6 U^6(\zeta), \\ U''(\zeta) &= h_2 U(\zeta) + 2h_4 U^3(\zeta) + 3h_6 U^5(\zeta), \end{aligned} \tag{13}$$

where $h_i (i = 0, 2, 4, 6)$ are real constants that will be discovered later.

Step-4: It is well known that the answer to Eq. (13) is as follows;

$$U(\zeta) = \frac{P(\zeta)}{\sqrt{fP^2(\zeta) + g}}, \tag{14}$$

provided that $0 < fP^2(\zeta) + g$ and $P(\zeta)$ is the Jacobi elliptic equation solution

$$P'^2(\zeta) = l_0 + l_2 P^2(\zeta) + l_4 P^4(\zeta), \tag{15}$$

where $l_i (i = 0, 2, 4)$ are unknown constants to be determined, f and g are given by

$$\begin{aligned} f &= \frac{h_4(l_2 - h_2)}{(l_2 - h_2)^2 + 3l_0 l_4 - 2l_2(l_2 - h_2)}, \\ g &= \frac{3l_0 h_4}{(l_2 - h_2)^2 + 3l_0 l_4 - 2l_2(l_2 - h_2)}, \end{aligned} \tag{16}$$

under the restriction condition

$$h_4^2(l_2 - h_2)[9l_0 l_4 - (l_2 - h_2)(2l_2 + h_2)] + 3h_6[-l_2^2 + h_2^2 + 3l_0 l_4]^2 = 0. \tag{17}$$

Step-5: According to [28], it is well known that the Jacobi elliptic solutions of Eq. (15) can be calculated when $0 < m < 1$. We can have the exact solutions of Eq. (9) by substituting Eqs. (14) and (15) into Eq. (12).

Function	$m \to 1$	$m \to 0$	Function	$m \to 1$	$m \to 0$
$sn(\zeta, m)$	$tanh(\zeta)$	$sin(\zeta)$	$ds(\zeta, m)$	$csch(\zeta)$	$csc(\zeta)$
$cn(\zeta, m)$	$sech(\zeta)$	$cos(\zeta)$	$sc(\zeta, m)$	$sinh(\zeta)$	$tan(\zeta)$
$dn(\zeta, m)$	$sech(\zeta)$	1	$sd(\zeta, m)$	$sinh(\zeta)$	$sin(\zeta)$
$ns(\zeta, m)$	$coth(\zeta)$	$csc(\zeta)$	$nc(\zeta, m)$	$cosh(\zeta)$	$sec(\zeta)$
$cs(\zeta, m)$	$csch(\zeta)$	$cot(\zeta)$	$cd(\zeta, m)$	1	$cos(\zeta)$

4 Application of the φ^6-model expansion method

The Kerr law of nonlinearity is derived from the fact that a light wave in an optical fiber experiences nonlinear reactions due to non-harmonic electron motion in the presence of an external electric field. Since $F(u) = u$ for Kerr law nonlinearity, Eq. (4) is reduced to [33]

$$iq_t + aq_{xx} + c(|q|^2)q = \frac{\beta}{|q|^2 q^*}\left[2|q|^2(|q|^2)_{xx} - \left\{(|q|^2)_x\right\}^2\right] + \gamma q, \tag{18}$$

and Eq. (7) is transformed

$$-\left(ak^2 + \gamma + \omega\right)P + cP^3 + \lambda^2(a - 4\beta)P'' = 0, \tag{19}$$

from Eq. (19), we get $N = 1$ by balancing P'' with P^3, we can obtain the following by substituting $N = 1$ in Eq. (12)

$$P(\zeta) = \alpha_0 + \alpha_1 U(\zeta) + \alpha_2 U^2(\zeta), \tag{20}$$

where α_0, α_1 and α_2 are constants to be determined.
We obtain the following algebraic equations by substituting Eq. (20) along with Eq. (13) into Eq. (19) and setting the coefficients of all powers of $U^i(\zeta)$, $i = 0, 1, \ldots, 6$ to be equal to zero;

$$\begin{aligned}
&U^0(\zeta);\ -\alpha_0\left(ak^2 + \gamma + \omega - c\alpha_0^2\right) + 2a\lambda^2 h_0\alpha_2 - 8\beta\lambda^2 h_0\alpha_2 = 0,\\
&U^1(\zeta);\ -\alpha_1\left(ak^2 + \gamma + \omega\right) + a\lambda^2 h_2\alpha_1 - 4\beta\lambda^2 h_2\alpha_1 + 3c\alpha_0^2\alpha_1 = 0,\\
&U^2(\zeta):\ 3c\alpha_0\alpha_1^2 - \alpha_2\left(ak^2 + \gamma + \omega\right) + 4a\lambda^2 h_2\alpha_2 - 16\beta\lambda^2 h_2\alpha_2 + 3c\alpha_0^2\alpha_2 = 0,\\
&U^3(\zeta):\ 2a\lambda^2 h_4\alpha_1 - 8\beta\lambda^2 h_4\alpha_1 + c\alpha_1^3 + 6c\alpha_0\alpha_1\alpha_2 = 0,\\
&U^4(\zeta):\ 6a\lambda^2 h_4\alpha_2 - 24\beta\lambda^2 h_4\alpha_2 + 3c\alpha_1^2\alpha_2 + 3c\alpha_0\alpha_2^2 = 0,\\
&U^5(\zeta):\ 3a\lambda^2 h_6\alpha_1 - 12\beta\lambda^2 h_6\alpha_1 + 3c\alpha_1\alpha_2^2 = 0,\\
&U^6(\zeta):\ 8a\lambda^2 h_6\alpha_2 - 32\beta\lambda^2 h_6\alpha_2 + c\alpha_2^3 = 0,
\end{aligned}$$

we get the following result after solving the resulting system:

$$\begin{aligned}
&\alpha_0 = 0,\quad \alpha_1 = \frac{\sqrt{2h_4}\sqrt{-a + 4\beta}\lambda}{\sqrt{c}},\quad \alpha_2 = 0,\\
&h_2 = \frac{ak^2 + \gamma + \omega}{(a - 4\beta)\lambda^2},\quad h_6 = 0.
\end{aligned} \tag{21}$$

In view of Eqs. (14), (20) and (21) along with the Jacobi elliptic functions in the table above, we obtain the following exact solutions of Eq. (18).
1. If $l_0 = 1$, $l_2 = -(1 + m^2)$, $l_4 = m^2$, $0 < m < 1$, then $P(\zeta) = sn(\zeta, m)$ or $P(\zeta) = cd(\zeta, m)$, and we have

$$q_{1,1}(x,t) = \frac{\sqrt{2h_4}\sqrt{-a + 4\beta}\lambda}{\sqrt{c}}\left[\frac{sn(\zeta, m)}{\sqrt{f\,(sn(\zeta, m))^2 + g}}\right]e^{i(-kx + wt + \theta)}, \tag{22}$$

or

$$q_{1,2}(x,t) = \frac{\sqrt{2h_4}\sqrt{-a + 4\beta}\lambda}{\sqrt{c}}\left[\frac{cd(\zeta, m)}{\sqrt{f\,(cd(\zeta, m))^2 + g}}\right]e^{i(-kx + wt + \theta)}, \tag{23}$$

such that $0 < c$, $\zeta = \lambda(x - vt)$ and f and g in Eqs. (16) are given by

$$\begin{aligned}
f &= \frac{(1 + m^2 + h_2)h_4}{1 - m^2 + m^4 - h_2^2},\\
g &= \frac{-3h_4}{1 - m^2 + m^4 - h_2^2},
\end{aligned} \tag{24}$$

under the restriction condition

$$-h_4^2\left(-1 - m^2 - h_2\right)\left(-1 + 2m^2 - h_2\right)\left(-2 + m^2 + h_2\right) = 0. \tag{25}$$

If $m \to 1$, then the dark optical soliton is obtained

$$q_{1,3}(x,t) = \frac{\sqrt{2h_4}\sqrt{-a+4\beta}\lambda \tanh(\zeta)}{\sqrt{c}\sqrt{\frac{(a-4\beta)\lambda^2 h_4\left(-3(a-4\beta)\lambda^2+(ak^2+\gamma+\omega+2(a-4\beta)\lambda^2)\tanh^2(\zeta)\right)}{-(ak^2+\gamma+\omega)^2+(a-4\beta)^2\lambda 4}}} e^{i(-kx+wt+\theta)}, \tag{26}$$

such that

$$-h_4^2(2+h_2)\left[-1+h_2\right]^2 = 0. \tag{27}$$

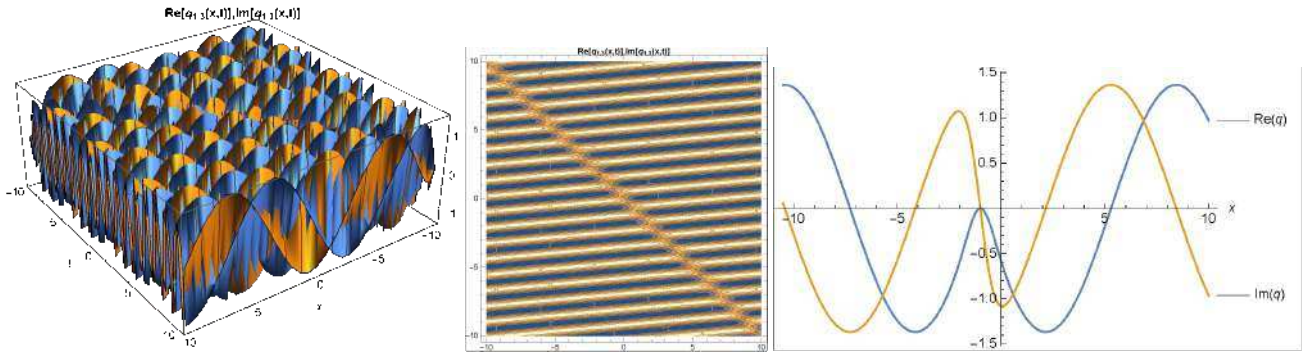

Figure 1. The numerical simulations corresponding to $|q_{1,3}|$ given by Eq. (26), for $m = 1$; (a) is the 3D graphic while (b) is the contour and (c) is the 2D graphic

If $m \to 0$, then the periodic solution is obtained

$$q_{1,4}(x,t) = \frac{\sqrt{2h_4}\sqrt{-a+4\beta}\lambda \sin(\zeta)}{\sqrt{c}\sqrt{\frac{(a-4\beta)\lambda^2 h_4\left(-3(a-4\beta)\lambda^2+(ak^2+\gamma+\omega+(a-4\beta)\lambda^2)\sin^2(\zeta)\right)}{-(ak^2+\gamma+\omega)^2+(a-4\beta)^2\lambda 4}}} e^{i(-kx+wt+\theta)}, \tag{28}$$

such that

$$h_4^2(-1-h_2)\left[(-2+h_2)(1+h_2)\right] = 0. \tag{29}$$

2. If $l_0 = 1-m^2$, $l_2 = 2m^2-1$, $l_4 = -m^2$, $0 < m < 1$, then $P(\zeta) = cn(\zeta, m)$, therefore

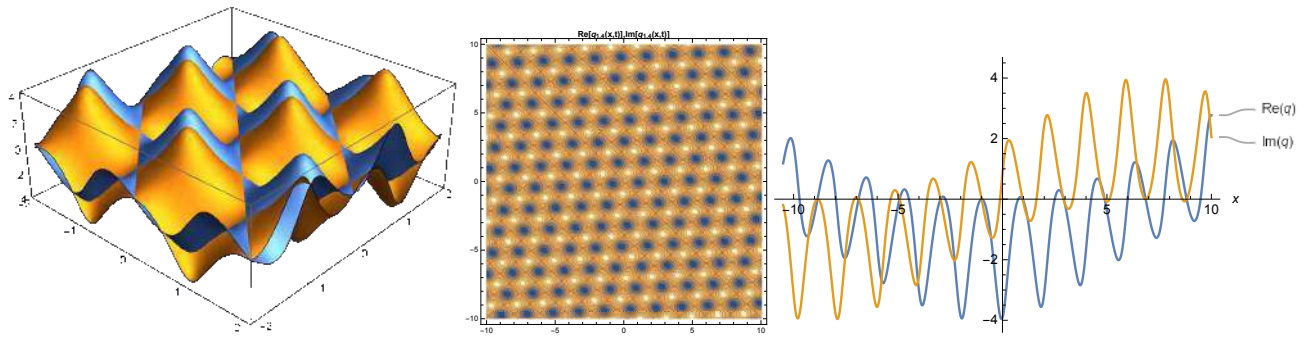

Figure 2. The numerical simulations corresponding to $|q_{1,4}|$ given by Eq. (28), for $m = 0$; (a), (b) and (c) are the 3D graphic, contour and 2D graphic, respectively

$$q_2(x,t) = \frac{\sqrt{2h_4}\sqrt{-a+4\beta}\lambda}{\sqrt{c}}\left[\frac{cn(\zeta,m)}{\sqrt{f\,(cn(\zeta,m))^2+g}}\right] e^{i(-kx+wt+\theta)}, \tag{30}$$

where f and g are determined by

$$f = -\frac{(-1+2m^2-h_2)h_4}{1-m^2+m^4-h_2^2}, \tag{31}$$
$$g = \frac{3\left(-1+m^2\right)h_4}{1-m^2+m^4-h_2^2},$$

under the constraint condition

$$h_4^2\left(-1+2m^2-h_2\right)\left[\left(-2+m^2+h_2\right)\left(1+m^2+h_2\right)\right] = 0. \tag{32}$$

If $m \to 1$, then the bright optical soliton solution is retrieved

$$q_{2,1}(x,t) = \frac{\sqrt{2h_4}\sqrt{-a+4\beta}\lambda sech(\zeta)}{\sqrt{c}\sqrt{\frac{(a-4\beta)\lambda^2 h_4 sech^2(\zeta)}{ak^2+\gamma+\omega+(a-4\beta)\lambda^2}}}e^{i(-kx+wt+\theta)}, \tag{33}$$

provided that

$$h_4^2(1-h_2)\left[h_2^2+h_2-2\right] = 0. \tag{34}$$

If $m \to 0$, then the periodic solution is obtained

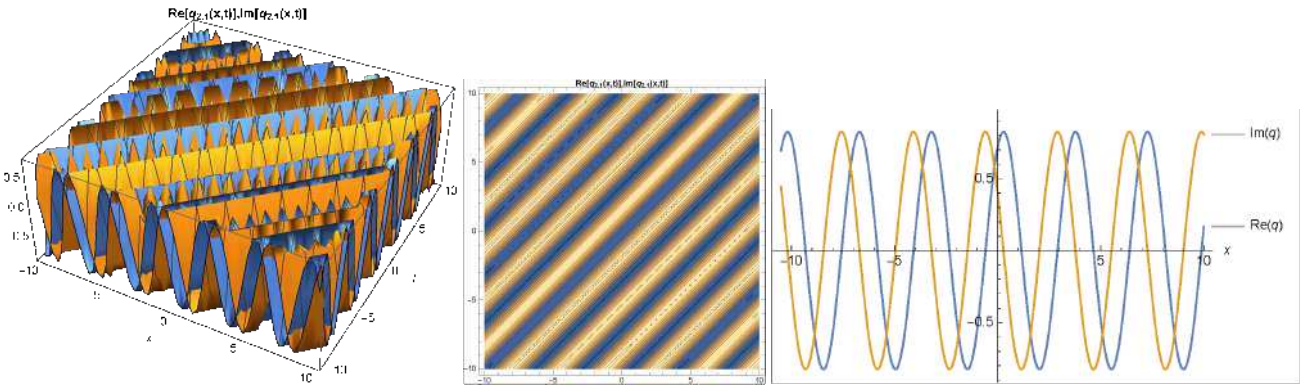

Figure 3. The numerical simulations corresponding to $|q_{2,1}|$ given by Eq. (33), for $m = 1$; (a), (b) and (c) are the 3D graphic, contour and 2D graphic, respectively

$$q_{2,2}(x,t) = \frac{\sqrt{2h_4}\sqrt{-a+4\beta}\lambda\sin(\zeta)}{\sqrt{c}\sqrt{\frac{(a-4\beta)\lambda^2 h_4\left(-3(a-4\beta)\lambda^2+\left(ak^2+\gamma+\omega+(a-4\beta)\lambda^2\right)\sin^2(\zeta)\right)}{-(ak^2+\gamma+\omega)^2+(a-4\beta)^2\lambda^4}}}e^{i(-kx+wt+\theta)}, \tag{35}$$

such that

$$h_4^2(-1-h_2)\left[(-2+h_2)(1+h_2)\right] = 0. \tag{36}$$

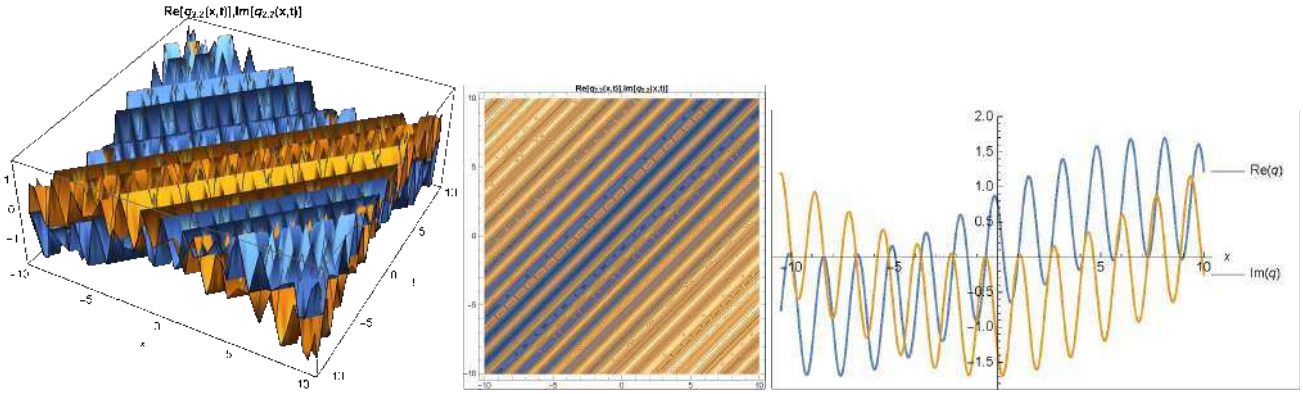

Figure 4. The numerical simulations corresponding to $|q_{2,2}|$ given by Eq. (35), for $m = 0$; (a), (b) and (c) are the 3D graphic, contour and 2D graphic, respectively

3. If $l_0 = m^2 - 1$, $l_2 = 2 - m^2$, $l_4 = -1$, $0 < m < 1$, then $P(\zeta) = dn(\zeta, m)$ which gives

$$q_3(x,t) = \frac{\sqrt{2h_4}\sqrt{-a+4\beta}\lambda}{\sqrt{c}}\left[\frac{dn(\zeta,m)}{\sqrt{f\,(dn(\zeta,m))^2+g}}\right]e^{i(-kx+wt+\theta)}, \tag{37}$$

where f and g are determined by

$$f = \frac{(-2+m^2+h_2)h_4}{1-m^2+m^4-h_2^2}, \qquad g = \frac{-3\left(-1+m^2\right)h_4}{1-m^2+m^4-h_2^2}, \tag{38}$$

under the restriction condition

$$h_4^2\left(2-m^2-h_2\right)\left[-\left(-1+2m^2+h_2\right)\left(1+m^2+h_2\right)\right] = 0. \tag{39}$$

If $m \to 1$, then the bright optical soliton solution is obtained

$$q_{3,1}(x,t) = \frac{\sqrt{2h_4}\sqrt{-a+4\beta}\lambda sech(\zeta)}{\sqrt{c}\sqrt{\frac{-(a-4\beta)\lambda^2h_4sech^2(\zeta)}{ak^2+\gamma+\omega+(a-4\beta)\lambda^2}}}e^{i(-kx+wt+\theta)}, \tag{40}$$

provided that

$$h_4^2(1-h_2)\left[-2+h_2+h_2^2\right] = 0. \tag{41}$$

If $m \to 0$, then the rational solution is obtained

$$q_{3,2}(x,t) = \frac{\sqrt{2h_4}\sqrt{-a+4\beta}\lambda}{\sqrt{c}\sqrt{\frac{-(a-4\beta)\lambda^2h_4}{4\beta\lambda^2+\gamma+\omega+a(k-\lambda)(k+\lambda)}}}e^{i(-kx+wt+\theta)}, \tag{42}$$

such that

$$h_4^2(2-h_2)\left[(1+h_2)^2\right] = 0. \tag{43}$$

4. If $l_0 = m^2$, $l_2 = -\left(1+m^2\right)$, $l_4 = 1$, $0 < m < 1$, $P(\zeta) = ns(\zeta, m)$ or $P(\zeta) = dc(\zeta, m)$ then

$$q_{4,1}(x,t) = \frac{\sqrt{2h_4}\sqrt{-a+4\beta}\lambda}{\sqrt{c}}\left[\frac{ns(\zeta,m)}{\sqrt{f\,(ns(\zeta,m))^2+g}}\right]e^{i(-kx+wt+\theta)}, \tag{44}$$

or

$$q_{4,2}(x,t) = \frac{\sqrt{2h_4}\sqrt{-a+4\beta}\lambda}{\sqrt{c}}\left[\frac{dc(\zeta,m)}{\sqrt{f\,(dc(\zeta,m))^2+g}}\right]e^{i(-kx+wt+\theta)}, \tag{45}$$

where f and g are given by

$$f = \frac{(1+m^2+h_2)h_4}{1-m^2+m^4-h_2^2},$$
$$g = \frac{-3m^2h_4}{1-m^2+m^4-h_2^2}, \tag{46}$$

under the constraint condition

$$h_4^2\left(-1-m^2-h_2\right)\left[-\left(-1+2m^2-h_2\right)\left(-2+m^2+h_2\right)\right] = 0. \tag{47}$$

If $m \to 1$, then the dark singular soliton solution is obtained

$$q_{4,3}(x,t) = \frac{\sqrt{2h_4}\sqrt{-a+4\beta}\lambda\coth(\zeta)}{\sqrt{c}\sqrt{\frac{(a-4\beta)\lambda^2\left(-3(a-4\beta)\lambda^2+\left(ak^2+\gamma+\omega+2(a-4\beta)\lambda^2\right)\coth^2(\zeta)\right)h_4}{-\left(ak^2+\gamma+\omega\right)^2+(a-4\beta)^2\lambda^4}}}e^{i(-kx+wt+\theta)}, \tag{48}$$

such that

$$h_4^2\left(-2-h_2\right)\left[\left(-1+h_2\right)^2\right] = 0. \tag{49}$$

If $m \to 0$, then the periodic solution is obtained

$$q_{4,4}(x,t) = \frac{\sqrt{2h_4}\sqrt{-a+4\beta}\lambda\csc(\zeta)}{\sqrt{c}\sqrt{\frac{-(a-4\beta)\lambda^2h_4\csc^2(\zeta)}{4\beta\lambda^2+\gamma+\omega+a(k-\lambda)(k+\lambda)}}}e^{i(-kx+wt+\theta)}, \tag{50}$$

such that

$$h_4^2\left(-1-h_2\right)\left[\left(-2+h_2\right)\left(1+h_2\right)\right] = 0. \tag{51}$$

5. If $l_0 = -m^2$, $l_2 = 2m^2-1$, $l_4 = 1-m^2$, $0 < m < 1$, then $P(\zeta) = nc(\zeta,m)$ and we have

$$q_5(x,t) = \frac{\sqrt{2h_4}\sqrt{-a+4\beta}\lambda}{\sqrt{c}}\left[\frac{nc(\zeta,m)}{\sqrt{f\,(nc(\zeta,m))^2+g}}\right]e^{i(-kx+wt+\theta)}, \tag{52}$$

where f and g are given by

$$f = \frac{-(-1+2m^2-h_2)h_4}{1-m^2+m^4-h_2^2},$$
$$g = \frac{3m^2h_4}{1-m^2+m^4-h_2^2}, \tag{53}$$

under the constraint condition

$$h_4^2\left(-1+2m^2-h_2\right)\left[\left(-2+m^2+h_2\right)\left(1+m^2+h_2\right)\right] = 0. \tag{54}$$

If $m \to 1$, then the singular soliton solution is obtained

$$q_{5,1}(x,t) = \frac{\sqrt{2h_4}\sqrt{-a+4\beta}\lambda\cosh(\zeta)}{\sqrt{c}\sqrt{\frac{-(a-4\beta)\lambda^2\left(-3(a-4\beta)\lambda^2-(4\beta\lambda^2+\gamma+\omega+a(k-\lambda)(k+\lambda))\cosh^2(\zeta)\right)h_4}{-(ak^2+\gamma+\omega)^2+(a-4\beta)^2\lambda 4}}}e^{i(-kx+wt+\theta)}, \tag{55}$$

such that

$$h_4^2(1-h_2)\left[-2+h_2+h_2^2\right] = 0. \tag{56}$$

If $m \to 0$, then the periodic solution is obtained

$$q_{5,2}(x,t) = \frac{\sqrt{2h_4}\sqrt{-a+4\beta}\lambda\sec(\zeta)}{\sqrt{c}\sqrt{\frac{-(a-4\beta)\lambda^2\sec^2(\zeta)h_4}{4\beta\lambda^2+\gamma+\omega+a(k-\lambda)(k+\lambda)}}}e^{i(-kx+wt+\theta)}, \tag{57}$$

such that

$$h_4^2(-1-h_2)\left[(-2+h_2)(1+h_2)\right] = 0. \tag{58}$$

6. If $l_0 = -1$, $l_2 = 2-m^2$, $l_4 = -\left(1-m^2\right)$, $0 < m < 1$, then $P(\zeta) = nd(\zeta, m)$ and we have

$$q_6(x,t) = \frac{\sqrt{2h_4}\sqrt{-a+4\beta}\lambda}{\sqrt{c}}\left[\frac{nd(\zeta,m)}{\sqrt{f\left(nd(\zeta,m)\right)^2+g}}\right]e^{i(-kx+wt+\theta)}, \tag{59}$$

where f and g are given by

$$f = \frac{(-2+m^2+h_2)h_4}{1-m^2+m4-h_2^2}, \tag{60}$$
$$g = \frac{3h_4}{1-m^2+m4-h_2^2},$$

under the constraint condition

$$h_4^2\left(2-m^2-h_2\right)\left[-\left(-1+2m^2-h_2\right)\left(1+m^2+h_2\right)\right] = 0. \tag{61}$$

7. If $l_0 = 1$, $l_2 = 2-m^2$, $l_4 = 1-m^2$, $0 < m < 1$ $P(\zeta) = sc(\zeta, m)$ then we have

$$q_7(x,t) = \frac{\sqrt{2h_4}\sqrt{-a+4\beta}\lambda}{\sqrt{c}}\left[\frac{sc(\zeta,m)}{\sqrt{f\left(sc(\zeta,m)\right)^2+g}}\right]e^{i(-kx+wt+\theta)}, \tag{62}$$

where f and g are given by

$$f = \frac{(-2+m^2+h_2)h_4}{1-m^2+m4-h_2^2}, \tag{63}$$
$$g = \frac{-3h_4}{1-m^2+m4-h_2^2},$$

under the constraint condition

$$h_4^2\left(2-m^2-h_2\right)\left[-\left(-1+2m^2-h_2\right)\left(1+m^2+h_2\right)\right] = 0. \tag{64}$$

If $m \to 1$, then the singular soliton solution is obtained

$$q_{7,1}(x,t) = \frac{\sqrt{2h_4}\sqrt{-a+4\beta}\lambda\sinh(\zeta)}{\sqrt{c}\sqrt{\frac{-(a-4\beta)\lambda^2\left(3(a-4\beta)\lambda^2-(4\beta\lambda^2+\gamma+\omega+a(k-\lambda)(k+\lambda))\sinh^2(\zeta)\right)h_4}{-(ak^2+\gamma+\omega)^2+(a-4\beta)^2\lambda 4}}}e^{i(-kx+wt+\theta)}, \tag{65}$$

such that

$$h_4^2\left(1-h_2\right)\left[-2+h_2+h_2^2\right]=0. \tag{66}$$

If $m \to 0$, then the periodic solution is obtained

$$q_{7,2}(x,t)=\frac{\sqrt{2h_4}\sqrt{-a+4\beta}\lambda\tan(\zeta)}{\sqrt{c}\sqrt{\frac{(a-4\beta)\lambda^2(-3(a-4\beta)\lambda^2+(ak^2+\gamma+\omega-2(a-4\beta)\lambda^2)\tan^2(\zeta))h_4}{-(ak^2+\gamma+\omega)^2+(a-4\beta)^2\lambda^4}}}e^{i(-kx+wt+\theta)}, \tag{67}$$

such that

$$h_4^2\left(2-h_2\right)\left[\left(1+h_2\right)^2\right]=0. \tag{68}$$

8. If $l_0=1$, $l_2=2m^2-1$, $l_4=-m^2\left(1-m^2\right)$, $0<m<1$, then $P(\zeta)=sd(\zeta,m)$ and we have

$$q_8(x,t)=\frac{\sqrt{2h_4}\sqrt{-a+4\beta}\lambda}{\sqrt{c}}\left[\frac{sd(\zeta,m)}{\sqrt{f\left(sd(\zeta,m)\right)^2+g}}\right]e^{i(-kx+wt+\theta)}, \tag{69}$$

where f and g are given by

$$\begin{aligned} f&=\frac{(-1+2m^2-h_2)h_4}{1-m^2+m^4-h_2^2},\\ g&=\frac{-3h_4}{1-m^2+m^4-h_2^2}, \end{aligned} \tag{70}$$

under the constraint condition

$$h_4^2\left(-1+2m^2-h_2\right)\left[\left(-2+m^2+h_2\right)\left(1+m^2+h_2\right)\right]=0. \tag{71}$$

9. If $l_0=1-m^2$, $l_2=2-m^2$, $l_4=1$, $0<m<1$, then $P(\zeta)=cs(\zeta,m)$ and we have

$$q_9(x,t)=\frac{\sqrt{2h_4}\sqrt{-a+4\beta}\lambda}{\sqrt{c}}\left[\frac{cs(\zeta,m)}{\sqrt{f\left(cs(\zeta,m)\right)^2+g}}\right]e^{i(-kx+wt+\theta)}, \tag{72}$$

where f and g are given by

$$\begin{aligned} f&=\frac{(-2+m^2+h_2)h_4}{1-m^2+m^4-h_2^2},\\ g&=\frac{3(-1+m^2)h_4}{1-m^2+m^4-h_2^2}, \end{aligned} \tag{73}$$

under the constraint condition

$$h_4^2\left(2-m^2-h_2\right)\left[-\left(-1+2m^2-h_2\right)\left(1+m^2+h_2\right)\right]=0. \tag{74}$$

If $m \to 1$, then the singular soliton solution is obtained

$$[q_{9,1}(x,t)=\frac{\lambda\sqrt{2h_4}\sqrt{-a+4\beta}csch(\zeta)}{\sqrt{c}\sqrt{\frac{-h_4(a-4\beta)\lambda^2csch^2(\zeta)}{ak^2+\gamma+\omega+(a-4\beta)\lambda^2}}}e^{i(-kx+wt+\theta)}], \tag{75}$$

such that

$$h_4^2\left(1-h_2\right)\left[-2+h_2+h_2^2\right]=0. \tag{76}$$

If $m\to 0$, then the periodic solution is obtained

$$q_{9,2}\left(x,t\right)=\frac{\sqrt{2h_4}\sqrt{-a+4\beta}\lambda\cot(\zeta)}{\sqrt{c}\sqrt{\frac{-(a-4\beta)\lambda^2(3(a-4\beta)\lambda^2-(ak^2+\gamma+\omega-2(a-4\beta)\lambda^2)\cot^2(\zeta))h_4}{-(ak^2+\gamma+\omega)^2+(a-4\beta)^2\lambda^4}}}e^{i(-kx+wt+\theta)}, \tag{77}$$

such that

$$h_4^2\left(2-h_2\right)\left[\left(1+h_2\right)^2\right]=0. \tag{78}$$

10. If $l_0=-m^2\left(1-m^2\right)$, $l_2=2m^2-1$, $l_4=1$, $0<m<1$, then $P(\zeta)=ds(\zeta,m)$ and we have

$$q_{10}\left(x,t\right)=\frac{\sqrt{2h_4}\sqrt{-a+4\beta}\lambda}{\sqrt{c}}\left[\frac{ds(\zeta,m)}{\sqrt{f\left(ds(\zeta,m)\right)^2+g}}\right]e^{i(-kx+wt+\theta)}, \tag{79}$$

where f and g are given by

$$\begin{aligned} f&=\frac{-(-1+2m^2-h_2)h_4}{1-m^2+m^4-h_2^2},\\ g&=\frac{-3m^2(-1+m^2)h_4}{1-m^2+m^4-h_2^2}, \end{aligned} \tag{80}$$

under the constraint condition

$$h_4^2\left(-1+2m^2-h_2\right)\left[\left(-2+m^2+h_2\right)\left(1+m^2+h_2\right)\right]=0. \tag{81}$$

11. If $l_0=\frac{1-m^2}{4}$, $l_2=\frac{1+m^2}{2}$, $l_4=\frac{1-m^2}{4}$, $0<m<1$, then $P(\zeta)=nc(\zeta,m)\pm sc(\zeta,m)$ or $P(\zeta)=\frac{cn(\zeta,m)}{1\pm sn(\zeta,m)}$ and we have

$$q_{11,1}\left(x,t\right)=\frac{\sqrt{2h_4}\sqrt{-a+4\beta}\lambda}{\sqrt{c}}\left[\frac{nc(\zeta,m)\pm sc(\zeta,m)}{\sqrt{f\left(nc(\zeta,m)\pm sc(\zeta,m)\right)^2+g}}\right]e^{i(-kx+wt+\theta)}, \tag{82}$$

or

$$q_{11,2}\left(x,t\right)=\frac{\sqrt{2h_4}\sqrt{-a+4\beta}\lambda}{\sqrt{c}}\left[\frac{\frac{cn(\zeta,m)}{1\pm sn(\zeta,m)}}{\sqrt{f\left(\frac{cn(\zeta,m)}{1\pm sn(\zeta,m)}\right)^2+g}}\right]e^{i(-kx+wt+\theta)}, \tag{83}$$

where f and g are given by

$$\begin{aligned} f&=\frac{-8(1+m^2-2h_2)h_4}{1+14m^2+m^4-16h_2^2},\\ g&=\frac{12(-1+m^2)h_4}{1+14m^2+m^4-16h_2^2}, \end{aligned} \tag{84}$$

under the constraint condition

$$h_4^2\left(\frac{1}{2}\left(1+m^2-2h_2\right)\right)\left[\frac{1}{16}\left(1+(-6+m)m+4h_2\right)\left(1+m\left(6+m\right)+4h_2\right)\right]=0. \tag{85}$$

If $m \to 1$, then the combined singular soliton solution

$$q_{11,3}(x,t) = \frac{\sqrt{2h_4}\sqrt{-a+4\beta}\lambda\left(\sinh(\zeta)+\cosh(\zeta)\right)}{\sqrt{c}\sqrt{\frac{-(a-4\beta)\lambda^2(\sinh(\zeta)+\cosh(\zeta))^2 h_4}{ak^2+\gamma+\omega+(a-4\beta)\lambda^2}}} e^{i(-kx+wt+\theta)}, \tag{86}$$

or dark-bright optical soliton solition is obtained

$$q_{11,4}(x,t) = \frac{\lambda\sqrt{2h_4}\sqrt{-a+4\beta}\left(\frac{sech(\zeta)}{1+\tanh(\zeta)}\right)}{\sqrt{c}\sqrt{\frac{-h_4\lambda^2\left(\frac{sech(\zeta)}{1+\tanh(\zeta)}\right)^2(a-4\beta)}{ak^2+\gamma+\omega+(a-4\beta)\lambda^2}}} e^{i(-kx+wt+\theta)}, \tag{87}$$

such that

$$h_4^2(1-h_2)\left[-2+h_2+h_2^2\right] = 0. \tag{88}$$

If $m \to 0$, then the combined periodic solution is obtained

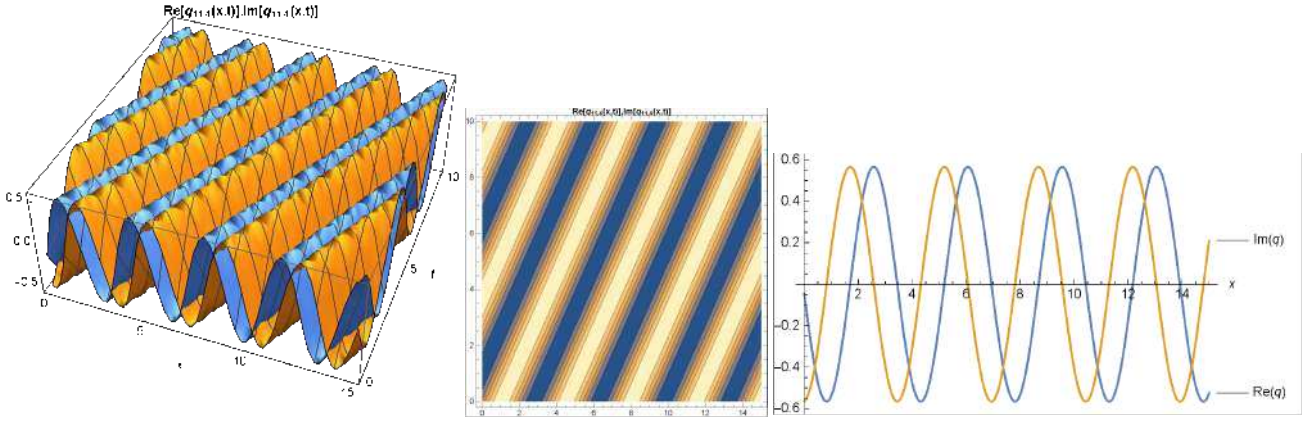

Figure 5. The numerical simulations corresponding to $|q_{11,4}|$ given by Eq. (87), for $m = 1$; (a), (b) and (c) are the 3D graphic, contour and 2D graphic, respectively

$$q_{11,5}(x,t) = \frac{\sqrt{h_4}\sqrt{-a+4\beta}\lambda\left(\sec(\zeta)+\tan(\zeta)\right)e^{i(-kx+wt+\theta)}}{\sqrt{2c}\sqrt{\frac{(a-4\beta)\lambda^2\left(4\left(ak^2+\gamma+\omega\right)-5(a-4\beta)\lambda^2+\left(4\left(ak^2+\gamma+\omega\right)+(a-4\beta)\lambda^2\right)\sin(\zeta)\right)h_4}{\left(16\left(ak^2+\gamma+\omega\right)^2-(a-4\beta)^2\lambda^4\right)(-1+\sin(\zeta))}}}, \tag{89}$$

or

$$q_{11,6}(x,t) = \frac{\frac{\sqrt{h_4}\sqrt{-a+4\beta}\lambda}{\sqrt{2c}(1+\sin(\zeta))}\cos(\zeta)e^{i(-kx+wt+\theta)}}{\sqrt{\frac{(a-4\beta)\lambda^2\left(-4\left(ak^2+\gamma+\omega\right)+5(a-4\beta)\lambda^2+\left(4\left(ak^2+\gamma+\omega\right)+(a-4\beta)\lambda^2\right)\sin(\zeta)\right)h_4}{\left(16\left(ak^2+\gamma+\omega\right)^2-(a-4\beta)^2\lambda^4\right)(1+\sin(\zeta))}}}, \tag{90}$$

such that

$$h_4^2\left(\frac{1}{2}-h_2\right)\left[\frac{1}{16}(1+4h_2)^2\right] = 0. \tag{91}$$

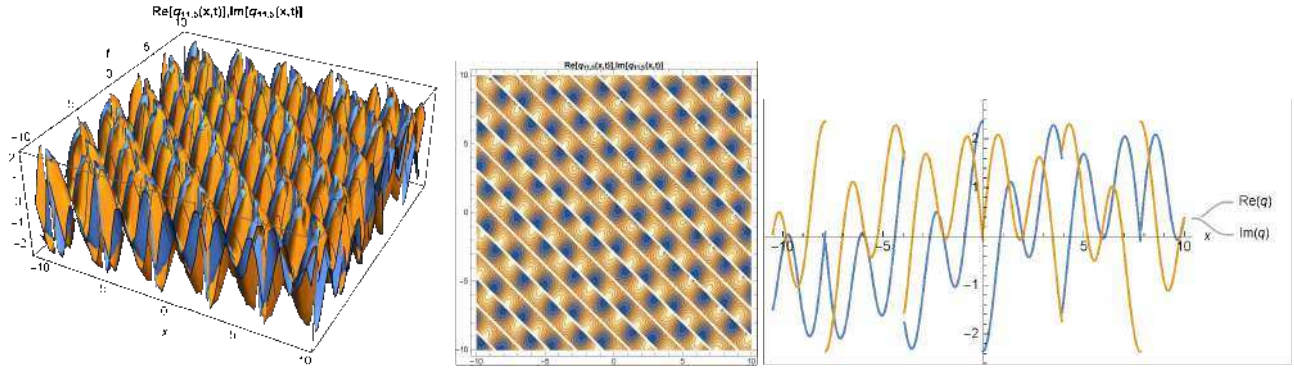

Figure 6. The numerical simulations corresponding to $|q_{11,5}|$ given by Eq. (89), for $m = 0$; (a), (b) and (c) are the 3D graphic, contour and 2D graphic, respectively

12. If $l_0 = \frac{-\left(1-m^2\right)^2}{4}$, $l_2 = \frac{1+m^2}{2}$, $l_4 = \frac{-1}{4}$, $0 < m < 1$, then $P(\zeta) = mcn(\zeta, m) \pm dn(\zeta, m)$ and we have

$$q_{12}(x,t) = \frac{\sqrt{2h_4}\sqrt{-a+4\beta}\lambda}{\sqrt{c}}\left[\frac{mcn(\zeta,m)\pm dn(\zeta,m)}{\sqrt{f\left(mcn(\zeta,m)\pm dn(\zeta,m)\right)^2+g}}\right]e^{i(-kx+wt+\theta)}, \tag{92}$$

where f and g are given by

$$f = \frac{-8(1+m^2-2h_2)h_4}{1+14m^2+m^4-16h_2^2},$$
$$g = \frac{12(-1+m^2)^2h_4}{1+14m^2+m^4-16h_2^2}, \tag{93}$$

under the constraint condition

$$h_4^2\left(\frac{1}{2}\left(1+m^2-2h_2\right)\right)\left[\frac{1}{16}\left(1+(-6+m)m+4h_2\right)\left(1+m(6+m)+4h_2\right)\right] = 0. \tag{94}$$

13. If $l_0 = \frac{1}{4}$, $l_2 = \frac{1-2m^2}{2}$, $l_4 = \frac{1}{4}$, $0 < m < 1$, then $P(\zeta) = \frac{sn(\zeta,m)}{1\pm cn(\zeta,m)}$ and we have

$$q_{13}(x,t) = \frac{\sqrt{2h_4}\sqrt{-a+4\beta}\lambda}{\sqrt{c}}\left[\frac{\frac{sn(\zeta,m)}{1\pm cn(\zeta,m)}}{\sqrt{f\left(\frac{sn(\zeta,m)}{1\pm cn(\zeta,m)}\right)^2+g}}\right]e^{i(-kx+wt+\theta)}, \tag{95}$$

where f and g are given by

$$f = \frac{8(-1+2m^2+2h_2)h_4}{1-16m^2+16m^4-16h_2^2},$$
$$g = \frac{-12h_4}{1-16m^2+16m^4-16h_2^2}, \tag{96}$$

under the constraint condition

$$h_4^2\left(\frac{1}{2}-m^2-h_2\right)\left[\frac{1}{16}+2m^2-2m^4+\left(\frac{1}{2}-m^2\right)h_2+h_2^2\right] = 0. \tag{97}$$

If $m \to 1$, then the combined soliton solution is obtained

$$q_{13,1}(x,t) = \frac{\frac{\sqrt{h_4}\sqrt{-a+4\beta}\lambda}{2\sqrt{c}}\tanh(\zeta)e^{i(-kx+wt+\theta)}}{\sqrt{\frac{(a-4\beta)\lambda^2\cosh^2(\frac{\zeta}{2})sech(\zeta)\left(-4\left(ak^2+\gamma+\omega\right)+(a-4\beta)\lambda^2+\left(4\left(ak^2+\gamma+\omega\right)+5(a-4\beta)\lambda^2\right)sech(\zeta)\right)h_4}{\left(16\left(ak^2+\gamma+\omega\right)^2-(a-4\beta)^2\lambda^4\right)}}}, \tag{98}$$

such that

$$h_4^2\left(\frac{-1}{2}-h_2\right)\left[\frac{1}{16}(1-4h_2)^2\right]=0. \tag{99}$$

If $m\to 0$, then the combined periodic solution is obtained

$$q_{13,2}(x,t)=\frac{\frac{\sqrt{h_4}\sqrt{-a+4\beta}\lambda}{2\sqrt{c}}\sin(\zeta)e^{i(-kx+wt+\theta)}}{\sqrt{\frac{(a-4\beta)\lambda^2\cos^2(\frac{\zeta}{2})(-4(ak^2+\gamma+\omega)+5(a-4\beta)\lambda^2+(4(ak^2+\gamma+\omega)+(a-4\beta)\lambda^2)\cos(\zeta))h_4}{(16(ak^2+\gamma+\omega)^2-(a-4\beta)^2\lambda^4)}}}, \tag{100}$$

such that

$$h_4^2\left(\frac{1}{2}-h_2\right)\left[\frac{1}{16}(1+4h_2)^2\right]=0. \tag{101}$$

14. If $l_0=\frac{1}{4}$, $l_2=\frac{1+m^2}{2}$, $l_4=\frac{\left(1-m^2\right)^2}{4}$, $0<m<1$, then $P(\zeta)=\frac{sn(\zeta,m)}{cn(\zeta,m)\pm dn(\zeta,m)}$ and we have

$$q_{14}(x,t)=\frac{\sqrt{2h_4}\sqrt{-a+4\beta}\lambda}{\sqrt{c}}\left[\frac{\frac{sn(\zeta,m)}{cn(\zeta,m)\pm dn(\zeta,m)}}{\sqrt{f\left(\frac{sn(\zeta,m)}{cn(\zeta,m)\pm dn(\zeta,m)}\right)^2+g}}\right]e^{i(-kx+wt+\theta)}, \tag{102}$$

where f and g are given by

$$\begin{aligned} f&=\frac{-8(1+m^2-2h_2)h_4}{1+14m^2+m^4-16h_2^2},\\ g&=\frac{-12h_4}{1+14m^2+m^4-16h_2^2}, \end{aligned} \tag{103}$$

under the constraint condition

$$h_4^2\left(\frac{1}{2}\left(1+m^2-2h_2\right)\right)\left[\frac{1}{16}(1+(-6+m)m+4h_2)(1+m(6+m)+4h_2)\right]=0. \tag{104}$$

If $m\to 1$, then the singular soliton solution is obtained

$$q_{14,1}(x,t)=\frac{\frac{\sqrt{2h_4}\sqrt{-a+4\beta}\lambda}{\sqrt{c}}\sinh(\zeta)}{\sqrt{\frac{-(a-4\beta)\lambda^2\left(3(a-4\beta)\lambda^2-(4\beta\lambda^2+\gamma+\omega+a(k-\lambda)(k+\lambda))\sinh^2(\zeta)\right)h_4}{-(ak^2+\gamma+\omega)^2+(a-4\beta)^2\lambda^4}}}e^{i(-kx+wt+\theta)}, \tag{105}$$

such that

$$h_4^2(1-h_2)\left[-2+h_2+h_2^2\right]=0. \tag{106}$$

If $m\to 0$, then the combined periodic solution is obtained

$$q_{14,2}(x,t)=\frac{\frac{\sqrt{h_4}\sqrt{-a+4\beta}\lambda\sin(\zeta)}{2\sqrt{c}}e^{i(-kx+wt+\theta)}}{\sqrt{\frac{(a-4\beta)\lambda^2\cos^2(\frac{\zeta}{2})(-4(ak^2+\gamma+\omega)+5(a-4\beta)\lambda^2+(4(ak^2+\gamma+\omega)+(a-4\beta)\lambda^2)\cos(\zeta))h_4}{(16(ak^2+\gamma+\omega)^2-(a-4\beta)^2\lambda^4)}}}, \tag{107}$$

such that

$$h_4^2\left(\frac{1}{2}-h_2\right)\left[\frac{1}{16}(1+4h_2)^2\right]=0. \tag{108}$$

5 Result and discussion

This study used the newly created φ^6—model expansion method to get dark, bright, singular, periodic and combined soliton solutions to the complex Ginzburg-Landau equation (CGLE) with Kerr law in nonlinear optics. The Kerr law of nonlinearity is a result of the nonlinear reactions that an external electric field-induced nonharmonic motion of trapped electrons in molecules induces in a light wave in an optical fiber. The constraint conditions ensure the existence of these solutions.
The graphics in Figures 1, 3 and 5 show the behavior of dark, bright and dark-bright solitons together with periodic and combined periodic wave solutions at any given time, which is important in the transmission of energy from one location to another. Furthermore, to examine the physical implications of the parameters in the transformation, which is known as the classical wave transformation represented by Eqs. (1) and (2). The physical meanings of the parameters in the solution of Eqs. (26), (28), (33), (35), (87) and (89) traveling waves, which contain numerous mathematical constants. It is the internal dynamics of the traveling wave for various parameter values. We may conclude that the traveling wave behavior alters for different values of each. The simulation is performed for several values of the wave frequency in order to examine the changes in the dark and bright solitons more clearly. Similarly, a similar discussion can be made for other physical parameters as well as various traveling wave solutions.

6 Conclcusion

This work investigates the complex Ginzburg–Landau equation (CGLE) with Kerr law in nonlinear optics, which represents soliton propagation in the presence of a detuning factor. The scheme's benefit is that the solutions are first recovered in terms of Jacobi's elliptic function. When a result, as the limiting values of the modulus of ellipticity approach 0 or unity, solitons or singular-periodic solutions are produced. The φ^6-model expansion approach is used to find dark, bright, dark-bright or combined, singular and combined singular optical soliton solutions to the CGL model with Kerr law. The φ^6-model expansion approach is found to be efficient for constructing optical soliton solutions for most nonlinear physical phenomena. The results presented in this study are intended to improve the CGLE's nonlinear dynamical characteristics. The findings of this study might assist in comprehending some of the physical implications of various nonlinear physics models. The hyperbolic sine, for example, appears in the calculation of the Roche limit and gravitational potential of a cylinder, while the hyperbolic cotangent appears in the Langevin function for magnetic polarization. In order to take into account slow-light pulses, the model will also be examined using fractional temporal evolution.

Declarations

List of abbreviations

CGLE: Complex Ginzburg-Landau Equation
GVE: Group Velocity Dispersion
NPDEs: Nonlinear Partial Differential Equations

Consent for publication

Not applicable.

Conflicts of interest

The authors declare that they have no conflict of interests.

Funding

No funding was used in this study.

Author's contributions

I.M.A.: Conceptualization, Methodology, Software, Visualization, Investigation, Supervision, Software, Validation, Writing-Reviewing and Editing. A.Y.: Conceptualization, Methodology Writing-Original draft preparation. Visualization, Investigation, Supervision, Software, Validation, Writing-Reviewing and Editing. All authors discussed the results and contributed to the final manuscript.

Acknowledgements

We appreciate the opportunities provided by Firat University for this study, which was carried out as part of the doctoral thesis research.

References

[1] Isah, M.A., & Külahcı, M.A. A study on null cartan curve in Minkowski 3-space. *Applied Mathematics and Nonlinear Sciences*, 5(1), 413-424, (2020). [CrossRef]

[2] Isah, M.A., & Külahcı, M.A. Involute Curves in 4-dimensional Galilean space G4. *In Conference Proceedings of Science and Technology*, 2(2), 134-141, (2019).
[3] Isah, M.A., Isah, I., Hassan, T.L., & Usman, M. Some characterization of osculating curves according to darboux frame in three dimensional euclidean space. *International Journal of Advanced Academic Research*, 7(12), 47-56, (2021).
[4] Isah, M.A., & Külahçı, M.A. Special curves according to bishop frame in minkowski 3-space. *Applied Mathematics and Nonlinear Sciences*, 5(1), 237-248, (2020). [CrossRef]
[5] Aydin, M.E., Mihai, A., & Yokus, A. Applications of fractional calculus in equiaffine geometry: plane curves with fractional order. *Mathematical Methods in the Applied Sciences*, 44(17), 13659-13669, (2021). [CrossRef]
[6] Myint-U, T., & Debnath, L. Linear partial differential equations for scientists and engineers. *Springer Science & Business Media*, Boston, (2007).
[7] Duran, S. Breaking theory of solitary waves for the Riemann wave equation in fluid dynamics. *International Journal of Modern Physics B*, 35(09), 2150130, (2021). [CrossRef]
[8] Hasegawa, A. Optical solitons in fibers. *In Optical solitons in fibers* (pp. 1-74). Springer, Berlin, Heidelberg, (1989).
[9] Yokuş, A., Durur, H., & Duran, S. Simulation and refraction event of complex hyperbolic type solitary wave in plasma and optical fiber for the perturbed Chen-Lee-Liu equation. *Optical and Quantum Electronics*, 53(7), 1-17, (2021). [CrossRef]
[10] Kivshar, Y.S., & Agrawal, G.P. Optical solitons: from fibers to photonic crystals. *Academic Press*, (2003).
[11] Hasegawa, A., & Kodama, Y. Signal transmission by optical solitons in monomode fiber. *Proceedings of the IEEE*, 69(9), 1145-1150, (1981). [CrossRef]
[12] Kaya, D., & Yokus, A. A numerical comparison of partial solutions in the decomposition method for linear and nonlinear partial differential equations. *Mathematics and Computers in Simulation*, 60(6), 507-512, (2002). [CrossRef]
[13] Durur, H. Energy-carrying wave simulation of the Lonngren-wave equation in semiconductor materials. *International Journal of Modern Physics B*, 35(21), 2150213, (2021). [CrossRef]
[14] Gao, W., Silambarasan, R., Baskonus, H.M., Anand, R.V., & Rezazadeh, H. Periodic waves of the non dissipative double dispersive micro strain wave in the micro structured solids. *Physica A: Statistical Mechanics and its Applications*, 545, 123772, (2020). [CrossRef]
[15] Yokuş, A., Durur, H., & Abro, K.A. Symbolic computation of Caudrey–Dodd–Gibbon equation subject to periodic trigonometric and hyperbolic symmetries. *The European Physical Journal Plus*, 136(4), 1-16, (2021). [CrossRef]
[16] Yokuş, A. Construction of different types of traveling wave solutions of the relativistic wave equation associated with the Schrödinger equation. *Mathematical Modelling and Numerical Simulation with Applications*, 1(1), 24-31, (2021). [CrossRef]
[17] Tarla, S., Ali, K.K., Yilmazer, R., & Osman, M.S. New optical solitons based on the perturbed Chen-Lee-Liu model through Jacobi elliptic function method. *Optical and Quantum Electronics*, 54(2), 1-12, (2022). [CrossRef]
[18] Tarla, S., Ali, K.K., Sun, T.C., Yilmazer, R., & Osman, M.S. Nonlinear pulse propagation for novel optical solitons modeled by Fokas system in monomode optical fibers. *Results in Physics*, 36, 105381, (2022). [CrossRef]
[19] Duran, S., & Karabulut, B. Nematicons in liquid crystals with Kerr Law by sub-equation method. *Alexandria Engineering Journal*, 61(2), 1695-1700, (2022). [CrossRef]
[20] Yokus, A., & Tuz, M. An application of a new version of (G'/G)-expansion method. In AIP Conference Proceedings 1798(1), 020165. AIP Publishing LLC, (2017). [CrossRef]
[21] Kaya, D., Yokuş, A., & Demiroğlu, U. Comparison of exact and numerical solutions for the Sharma-Tasso-Olver equation. *In Numerical Solutions of Realistic Nonlinear Phenomena* (pp. 53-65). Springer, Cham (2020).
[22] Baskonus, H.M., Gao, W., Rezazadeh, H., Mirhosseini-Alizamini, S.M., Baili, J., Ahmad, H., & Gia, T.N. New classifications of nonlinear Schrödinger model with group velocity dispersion via new extended method. *Results in Physics*, 31, 104910, (2021). [CrossRef]
[23] Yokus, A., & Isah, M.A. Stability analysis and solutions of (2+1)-Kadomtsev–Petviashvili equation by homoclinic technique based on Hirota bilinear form. *Nonlinear Dynamics*, 1-12, (2022). [CrossRef]
[24] Khan, A., Khan, A., & Sinan, M. Ion temperature gradient modes driven soliton and shock by reduction perturbation method for electron-ion magneto-plasma. *Mathematical Modelling and Numerical Simulation with Applications*, 2(1), 1-12, (2022). [CrossRef]
[25] Yokus, A., & Isah, M.A. Investigation of internal dynamics of soliton with the help of traveling wave soliton solution of Hamilton amplitude equation. *Optical and Quantum Electronics*, 54(8), 1-21, (2022). [CrossRef]
[26] Zhou, Q., Xiong, X., Zhu, Q., Liu, Y., Yu, H., Yao, P., ... & Belicd, M. Optical solitons with nonlinear dispersion in polynomial law medium. *Journal of Optoelectronics and Advanced Materials*, 17(1-2), 82-86, (2015).
[27] Zayed, E.M., & Al-Nowehy, A.G. Many new exact solutions to the higher-order nonlinear Schrödinger equation with derivative non-Kerr nonlinear terms using three different techniques. *Optik*, 143, 84-103, (2017). [CrossRef]
[28] Zayed, E.M., Al-Nowehy, A.G., & Elshater, M.E. New-model expansion method and its applications to the resonant nonlinear Schrödinger equation with parabolic law nonlinearity. *The European Physical Journal Plus*, 133(10), 417, (2018). [CrossRef]
[29] Mehdizadeh Khalsaraei, M., Shokri, A., Noeiaghdam, S., & Molayi, M. Nonstandard Finite Difference Schemes for an SIR Epidemic Model. *Mathematics*, 9(23), 3082, (2021). [CrossRef]
[30] Zarin, R., Ahmed, I., Kumam, P., Zeb, A., & Din, A. Fractional modeling and optimal control analysis of rabies virus under the convex incidence rate. *Results in Physics*, 28, 104665, (2021). [CrossRef]
[31] Khan, A., Zarin, R., Khan, S., Saeed, A., Gul, T., & Humphries, U.W. Fractional dynamics and stability analysis of COVID-19 pandemic model under the harmonic mean type incidence rate. *Computer Methods in Biomechanics and Biomedical Engineering*, 25(6), 619-640, (2022). [CrossRef]
[32] Zarin, R., Ahmed, I., Kumam, P., Zeb, A., & Din, A. Fractional modeling and optimal control analysis of rabies virus under the convex incidence rate. *Results in Physics*, 28, 104665, (2021). [CrossRef]
[33] Chu, Y., Shallal, M.A., Mirhosseini-Alizamini, S.M., Rezazadeh, H., Javeed, S., & Baleanu, D. Application of modified extended Tanh technique for solving complex Ginzburg–Landau equation considering Kerr law nonlinearity. *CMC-Computers Materials & Continua*, 66(2), 1369-1378, (2021). [CrossRef]
[34] Arnous, A.H., Seadawy, A.R., Alqahtani, R.T., & Biswas, A. Optical solitons with complex Ginzburg–Landau equation by

modified simple equation method. *Optik*, 144, 475-480, (2017). [CrossRef]
[35] Liu, W., Yu, W., Yang, C., Liu, M., Zhang, Y., & Lei, M. Analytic solutions for the generalized complex Ginzburg–Landau equation in fiber lasers. *Nonlinear Dynamics*, 89(4), 2933-2939, (2017). [CrossRef]
[36] Kudryashov, N.A. First integrals and general solution of the complex Ginzburg-Landau equation. *Applied Mathematics and Computation*, 386, 125407, (2020). [CrossRef]
[37] Rezazadeh, H. New solitons solutions of the complex Ginzburg-Landau equation with Kerr law nonlinearity. *Optik*, 167, 218-227, (2018). [CrossRef]
[38] Mirzazadeh, M., Ekici, M., Sonmezoglu, A., Eslami, M., Zhou, Q., Kara, A.H., ... & Belić, M. Optical solitons with complex Ginzburg–Landau equation. *Nonlinear Dynamics*, 85(3), 1979-2016, (2016). [CrossRef]
[39] Osman, M.S., Ghanbari, B., & Machado, J.A.T. New complex waves in nonlinear optics based on the complex Ginzburg-Landau equation with Kerr law nonlinearity. *The European Physical Journal Plus*, 134(1), 1-10, (2019). [CrossRef]
[40] Ahmed, I., Seadawy, A.R., & Lu, D. Combined multi-waves rational solutions for complex Ginzburg–Landau equation with Kerr law of nonlinearity. *Modern Physics Letters A*, 34(03), 1950019, (2019). [CrossRef]
[41] Sajid, N., & Akram, G. Novel solutions of Biswas-Arshed equation by newly ϕ^6-model expansion method. *Optik*, 211, 164564, (2020). [CrossRef]

Mathematical Modelling and Numerical Simulation with Applications (MMNSA) (https://www.mmnsa.org)

Mathematical Modelling and Numerical Simulation with Applications, 2022, 2(3), 164–176

https://www.mmnsa.org
ISSN Online: 2791-8564 / Open Access
https://doi.org/10.53391/mmnsa.2022.013

RESEARCH PAPER

Stability characterization of a fractional-order viral system with the non-cytolytic immune assumption

Mouhcine Naim [1,†], Yassine Sabbar [2,†,*] and Anwar Zeb [3,†]

[1]Laboratory of Analysis, Modeling and Simulation, Department of Mathematics and Computer Science, Faculty of Sciences Ben M'sik, Hassan II University, Casablanca, Morocco, [2]LPAIS Laboratory, Faculty of Sciences Dhar El Mahraz, Sidi Mohamed Ben Abdellah University, Fez, Morocco, [3]Department of Mathematics, COMSATS University Islamabad, Abbottabad Campus, Abbottabad 22060, Khyber Pakhtunkhwa, Pakistan

*Corresponding Author
†naimmouhcine2013@gmail.com (Mouhcine Naim); yassine.sabbar@usmba.ac.ma (Yassine Sabbar); anwar@cuiatd.edu.pk (Anwar Zeb)

Abstract

This article deals with a Caputo fractional-order viral model that incorporates the non-cytolytic immune hypothesis and the mechanism of viral replication inhibition. Firstly, we establish the existence, uniqueness, non-negativity and boundedness of the solutions of the proposed viral model. Then, we point out that our model has the following three equilibrium points: equilibrium point without virus, equilibrium state without immune system, and equilibrium point activated by immunity with humoral feedback. By presenting two critical quantities, the asymptotic stability of all said steady points is examined. Finally, we examine the finesse of our results by highlighting the impact of fractional derivatives on the stability of the corresponding steady points.

Key words: Viral model; non-cytolytic; immunity; fractional-order formulation; stability
AMS 2020 Classification: 26A33; 34A08; 45M10

1 Introduction

Mathematical modeling has become necessary to comprise our world and to study phenomena on time and space scales that are difficult to scope empirically [1]. Mathematics applied in virology seeks to investigate the interactions of viruses with the biological environment and their powerful influence on living organisms, both plants and animals. Viruses are scrutinized at different scales: molecular, cellular, in the body and, in the case of an epidemic, in the ecosystem or society as a whole [2]. Virological modeling also examines and models the spread of viruses at the population level. It starts from when they cross species barriers, until policy measures are put in place to reduce and treat disease. At this scale, the humanities can be called in as reinforcements. Specifically, it concentrates on structures, diffusion, dynamics, and immune capabilities of infections [3]. The blending of mathematical tools with virology pursues to predict the long-run attitude of a virus under certain conditions in order to help eradicate or control the infection. In terms of scientific research, the description of virus-cell interactions with different types of immune responses is a rich subject of interest for many researchers [4]. Thus, a number of studies have been devoted to the analysis of viral systems with a specific immune response combining humoral and cellular immunizations [5]. These two characteristics are types of adaptive immune reactions that permit the human organism to safeguard itself from threatening agents such as bacterial microorganisms, viruses and toxins, in a targeted way.

➤ **Received:** 29.07.2022 ➤ **Revised:** 22.09.2022 ➤ **Accepted:** 24.09.2022 ➤ **Published:** 25.09.2022

Recovery from infected cells is an important hypothesis along with the immune response. For this reason, it is appropriate to propose a viral model including the healing average of damaging cells employing the non-cytolytic immune feedback under humoral resistance. On the other hand, the host immune response during viral infection can be usually splitted into lytic and non-lytic elements [6], where the lytic elements kill the damaged cells, while the non-lytic elements prohibit viral replication through soluble media produced by immune cells. For example, in the case of SARS-CoV-2 infection, some authors have considered target cell models by proposing a framework with lytic and non-lytic immune responses to understand virus spread within the human body [7]. The human immune system consists of both innate and adaptive immune responses. While the adaptive immune system is quick and efficient in targeting invasions by previously encountered pathogens, its role in host defense in the early days of a new infection is secondary to the innate immune system. Motivated by these facts, Dhar et al. [4] exhibited the following viral system with non-cytolytic immune assumption:

$$\begin{cases} \mathbf{U}'(t) = \varphi - \mathfrak{h}_1\mathbf{U}(t) - \mathfrak{b}\mathbf{U}(t)\mathbf{Y}(t)\overbrace{(1+q\mathbf{W}(t))^{-1}}^{\text{Inhibition rate}} + \xi\mathbf{X}(t), \\ \mathbf{X}'(t) = \mathfrak{b}\mathbf{U}(t)\mathbf{Y}(t)(1+q\mathbf{W}(t))^{-1} - \mathfrak{h}_2\mathbf{X}(t) - \xi\mathbf{X}(t), \\ \mathbf{Y}'(t) = k\mathbf{X}(t) - \mathfrak{h}_3\mathbf{Y}(t) - p\mathbf{Y}(t)\mathbf{W}(t), \\ \mathbf{W}'(t) = c\mathbf{Y}(t)\mathbf{W}(t) - \mathfrak{h}_4\mathbf{W}(t), \end{cases} \tag{1}$$

with positive started data. Here, **U**, **X**, **Y** and **W** indicate in that order, susceptible uninfected cells, infected cells, free virus and B lymphocytes (cells used in the humoral immune process of the adaptive immune system). Regarding the positive parameters of system (1), φ indicates the inflow of **U** cells, k designates the produce ratio of **Y**, c is the growth rate of B lymphocytes, $\mathfrak{h}_1$, $\mathfrak{h}_2$, $\mathfrak{h}_3$ and $\mathfrak{h}_4$ are the natural mortality rates of **U**, **X**, **Y** and **W** cells respectively, p is the neutralizing rate of antibodies produced by B cells, ξ is the healing rate of infected cell due to the antiviral activity, and $\mathfrak{b}$ is the contamination rate. The expression $(1+q\mathbf{W})$ designates the rate at which the non-lytic process prevents viral growth, where q is the non-lytic force. To facilitate the understanding of the rest of this article, we summarize the transfer mechanisms of the model mentioned above by the diagram shown in Figure 1.

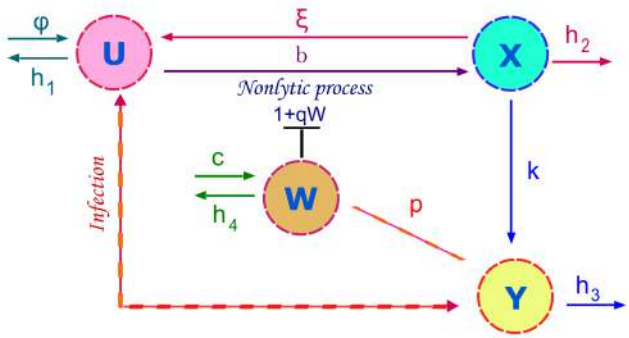

Figure 1. *Compartment diagram of the viral system* (1).

In [4], the authors established the steady points of system (1) and studied their asymptotic stability. Specifically, they provided the critical value between the disappearance and continuation of the infection. The results obtained in [4] are interesting and help us to understand the long term of the infection under some local characteristics of the classical order derivative. This type of mathematical formulation has certain limits, and the system (1) can be improved and updated by considering the fractional framework.

Fractional derivatives is a generalization of the integer order derivative to an arbitrary order, which is originated from the L'Hospital letter to Leibniz discussing the meaning of the derivative or what does the derivative of order $\frac{1}{2}$ or $\sqrt{2}$ of a function mean in 1695. Several definitions of fractional derivatives have been introduced. Among them, the Riemann–Liouville and Caputo's derivative are widely used in the literature. The fractional order derivative used in this paper is in the sense of Caputo definition, which is a modification of the Riemann-Liouville integral definition, and has the advantage that the initial values for fractional differential equations with Caputo derivatives take the same form as that for integer order differential equations [8, 9, 10]. Also, another advantage of this definition is that the Caputo derivative of a constant is zero. Memory effect is an essential characteristic of fractional-order derivatives which made fractional calculus and its applications widely used in many fields of science and engineering [11, 12, 13, 14, 15, 16, 17]. Obviously, this feature is very relevant for modeling the spread of infections [18, 19, 20, 21, 22, 23, 24]. For this reason, many researchers have adopted this analytical vision [25, 26, 27, 28, 29, 30, 31]. In [32], the authors derived a non-integer order system for the co-infection mechanisms. They inferred that the fractional formulation matches real data of certain viral problems. Analytically, they examined the stability property of the proposed viral model. To model the virological memory effects, the authors in [33], presented a fractional order viral model. They analyzed the long-term dynamics of the constructed model. As a real-world application, the authors in [34], proposed a fractional feeding system to illustrate the complexity of the spread of COVID-19. They presented an advanced analysis by discussing the attitude of viral propagation phenomena. In

accordance with the above arguments and works, we improve system (1) by using the fractional formulation as follows:

$$\begin{cases} {}_0^{\mathcal{C}}\mathbb{F}^{\sigma}\mathbf{U}(t) = & \varphi - \hbar_1\mathbf{U}(t) - \mathfrak{b}\mathbf{U}(t)\mathbf{Y}(t)\big(1+q\mathbf{W}(t)\big)^{-1} + \xi\mathbf{X}(t), \\ {}_0^{\mathcal{C}}\mathbb{F}^{\sigma}\mathbf{X}(t) = & \mathfrak{b}\mathbf{U}(t)\mathbf{Y}(t)\big(1+q\mathbf{W}(t)\big)^{-1} - \hbar_2\mathbf{X}(t) - \xi\mathbf{X}(t), \\ {}_0^{\mathcal{C}}\mathbb{F}^{\sigma}\mathbf{Y}(t) = & k\mathbf{X}(t) - \hbar_3\mathbf{Y}(t) - p\mathbf{Y}(t)\mathbf{W}(t), \\ {}_0^{\mathcal{C}}\mathbb{F}^{\sigma}\mathbf{W}(t) = & c\mathbf{Y}(t)\mathbf{W}(t) - \hbar_4\mathbf{W}(t), \end{cases} \tag{2}$$

where ${}_0^{\mathcal{C}}\mathbb{F}^{\sigma}$ is the Caputo fractional derivative and $\sigma \in (0,1]$ is its related order. The Caputo fractional derivative of order $\sigma \in (0,1]$ for a function $\mathfrak{f} \in \mathcal{C}(\mathbb{R}_+,\mathbb{R})$ is expressed as follows [35]:

$${}_0^{\mathcal{C}}\mathbb{F}^{\sigma}\mathfrak{f}(t) = \frac{1}{\Gamma(1-\sigma)}\int_0^t (t-s)^{-\sigma}\mathfrak{f}'(s)ds,$$

where Γ is the Gamma function and $\Gamma(\sigma) = \int_0^{\infty} t^{\sigma-1}e^{-t}dt$.
Note that, the fractional order formulation (2) is converted to ordinary differential equations system when $\sigma = 1$. Therefore, the model studied in [4] is a special case of system (1) when $\sigma = 1$.
The axial problematic of this research is to explore some long-run characteristics of the viral system (2) which adopts the non-integer order derivative. It is well known that stability analysis is an important property of dynamical systems. It provides a good overview of the long term of the studied phenomenon. Unlike classical investigations, in this survey, we concentrate on exploring the influence of fractional derivative on said features; and this is the main part of our contribution.
The remaining of this article is structured as follows: we begin in Section 2 by proving the well-posedness of our enhanced model in the sense that it has a unique nonnegative and bounded solution, defining the steady points $\mathbb{S}^{\circ}$, $\mathbb{S}_1^{\star}$, $\mathbb{S}_2^{\star}$ of system (2) and their related critical quantities $\mathcal{T}_{\circ}$ and $\mathcal{T}_1$. These two threshold conditions make it possible to sort the dynamic behavior of our system. In Section 3, we present our main theoretical findings on the stability of our dynamical system. In Section 4, we belay the exactitude of our outcomes by discussing the impact of non-integer orders on the stability behavior of system (2).

2 Well-posedness and definition of possible steady points

The first concern in analyzing the dynamical properties of a mathematical population system is to know whether it is well-posed or not, and we mean by well-posedness here that the system admits a unique, non-negative, and global-in-time solution. In this section, we will provide a suitable hypothetical framework under which the well-posedness of system (2) is guaranteed. Moreover, we will show that our model has three equilibrium points.

Existence, nonnegativity and boundedness of solutions

Before going the main result of this section, we first give the following useful lemma which will be involved in the sequel.

Lemma 1 *[36]. Assume that $\mathfrak{f}$ and ${}_0^{\mathcal{C}}\mathbb{F}^{\sigma}\mathfrak{f}$ are continuous functions on the interval $[\mathbf{a},\mathbf{b}]$, and $\sigma \in (0,1]$, then we have*

(i) If ${}_0^{\mathcal{C}}\mathbb{F}^{\sigma}\mathfrak{f}(t) \geq 0$ for all $t \in [\mathbf{a},\mathbf{b}]$, then $\mathfrak{f}$ is nondecreasing on $[\mathbf{a},\mathbf{b}]$,
(ii) If ${}_0^{\mathcal{C}}\mathbb{F}^{\sigma}\mathfrak{f}(t) \leq 0$ for all $t \in [\mathbf{a},\mathbf{b}]$, then $\mathfrak{f}$ is nonincreasing on $[\mathbf{a},\mathbf{b}]$.

Theorem 1 *The fractional model (2) with any nonnegative initial condition is well-posed in the sense that it has a unique nonnegative and bounded solution.*

Proof From Theorem 3.1 and Remark 3.2 in [37], we can prove the existence and uniqueness of the solution of system (2).
Now, we show the nonnegativity of this solution. From system (2), one can deduce that

$${}_0^{\mathcal{C}}\mathbb{F}^{\sigma}\mathbf{U}\Big|_{\mathbf{U}=0} = \varphi + \xi\mathbf{X} > 0 \quad \text{for all } \mathbf{X},\mathbf{Y},\mathbf{W} \geq 0,$$

$${}_0^{\mathcal{C}}\mathbb{F}^{\sigma}\mathbf{X}\Big|_{\mathbf{X}=0} = \frac{\mathfrak{b}\mathbf{U}\mathbf{Y}}{1+q\mathbf{W}} \geq 0 \quad \text{for all } \mathbf{U},\mathbf{Y},\mathbf{W} \geq 0,$$

$${}_0^{\mathcal{C}}\mathbb{F}^{\sigma}\mathbf{Y}\Big|_{\mathbf{Y}=0} = k\mathbf{X} \geq 0 \quad \text{for all } \mathbf{U},\mathbf{X},\mathbf{W} \geq 0,$$

$${}_0^{\mathcal{C}}\mathbb{F}^{\sigma}\mathbf{W}\Big|_{\mathbf{W}=0} = 0 \geq 0 \quad \text{for all } \mathbf{U},\mathbf{X},\mathbf{Y} \geq 0.$$

By utilizing Lemma 1, we deduce that the solution of the fractional order system (2) is nonnegative. Now, we check the boundedness of the solution. For this purpose, we define the following function

$$\mathcal{N}(t) = \mathbf{U}(t) + \mathbf{X}(t) + \frac{\hbar_2}{2k}\mathbf{Y}(t) + \frac{p\hbar_2}{2kc}\mathbf{W}(t).$$

Thus,

$${}_0^{\mathcal{C}}\mathbb{F}^{\sigma}\mathcal{N}(t) = \varphi - \hbar_1\mathbf{U}(t) - \frac{\hbar_2}{2}\mathbf{X}(t) - \frac{\hbar_2\hbar_3}{2k}\mathbf{Y}(t) - \frac{p\hbar_2\hbar_4}{2kc}\mathbf{W}(t) \leq \varphi - d\mathcal{N}(t),$$

where $d = \min\left\{\hbar_1, \frac{\hbar_2}{2}, \hbar_3, \hbar_4\right\}$. Then, by Lemma 3 in [38], we obtain that

$$\mathcal{N}(t) \leq \left(\mathcal{N}(0) - \frac{\varphi}{d}\right)\mathcal{M}_\sigma\left(-dt^\sigma\right) + \frac{\varphi}{d},$$

where $\mathcal{M}_\sigma(z) = \sum_{j=0}^{\infty} \frac{z^j}{\Gamma(\sigma j+1)}$ is the Mittag-Leffler function of parameter σ [39]. Hence, $\limsup_{t\to\infty} \mathcal{N}(t) \leq \frac{\varphi}{d}$, Therefore, the solution of system (2) is bounded. ■

The steady states

Definition 1 *[40]. $\mathcal{O}^*$ is an equilibrium point of the system ${}_0^C\mathbb{F}^\sigma \mathfrak{f}(t) = \mathcal{P}(t, \mathfrak{f}(t))$, $\sigma \in (0,1]$, if $\mathcal{P}(t, \mathcal{O}^*) = 0$.*

The model (2) admits three biological steady points. Effortlessly, one can first deduce that the system (2) always has a virus-clear steady point

$$\mathbb{S}^\circ = (\mathbf{U}^\circ, 0, 0, 0) = \left(\frac{\varphi}{\hbar_1}, 0, 0, 0\right).$$

Then, we obtain the following basic reproduction number:

$$\mathcal{T}_\circ = \frac{\mathfrak{b}k\mathbf{U}^\circ}{\hbar_3(\hbar_2 + \xi)}.$$

Biologically, $\mathcal{T}_\circ$ indicates the mean density of the newly contaminated cells generated from one tainted cell at the beginning of the infection. If $\mathcal{T}_\circ > 1$, system (2) has the following immunity-free steady point:

$$\mathbb{S}_1^\star = (\mathbf{U}_1^\star, \mathbf{X}_1^\star, \mathbf{Y}_1^\star, 0) = \left(\frac{\hbar_3(\hbar_2 + \xi)}{\mathfrak{b}k}, \frac{\hbar_1\hbar_3(\hbar_2 + \xi)}{\mathfrak{b}\hbar_2 k}(\mathcal{T}_\circ - 1), \frac{k}{\hbar_3}\mathbf{X}_1^\star, 0\right).$$

Now, we set

$$\mathcal{T}_1 = \frac{c}{\hbar_4}\mathbf{Y}_1^\star = \frac{c\hbar_1(\hbar_2 + \xi)}{\mathfrak{b}\hbar_2\hbar_4}(\mathcal{T}_\circ - 1),$$

which is the immune response critical value. Explicitly, $\mathcal{T}_1$ refers to the average density of new immune cells provided by an immune cell over its natural mean lifespan [4]. If $\mathcal{T}_1 > 1$, system (2) has an immunity-activated steady point with humoral response $\mathbb{S}_2^\star = (\mathbf{U}_2^\star, \mathbf{X}_2^\star, \mathbf{Y}_2^\star, \mathbf{W}_2^\star)$, where

$$\begin{aligned}
\mathbf{U}_2^\star &= \frac{c\varphi(\hbar_2 + \xi)(1 + q\mathbf{W}_2^\star)}{\mathfrak{b}\hbar_2\hbar_4 + c\hbar_1(\hbar_2 + \xi)(1 + q\mathbf{W}_2^\star)},\\
\mathbf{X}_2^\star &= \frac{\mathfrak{b}\varphi\hbar_4}{\mathfrak{b}\hbar_2\hbar_4 + c\hbar_1(\hbar_2 + \xi)(1 + q\mathbf{W}_2^\star)},\\
\mathbf{Y}_2^\star &= \frac{\hbar_4}{c},
\end{aligned}$$

and $\mathbf{W}_2^\star$ is the positive real root of the following equation

$$\Omega_1\mathbf{W}_2^{\star 2} + \Omega_2\mathbf{W}_2^\star + \Omega_3 = 0,$$

where

$$\begin{aligned}
\Omega_1 &= cpq\hbar_1\hbar_4(\hbar_2 + \xi),\\
\Omega_2 &= \mathfrak{b}p\hbar_2\hbar_4^2 + c\hbar_1\hbar_4(\hbar_2 + \xi)(p + \hbar_3 q),\\
\Omega_3 &= \mathfrak{b}\hbar_2\hbar_3\hbar_4^2(1 - \mathcal{T}_1).
\end{aligned}$$

The results of this subsection can be summarized in the following theorem.

Theorem 2 *The fractional system (2) has three steady points. That is,*

i. if $\mathcal{T}_\circ \leq 1$, then model (2) has a unique virus-clear steady point $\mathbb{S}^\circ$,
ii. if $\mathcal{T}_1 \leq 1 < \mathcal{T}_\circ$, then model (2) has a unique immunity-free steady point $\mathbb{S}_1^\star$ besides $\mathbb{S}^\circ$,
iii. if $\mathcal{T}_1 > 1$, then model (2) has a unique immunity-activated steady point with humoral response $\mathbb{S}_2^\star$ besides $\mathbb{S}^\circ$ and $\mathbb{S}_1^\star$.

3 Stability characterization

This section is dedicated to examining the stability of $\mathbb{S}^\circ$, $\mathbb{S}_1^\star$ and $\mathbb{S}_2^\star$. To analyze the local stability of the equilibria, we need the following lemma.

Lemma 2 *[41]. Consider the fractional order system*

$$ {}_0^C\mathbb{F}^\sigma x(t) = h(x(t)), \;\; x(0) = x_0, $$

where $\sigma \in (0,1]$, $x(t) \in \mathbb{R}^n$ *and* $h \in C^1(\mathbb{R}^n, \mathbb{R}^n)$. *An equilibrium point is locally asymptotically stable if all the eigenvalues* η_j $(j = 1, 2, \ldots, n)$ *of the Jacobian matrix* $\mathbb{M}^{\mathcal{J}} = \frac{\partial h}{\partial x}$ *evaluated at the equilibrium satisfy* $\left|\arg(\eta_j)\right| > \frac{\sigma\pi}{2}$, *and unstable if there exist an eigenvalue* η_j *such that* $\left|\arg(\eta_j)\right| < \frac{\sigma\pi}{2}$.

It should be noted that the Jacobian matrix of (2) at any steady point $\mathbb{S} = (\mathbf{U}, \mathbf{X}, \mathbf{Y}, \mathbf{W})$ is given as follows:

$$ \mathbb{M}^{\mathcal{J}} = \begin{pmatrix} -\hbar_1 - \frac{\flat\mathbf{Y}}{1+q\mathbf{W}} & \xi & -\frac{\flat\mathbf{U}}{1+q\mathbf{W}} & \frac{\flat q\mathbf{U}\mathbf{Y}}{(1+q\mathbf{W})^2} \\ \frac{\flat\mathbf{Y}}{1+q\mathbf{W}} & -\hbar_2 - \xi & \frac{\flat\mathbf{U}}{1+q\mathbf{W}} & -\frac{\flat q\mathbf{U}\mathbf{Y}}{(1+q\mathbf{W})^2} \\ 0 & k & -\hbar_3 - p\mathbf{W} & -p\mathbf{Y} \\ 0 & 0 & c\mathbf{W} & -\hbar_4 + c\mathbf{Y} \end{pmatrix}. \tag{3} $$

In order to prove the global stability, we need the two following lemmas.

Lemma 3 *[42]. Let* $o(t) \in \mathbb{R}_+$ *be a continuous and differentiable function. Then, for any* $t \geq 0$, $\sigma \in (0,1]$, *and* $o^* > 0$, *we have*

$$ {}_0^C\mathbb{F}^\sigma \left(o(t) - o^* - o^* \ln \frac{o(t)}{o^*} \right) \leq \left(1 - \frac{o^*}{o(t)} \right) {}_0^C\mathbb{F}^\sigma o(t). $$

Lemma 4 *[43]. Let* $o(t) \in \mathbb{R}_+$ *be a continuous and differentiable function. Then, for any* $t \geq 0$ *and* $\sigma \in (0,1]$, *we have*

$$ \frac{1}{2} {}_0^C\mathbb{F}^\sigma o^2(t) \leq o(t) \, {}_0^C\mathbb{F}^\sigma o(t). $$

We will also need the following fractional version of the well-known LaSalle's invariance principle.

Lemma 5 *[44]. Suppose* $\mathcal{E}$ *is a bounded closed set. Every solution of system* ${}_0^C\mathbb{F}^\sigma x(t) = f(x(t))$ *starts from a point in* $\mathcal{E}$ *and remains in* $\mathcal{E}$ *for all time. If* $\exists\, \mathcal{L} \in C^1(\mathcal{E}, \mathbb{R})$ *such that* ${}_0^C\mathbb{F}^\sigma \mathcal{L}(x(t)) \leq 0$. *Let* $D = \left\{ x \in \mathcal{E} : {}_0^C\mathbb{F}^\sigma \mathcal{L} = 0 \right\}$ *and* $\mathcal{M}$ *be the largest invariant set of D. Then every solution* $x(t)$ *originating in* $\mathcal{E}$ *tends to* $\mathcal{M}$ *as* $t \to \infty$. *In particular, if* $\mathcal{M} = \{0\}$, $x(t) \to 0$ *as* $t \to \infty$.

Stability of the virus-clear steady point $\mathbb{S}^\circ$

Theorem 3 *If* $\mathcal{T}_\circ < 1$, *then* $\mathbb{S}^\circ$ *is locally asymptotically stable for all* $\sigma \in (0,1]$. $\mathbb{S}^\circ$ *is unstable if* $\mathcal{T}_\circ > 1$.

Proof The characteristic equation of the Jacobian matrix (3) at $\mathbb{S}^\circ$ is given by

$$ (\eta + \hbar_1)(\eta + \hbar_4) \left[\eta^2 + (\hbar_2 + \hbar_3 + \xi)\eta + \hbar_3(\hbar_2 + \xi) - \flat k\mathbf{U}^\circ \right] = 0. \tag{4} $$

Plainly, equation (4) has two negative real roots $\eta_1 = -\hbar_1$ and $\eta_2 = -\hbar_4$, then $\left|\arg(\eta_{1,2})\right| = \pi > \frac{\sigma\pi}{2}$ for any $\sigma \in (0,1]$. The other two roots of (4) are governed by the following equation:

$$ \eta^2 + (\hbar_2 + \hbar_3 + \xi)\eta + \hbar_3(\hbar_2 + \xi)(1 - \mathcal{T}_\circ) = 0, \tag{5} $$

which has, by the Routh-Hurwitz criterion, two roots η_i $(i = 3, 4)$ with negative real parts if $\mathcal{T}_\circ < 1$. Thus, $\left|\arg(\eta_{3,4})\right| > \frac{\pi}{2} \geq \frac{\sigma\pi}{2}$ for any $\sigma \in (0,1]$ when $\mathcal{T}_\circ < 1$. If $\mathcal{T}_\circ > 1$, then equation (5) admits a positive real root η^*, then $\left|\arg(\eta^*)\right| = 0 < \frac{\sigma\pi}{2}$ for all $\sigma \in (0,1]$. Consequently, by Lemma 2, $\mathbb{S}^\circ$ is unstable if $\mathcal{T}_\circ > 1$ and locally asymptotically stable if $\mathcal{T}_\circ < 1$. ■

Theorem 4 *If* $\mathcal{T}_\circ \leq 1$, *then* $\mathbb{S}^\circ$ *is globally asymptotically stable for all* $\sigma \in (0,1]$.

Proof Let $\mathcal{L}_{\star\star}$ be the Lyapunov functional defined as

$$ \mathcal{L}_{\star\star}(t) = \mathbf{U}^\circ H\left(\frac{\mathbf{U}(t)}{\mathbf{U}^\circ}\right) + \mathbf{X}(t) + \frac{\flat\mathbf{U}^\circ}{\hbar_3}\mathbf{Y}(t) + \frac{\flat p\mathbf{U}^\circ}{c\hbar_3}\mathbf{W}(t) + \frac{\xi}{2(\hbar_1 + \hbar_2)\mathbf{U}^\circ}\left(\mathbf{U}(t) - \mathbf{U}^\circ + \mathbf{X}(t)\right)^2, $$

where $H(x) = x - 1 - \ln x,\ x > 0$. According to Lemma 3 and Lemma 4, we obtain

$$\begin{aligned}
{}_0^{\mathcal{C}}\mathbb{F}^{\sigma}\mathcal{L}_{\star\star} &\leq \left(1 - \frac{\mathbf{U}^{\circ}}{\mathbf{U}}\right) {}_0^{\mathcal{C}}\mathbb{F}^{\sigma}\mathbf{U} + {}_0^{\mathcal{C}}\mathbb{F}^{\sigma}\mathbf{X} + \frac{\mathfrak{b}\mathbf{U}^{\circ}}{\mathfrak{h}_3}\, {}_0^{\mathcal{C}}\mathbb{F}^{\sigma}\mathbf{Y} + \frac{\mathfrak{b}p\mathbf{U}^{\circ}}{c\mathfrak{h}_3}\, {}_0^{\mathcal{C}}\mathbb{F}^{\sigma}\mathbf{W} \\
&\quad + \frac{\xi}{(\mathfrak{h}_1 + \mathfrak{h}_2)\mathbf{U}^{\circ}} (\mathbf{U} - \mathbf{U}^{\circ} + \mathbf{X}) \left({}_0^{\mathcal{C}}\mathbb{F}^{\sigma}\mathbf{U} + {}_0^{\mathcal{C}}\mathbb{F}^{\sigma}\mathbf{X}\right) \\
&= \left(1 - \frac{\mathbf{U}^{\circ}}{\mathbf{U}}\right) \left(\varphi - \mathfrak{h}_1\mathbf{U} - \frac{\mathfrak{b}\mathbf{U}\mathbf{Y}}{1 + q\mathbf{W}} + \xi\mathbf{X}\right) + \frac{\mathfrak{b}\mathbf{U}\mathbf{Y}}{1 + q\mathbf{W}} - (\mathfrak{h}_2 + \xi)\mathbf{X} \\
&\quad + \frac{\mathfrak{b}\mathbf{U}^{\circ}}{\mathfrak{h}_3} (k\mathbf{X} - \mathfrak{h}_3\mathbf{Y} - p\mathbf{Y}\mathbf{W}) + \frac{\mathfrak{b}p\mathbf{U}^{\circ}}{c\mathfrak{h}_3} (c\mathbf{Y}\mathbf{W} - \mathfrak{h}_4\mathbf{W}) + \frac{\xi}{(\mathfrak{h}_1 + \mathfrak{h}_2)\mathbf{U}^{\circ}} (\mathbf{U} - \mathbf{U}^{\circ} + \mathbf{X}) (\varphi - \mathfrak{h}_1\mathbf{U} - \mathfrak{h}_2\mathbf{X}) \\
&= -\mathfrak{h}_1 \frac{(\mathbf{U} - \mathbf{U}^{\circ})^2}{\mathbf{U}} + \xi\mathbf{X}\left(1 - \frac{\mathbf{U}^{\circ}}{\mathbf{U}}\right) + \frac{\mathfrak{b}\mathbf{U}^{\circ}\mathbf{Y}}{1 + q\mathbf{W}} - (\mathfrak{h}_2 + \xi)\mathbf{X} - \mathfrak{b}\mathbf{U}^{\circ}\mathbf{Y} + \frac{\mathfrak{b}k\mathbf{U}^{\circ}}{\mathfrak{h}_3}\mathbf{X} - \frac{\mathfrak{b}p\mathfrak{h}_4\mathbf{U}^{\circ}}{c\mathfrak{h}_3}\mathbf{W} \\
&\quad - \frac{\xi}{(\mathfrak{h}_1 + \mathfrak{h}_2)\mathbf{U}^{\circ}} (\mathbf{U} - \mathbf{U}^{\circ} + \mathbf{X}) \left(\mathfrak{h}_1 (\mathbf{U} - \mathbf{U}^{\circ}) + \mathfrak{h}_2\mathbf{X}\right) \\
&= -\left(\mathfrak{h}_1\mathbf{U}^{\circ} + \xi\mathbf{X} + \frac{\xi\mathfrak{h}_1\mathbf{U}}{\mathfrak{h}_1 + \mathfrak{h}_2}\right) \frac{(\mathbf{U} - \mathbf{U}^{\circ})^2}{\mathbf{U}\mathbf{U}^{\circ}} - \frac{\mathfrak{h}_2\xi\mathbf{X}^2}{(\mathfrak{h}_1 + \mathfrak{h}_2)\mathbf{U}^{\circ}} - \frac{\mathfrak{b}q\mathbf{U}^{\circ}\mathbf{Y}\mathbf{W}}{1 + q\mathbf{W}} - \frac{\mathfrak{b}p\mathfrak{h}_4\mathbf{U}^{\circ}\mathbf{W}}{c\mathfrak{h}_3} + (\mathfrak{h}_2 + \xi)(\mathcal{T}_{\circ} - 1)\mathbf{X}.
\end{aligned}$$

Therefore, $\mathcal{T}_{\circ} \leq 1$ ensures that ${}_0^{\mathcal{C}}\mathbb{F}^{\sigma}\mathcal{L}_{\star\star} \leq 0$. Furthermore, it is easy to verify that the singleton $\{\mathbb{S}^{\circ}\}$ is the largest compact invariant set in $\left\{(\mathbf{U}, \mathbf{X}, \mathbf{Y}, \mathbf{W}) \in \mathbb{R}_+^4 : {}_0^{\mathcal{C}}\mathbb{F}^{\sigma}\mathcal{L}_{\star\star} = 0\right\}$. By Lemma 5, we infer that $\mathbb{S}^{\circ}$ is globally asymptotically stable if $\mathcal{T}_{\circ} \leq 1$ for all $\sigma \in (0, 1]$. ■

Stability of the immune-free steady point $\mathbb{S}_1^{\star}$

This subsection aims to analyze the stability of the immune-free steady point $\mathbb{S}_1^{\star}$ of the system (2). Obviously, we presume that $\mathcal{T}_{\circ} > 1$.

Theorem 5 *If $\mathcal{T}_1 < 1 < \mathcal{T}_{\circ}$, then $\mathbb{S}_1^{\star}$ is locally asymptotically stable for all $\sigma \in (0, 1]$. $\mathbb{S}_1^{\star}$ is unstable if $\mathcal{T}_1 > 1$.*

Proof At $\mathbb{S}_1^{\star}$, the characteristic equation of the Jacobian matrix (3) is given by

$$(\eta + \mathfrak{h}_4 - c\mathbf{Y}_1^{\star}) \left(\eta^3 + \Pi_2\eta^2 + \Pi_1\eta + \Pi_0\right) = 0, \tag{6}$$

where

$$\begin{aligned}
\Pi_2 &= \mathfrak{h}_1 + \mathfrak{h}_2 + \mathfrak{h}_3 + \xi + \mathfrak{b}\mathbf{Y}_1^{\star}, \\
\Pi_1 &= \mathfrak{h}_1 (\mathfrak{h}_2 + \mathfrak{h}_3 + \xi) + \mathfrak{b}\mathbf{Y}_1^{\star} (\mathfrak{h}_2 + \mathfrak{h}_3), \\
\Pi_0 &= \mathfrak{h}_2\mathfrak{h}_3\mathfrak{b}\mathbf{Y}_1^{\star}.
\end{aligned}$$

One of the roots of equation (6) is $\eta_1 = c\mathbf{Y}_1^{\star} - \mathfrak{h}_4 = \mathfrak{h}_4 (\mathcal{T}_1 - 1)$. Hence, $|\arg(\eta_1)| = \pi > \frac{\sigma\pi}{2}$ for all $\sigma \in (0, 1]$ if $\mathcal{T}_1 < 1$ and $|\arg(\eta_1)| = 0 < \frac{\sigma\pi}{2}$ for all $\sigma \in (0, 1]$ if $\mathcal{T}_1 > 1$. While the remaining roots are given by the solution to the following equation:

$$\eta^3 + \Pi_2\eta^2 + \Pi_1\eta + \Pi_0 = 0. \tag{7}$$

It is easy to remark that $\Pi_2 > 0$, $\Pi_1 > 0$ and $\Pi_0 > 0$. Therefore,

$$\Pi_2\Pi_1 - \Pi_0 = (\mathfrak{h}_1 + \mathfrak{h}_2 + \xi + \mathfrak{b}\mathbf{Y}_1^{\star}) \Pi_1 + \mathfrak{h}_1\mathfrak{h}_3 (\mathfrak{h}_2 + \mathfrak{h}_3 + \xi) + \mathfrak{h}_3^2\mathfrak{b}\mathbf{Y}_1^{\star} > 0.$$

Thus, by the Routh-Hurwitz criterion, all roots η_i $(i = 2, 3, 4)$ of (7) have negative real part, so that $|\arg(\eta_{2,3,4})| > \frac{\pi}{2} \geq \frac{\sigma\pi}{2}$ for all $\sigma \in (0, 1]$ if $\mathcal{T}_{\circ} > 1$. In accordance with Lemma 1, $\mathbb{S}_1^{\star}$ is unstable if $\mathcal{T}_1 > 1$ and locally asymptotically stable if $\mathcal{T}_1 < 1 < \mathcal{T}_{\circ}$. ■

Next, we analyze the global stability of $\mathbb{S}_1^{\star}$ by assuming the following hypothesis

$$\frac{\mathbf{Y}_1^{\star}}{\mathbf{Y}} - \frac{1}{1 + q\mathbf{W}} \leq 0. \tag{$\mathcal{H}$}$$

Theorem 6 *If $\mathcal{T}_1 \leq 1 < \mathcal{T}_{\circ} \leq 1 + \frac{\mathfrak{h}_2}{\xi}$ and $(\mathcal{H})$ holds, then $\mathbb{S}_1^{\star}$ is globally asymptotically stable for any $\sigma \in (0, 1]$.*

Proof Let $\mathcal{L}_{\dagger}$ be the Lyapunov functional defined as

$$\begin{aligned}
\mathcal{L}_{\dagger}(t) &= \mathbf{U}_1^{\star} H\left(\frac{\mathbf{U}(t)}{\mathbf{U}_1^{\star}}\right) + \mathbf{X}_1^{\star} H\left(\frac{\mathbf{X}(t)}{\mathbf{X}_1^{\star}}\right) + \frac{\mathfrak{b}\mathbf{U}_1^{\star}\mathbf{Y}_1^{\star}}{k\mathbf{X}_1^{\star}} \mathbf{Y}_1^{\star} H\left(\frac{\mathbf{Y}(t)}{\mathbf{Y}_1^{\star}}\right) + \frac{\mathfrak{b}p\mathbf{U}_1^{\star}\mathbf{Y}_1^{\star}}{ck\mathbf{X}_1^{\star}} \mathbf{W}(t) \\
&\quad + \frac{\xi}{2(\mathfrak{h}_1 + \mathfrak{h}_2)\mathbf{U}_1^{\star}} (\mathbf{U}(t) - \mathbf{U}_1^{\star} + \mathbf{X}(t) - \mathbf{X}_1^{\star})^2.
\end{aligned}$$

Applying the Caputo fractional derivative on system (2), we obtain

$$\begin{aligned}
{}_0^C\mathbb{F}^\sigma \mathcal{L}_\dagger \leq & \left(1-\frac{\mathbf{U}_1^\star}{\mathbf{U}}\right) {}_0^C\mathbb{F}^\sigma \mathbf{U} + \left(1-\frac{\mathbf{X}_1^\star}{\mathbf{X}}\right) {}_0^C\mathbb{F}^\sigma \mathbf{X} + \frac{\mathfrak{b}\mathbf{U}_1^\star\mathbf{Y}_1^\star}{k\mathbf{X}_1^\star}\left(1-\frac{\mathbf{Y}_1^\star}{\mathbf{Y}}\right) {}_0^C\mathbb{F}^\sigma \mathbf{Y} + \frac{\mathfrak{b}p\mathbf{U}_1^\star\mathbf{Y}_1^\star}{ck\mathbf{X}_1^\star} {}_0^C\mathbb{F}^\sigma \mathbf{W} \\
& + \frac{\xi}{(\mathfrak{h}_1+\mathfrak{h}_2)\mathbf{U}_1^\star}(\mathbf{U}-\mathbf{U}_1^\star+\mathbf{X}-\mathbf{X}_1^\star)\left({}_0^C\mathbb{F}^\sigma \mathbf{U} + {}_0^C\mathbb{F}^\sigma \mathbf{X}\right) \\
= & \left(1-\frac{\mathbf{U}_1^\star}{\mathbf{U}}\right)\left(\varphi-\mathfrak{h}_1\mathbf{U}-\frac{\mathfrak{b}\mathbf{U}\mathbf{Y}}{1+q\mathbf{W}}+\xi\mathbf{X}\right)+\left(1-\frac{\mathbf{X}_1^\star}{\mathbf{X}}\right)\left(\frac{\mathfrak{b}\mathbf{U}\mathbf{Y}}{1+q\mathbf{W}}-(\mathfrak{h}_2+\xi)\mathbf{X}\right) \\
& + \frac{\mathfrak{b}\mathbf{U}_1^\star\mathbf{Y}_1^\star}{k\mathbf{X}_1^\star}\left(1-\frac{\mathbf{Y}_1^\star}{\mathbf{Y}}\right)(k\mathbf{X}-\mathfrak{h}_3\mathbf{Y}-p\mathbf{Y}\mathbf{W})+\frac{\mathfrak{b}p\mathbf{U}_1^\star\mathbf{Y}_1^\star}{ck\mathbf{X}_1^\star}(c\mathbf{Y}\mathbf{W}-\mathfrak{h}_4\mathbf{W}) \\
& + \frac{\xi}{(\mathfrak{h}_1+\mathfrak{h}_2)\mathbf{U}_1^\star}(\mathbf{U}-\mathbf{U}_1^\star+\mathbf{X}-\mathbf{X}_1^\star)(\varphi-\mathfrak{h}_1\mathbf{U}-\mathfrak{h}_2\mathbf{X}).
\end{aligned}$$

Note that $\varphi = \mathfrak{h}_1\mathbf{U}_1^\star + \mathfrak{b}\mathbf{U}_1^\star\mathbf{Y}_1^\star - \xi\mathbf{X}_1^\star$, $\mathfrak{h}_2 + \xi = \frac{\mathfrak{b}\mathbf{U}_1^\star\mathbf{Y}_1^\star}{\mathbf{X}_1^\star}$ and $\mathfrak{h}_3 = \frac{k\mathbf{X}_1^\star}{\mathbf{Y}_1^\star}$. Therefore,

$$\begin{aligned}
{}_0^C\mathbb{F}^\sigma \mathcal{L}_\dagger \leq & \mathfrak{h}_1\left(1-\frac{\mathbf{U}_1^\star}{\mathbf{U}}\right)(\mathbf{U}_1^\star-\mathbf{U})+\xi(\mathbf{X}-\mathbf{X}_1^\star)\left(1-\frac{\mathbf{U}_1^\star}{\mathbf{U}}\right) \\
& + \mathfrak{b}\mathbf{U}_1^\star\mathbf{Y}_1^\star\left(3-\frac{\mathbf{U}_1^\star}{\mathbf{U}}+\frac{\mathbf{Y}}{\mathbf{Y}_1^\star}\frac{1}{1+q\mathbf{W}}-\frac{\mathbf{U}\mathbf{X}_1^\star\mathbf{Y}}{\mathbf{U}_1^\star\mathbf{X}\mathbf{Y}_1^\star}\frac{1}{1+q\mathbf{W}}-\frac{\mathbf{Y}}{\mathbf{Y}_1^\star}-\frac{\mathbf{X}\mathbf{Y}_1^\star}{\mathbf{X}_1^\star\mathbf{Y}}\right) \\
& + \frac{\mathfrak{b}p\mathbf{U}_1^\star\mathbf{Y}_1^\star}{k\mathbf{X}_1^\star}\left(\mathbf{Y}_1^\star-\frac{\mathfrak{h}_4}{c}\right)\mathbf{W}-\frac{\xi}{(\mathfrak{h}_1+\mathfrak{h}_2)\mathbf{U}_1^\star}(\mathbf{U}-\mathbf{U}_1^\star+\mathbf{X}-\mathbf{X}_1^\star)(\mathfrak{h}_1(\mathbf{U}-\mathbf{U}_1^\star)+\mathfrak{h}_2(\mathbf{X}-\mathbf{X}_1^\star)) \\
= & -\left(\mathfrak{h}_1\mathbf{U}_1^\star+\xi\mathbf{X}-\xi\mathbf{X}_1^\star+\frac{\xi\mathfrak{h}_1\mathbf{U}}{\mathfrak{h}_1+\mathfrak{h}_2}\right)\frac{(\mathbf{U}-\mathbf{U}_1^\star)^2}{\mathbf{U}\mathbf{U}_1^\star}-\frac{\xi\mathfrak{h}_2}{(\mathfrak{h}_1+\mathfrak{h}_2)\mathbf{U}_1^\star}(\mathbf{X}-\mathbf{X}_1^\star)^2 \\
& + \mathfrak{b}\mathbf{U}_1^\star\mathbf{Y}_1^\star\left(4-\frac{\mathbf{U}_1^\star}{\mathbf{U}}-(1+q\mathbf{W})-\frac{\mathbf{U}\mathbf{X}_1^\star\mathbf{Y}}{\mathbf{U}_1^\star\mathbf{X}\mathbf{Y}_1^\star}\frac{1}{1+q\mathbf{W}}-\frac{\mathbf{X}\mathbf{Y}_1^\star}{\mathbf{X}_1^\star\mathbf{Y}}\right) \\
& + \mathfrak{b}q\mathbf{U}_1^\star\mathbf{Y}_1^\star\left(1-\frac{\mathbf{Y}}{\mathbf{Y}_1^\star}\frac{1}{1+q\mathbf{W}}\right)\mathbf{W}+\frac{\mathfrak{h}_4\mathfrak{b}p\mathbf{U}_1^\star\mathbf{Y}_1^\star}{ck\mathbf{X}_1^\star}(\mathcal{T}_1-1)\mathbf{W}.
\end{aligned}$$

Employing the arithmetic-geometric means inequality, we obtain

$$4-\frac{\mathbf{U}_1^\star}{\mathbf{U}}-(1+q\mathbf{W})-\frac{\mathbf{U}\mathbf{X}_1^\star\mathbf{Y}}{\mathbf{U}_1^\star\mathbf{X}\mathbf{Y}_1^\star}\frac{1}{1+q\mathbf{W}}-\frac{\mathbf{X}\mathbf{Y}_1^\star}{\mathbf{X}_1^\star\mathbf{Y}}\leq 0.$$

From $(\mathcal{H})$, we have

$$1-\frac{\mathbf{Y}}{\mathbf{Y}_1^\star}\frac{1}{1+q\mathbf{W}}=\frac{\mathbf{Y}}{\mathbf{Y}_1^\star}\left(\frac{\mathbf{Y}_1^\star}{\mathbf{Y}}-\frac{1}{1+q\mathbf{W}}\right)\leq 0.$$

Further, we have

$$\mathfrak{h}_1\mathbf{U}_1^\star-\xi\mathbf{X}_1^\star=\frac{\mathfrak{h}_1\mathfrak{h}_3(\mathfrak{h}_2+\xi)}{\mathfrak{b}k}\left(1-\frac{\xi}{\mathfrak{h}_2}(\mathcal{T}_\circ-1)\right).$$

Thus, ${}_0^C\mathbb{F}^\sigma \mathcal{L}_\dagger \leq 0$ if $\mathcal{T}_1 \leq 1 < \mathcal{T}_\circ \leq 1+\frac{\mathfrak{h}_2}{\xi}$. Furthermore, the largest compact invariant set in $\left\{(\mathbf{U},\mathbf{X},\mathbf{Y},\mathbf{W})\in\mathbb{R}_+^4 : {}_0^C\mathbb{F}^\sigma \mathcal{L}_\dagger = 0\right\}$ is singleton $\{\mathbb{S}_1^\star\}$. By Lemma 5, $\mathbb{S}_1^\star$ is globally asymptotically stable if $\mathcal{T}_1 \leq 1 < \mathcal{T}_\circ \leq 1+\frac{\mathfrak{h}_2}{\xi}$. ■

Stability of immunity-activated steady point with humoral response $\mathbb{S}_2^\star$

In this subsection, we deal with the local stability of the steady point $\mathbb{S}_2^\star$. We begin our analysis by computing the characteristic equation of the Jacobian matrix (3) at $\mathbb{S}_2^\star$, we find

$$\eta^4+\mathcal{O}_3\eta^3+\mathcal{O}_2\eta^2+\mathcal{O}_1\eta+\mathcal{O}_0=0, \tag{8}$$

where

$$\begin{aligned}
\mathcal{O}_3 &= \mathfrak{h}_1+\mathfrak{h}_2+\mathfrak{h}_3+\xi+p\mathbf{W}_2^\star+\frac{\mathfrak{b}\mathbf{Y}_2^\star}{1+q\mathbf{W}_2^\star}>0, \\
\mathcal{O}_2 &= \mathfrak{h}_4p\mathbf{W}_2^\star+\mathfrak{h}_1(\mathfrak{h}_2+\mathfrak{h}_3+\xi+p\mathbf{W}_2^\star)+\frac{\mathfrak{b}\mathbf{Y}_2^\star}{1+q\mathbf{W}_2^\star}(\mathfrak{h}_2+\mathfrak{h}_3+p\mathbf{W}_2^\star)>0, \\
\mathcal{O}_1 &= \mathfrak{h}_4p\mathbf{W}_2^\star(\mathfrak{h}_1+\mathfrak{h}_2+\xi)+\frac{\mathfrak{b}\mathbf{Y}_2^\star}{1+q\mathbf{W}_2^\star}(\mathfrak{h}_4p\mathbf{W}_2^\star+\mathfrak{h}_2(\mathfrak{h}_3+p\mathbf{W}_2^\star))+\frac{kcq\mathfrak{b}\mathbf{U}_2^\star\mathbf{Y}_2^\star\mathbf{W}_2^\star}{(1+q\mathbf{W}_2^\star)^2}>0, \\
\mathcal{O}_0 &= \mathfrak{h}_1\mathfrak{h}_4p\mathbf{W}_2^\star(\mathfrak{h}_2+\xi)+\mathfrak{h}_2\mathfrak{h}_4p\mathbf{W}_2^\star\frac{\mathfrak{b}\mathbf{Y}_2^\star}{1+q\mathbf{W}_2^\star}+\mathfrak{h}_1kc\frac{\mathfrak{b}q\mathbf{U}_2^\star\mathbf{Y}_2^\star\mathbf{W}_2^\star}{(1+q\mathbf{W}_2^\star)^2}>0.
\end{aligned}$$

Thus, by the Routh-Hurwitz criterion, all roots η_j $(j = 1, 2, 3, 4)$ of (8) have negative real part if

$$\mathcal{O}_3\mathcal{O}_2 - \mathcal{O}_1 > 0 \quad \text{and} \quad \mathcal{O}_1\left(\mathcal{O}_3\mathcal{O}_2 - \mathcal{O}_1\right) - \mathcal{O}_3^2\mathcal{O}_0 > 0, \tag{9}$$

so that $\left|\arg(\eta_j)\right| > \frac{\pi}{2} \geq \frac{\sigma\pi}{2}$ for all $\sigma \in (0, 1]$ if $\mathcal{T}_1 > 1$. Hence, according to Lemma 1, we have the following theorem.

Theorem 7 *Assume that $\mathcal{T}_1 > 1$ and the condition (9) holds, then $\mathbb{S}_2^\star$ is locally asymptotically stable for all $\sigma \in (0, 1]$.*

Remark 1 *Theorems 3, 4, 5, 6 and 7 indicate theoretically that the Caputo derivatives have no influence on the stability of the equilibria $\mathbb{S}^\circ$, $\mathbb{S}_1^\star$ and $\mathbb{S}_2^\star$.*

4 Numerical results and discussions

In this section, and by utilizing the parameter values of the data listed in Table 1, we discuss the different results established previously in this article. The pivotal purpose is to examine the influence of fractional derivatives on the long-run behavior of our enhanced model (2). We will theoretically choose the parameters used in the simulations according to two criteria:
1. To verify and check appropriately the obtained analytical results in all cases.
2. To show numerically the sharpness of the obtained stability conditions. During the forthcoming numerical tests, the solution of our viral system (2) is supposed to be starting from the initial condition $\mathbf{U}(0) = 300$, $\mathbf{X}(0) = 7$, $\mathbf{Y}(0) = 4$, $\mathbf{W}(0) = 80$. Also, we deem from now on that the unity of time is one day.

Parameter	*Example 1*	*Example 2*	*Example 3*	*Source*
φ	2	2	6	Assumed
$\hbar_1$	0.01	0.01	0.01	[4]
$\mathfrak{b}$	0.01	0.02	0.02	[4]
q	0.5	0.5	0.5	[4]
ξ	0.01	0.01	0.01	[4]
$\hbar_2$	1.001	1.001	1.001	Assumed
$\hbar_3$	2.0003	2.0003	2.0003	Assumed
$\hbar_4$	0.3	0.3	0.3	[4]
k	0.9	2.9	2.9	Assumed
p	0.006	0.006	0.006	Assumed
c	0.1	0.1	0.1	[4]

Table 1. Some numerical values of the deterministic parameters used in the simulations

Remark 2 *In this section, we aim to numerically examine the impact of fractional derivatives on the long-term characteristics of the virus. For this reason, we simulate its progression using the parameters listed in Table 1. We mention that the parameters φ, $\mathfrak{b}$ and k are very sensitive and a slight variation in their values results in a significant dynamical bifurcation. Thus, we present some simulated scenarios in order to cover all cases of equilibrium stability.*

Example 1: Virus-clear steady point $\mathbb{S}^\circ$

To numerically probe the effect of fractional derivatives on the infection stability, we firstly assign to our system parameters the numerical values appearing in Table 1 - Example 1. A simple calculation gives $\mathcal{T}_\circ = 0.8911$ which is strictly less than one. From Theorem 2, there exists a virus-clear steady point $\mathbb{S}^\circ = (200, 0, 0, 0)$ of system (2). By choosing some arbitrary values of σ: 0.98; 0.94; 0.9; 0.88; 0.84; 0.8; 0.78; 0.76, we present the long-run behavior of the solutions in Figure 2. Specifically, in the case of $\sigma = 0.98$, we remark that the density of susceptible cells $\mathbf{U}$, after an initial slope, progressively rises and reaches the steady value $\frac{\varphi}{\hbar_1} = 200$. After a significant decrease followed by a gradual increase, the densities of $\mathbf{X}(t)$ and $\mathbf{Y}(t)$ return to decrease and end up being disappeared over time, while the density of $\mathbf{W}(t)$ decreases and converges to zero.
Now, by decreasing the value of σ to 0.94, we show that the solution suddenly changes its behavior shape, but finally converges to $\mathbb{S}^\circ$. To further exhibit this phenomenon, we choose various values between $\sigma = 0.94$ and $\sigma = 0.76$. We conclude that as the value of σ decreases, the solution slowly reaches the equilibrium $\mathbb{S}^\circ$. That is, the rate of convergence increases as the integer-order σ is closer to one. But, in all cases, solutions with different differentiation values reach the virus-clear state which actually confirms the result of Theorem 3. Consequently, the infection will be eradicated from the host body.

Example 2: Immune-free steady point $\mathbb{S}_1^\star$

In this example, we select the parameter values from Table 1 - Example 2. Then, we obtain $\mathcal{T}_\circ = 5.7426 > 1$ and $\mathcal{T}_1 = 0.7983 < 1$. In accordance with Theorem 2, the immune-free steady point $\mathbb{S}_1^\star$ exists since $\mathcal{T}_1 < 1 < \mathcal{T}_\circ$. To depict the effect of fractional derivatives on $\mathbb{S}_1^\star$, we arbitrarily select certain values of $\sigma = 0.98; 0.94; 0.9; 0.88; 0.84; 0.8; 0.78; 0.76$. In Figure 3, we see that after some pseudo periodic fluctuations, the densities of $\mathbf{U}(t)$, $\mathbf{X}(t)$ and $\mathbf{Y}(t)$ reach the stable level $\mathbf{U}_1^\star = 34.8276$, $\mathbf{X}_1^\star = 1.6517$ and $\mathbf{Y}_1^\star = 2.3950$, while the density of $\mathbf{W}(t)$ ultimately extinct. Since $\mathcal{T}_1 < 1 < \mathcal{T}_\circ$, the numerical outcome of this example confirms the stability result of Theorem 5. Hence, the infection becomes chronic one in the absence of persistent humoral immune response.

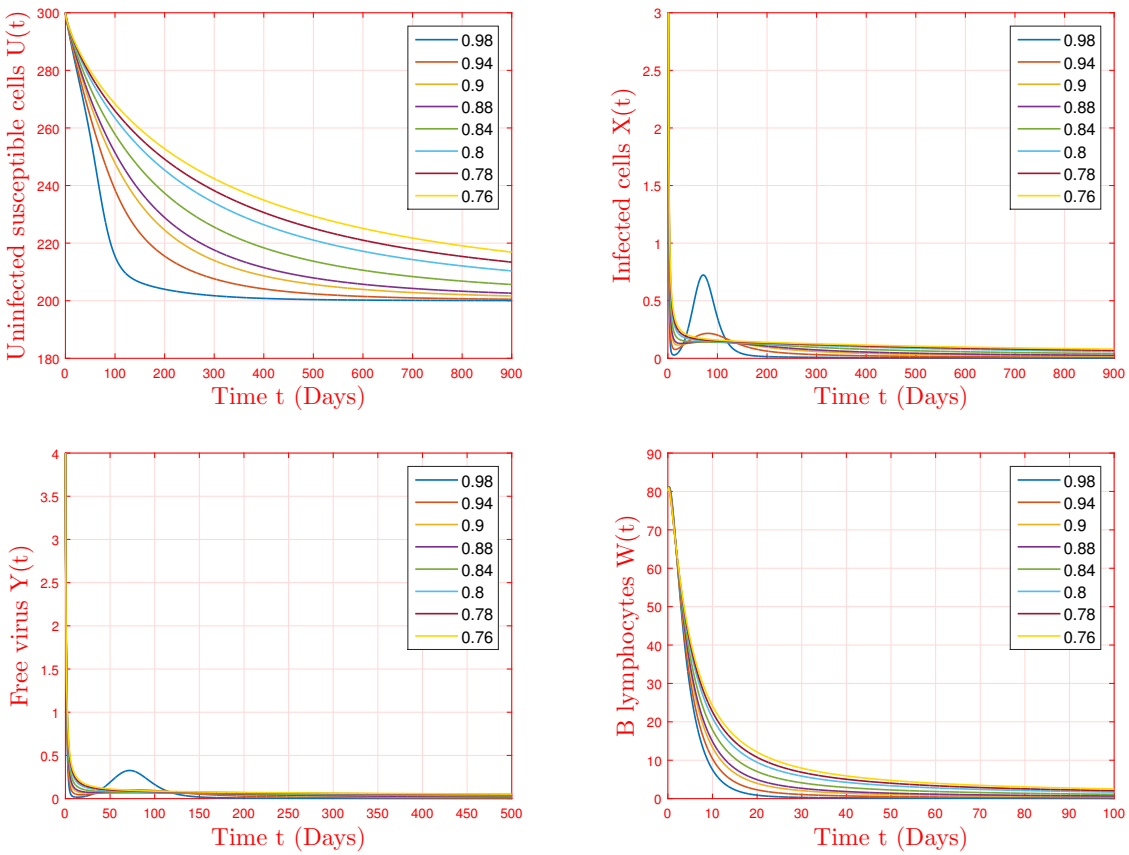

Figure 2. *Stability of the virus-clear steady point* $\mathbb{S}^{\circ} = (200, 0, 0, 0)$ *for different values of* $\sigma = 0.98; 0.94; 0.9; 0.88; 0.84; 0.8; 0.78; 0.76$.

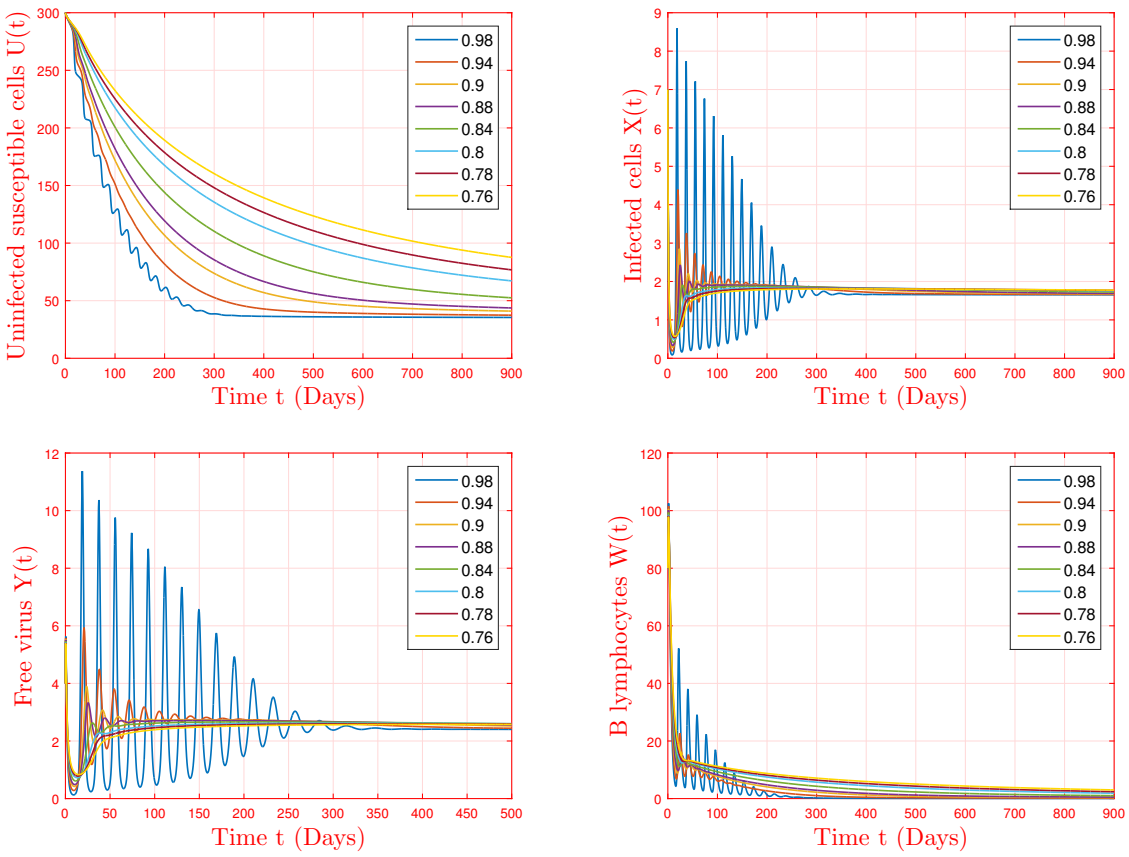

Figure 3. *Stability of the immune-free steady point* $\mathbb{S}_1^{\star} = (34.8276, 1.6517, 2.3950, 0)$ *for different values of* $\sigma = 0.98; 0.94; 0.9; 0.88; 0.84; 0.8; 0.78; 0.76$.

Example 3: Immunity-activated steady point with the humoral response $\mathbb{S}_2^\star$

Now, we choose the parameter values from Table 1 - Example 3. Then, we obtain $\mathcal{T}_1 = 2.7317 > 1$. In accordance with Theorem 2, there is an immunity-activated steady point with the humoral response $\mathbb{S}_2^\star$. Furthermore, we get

$$\mathcal{O}_3\mathcal{O}_2 - \mathcal{O}_1 = 0.3648 > 0,$$
$$\mathcal{O}_1\left(\mathcal{O}_3\mathcal{O}_2 - \mathcal{O}_1\right) - \mathcal{O}_3^2\mathcal{O}_0 = 0.2903 > 0,$$

then $\mathbb{S}_2^\star$ is asymptotically stable for different values of σ due to Theorem 7. From Figure 4, we remark that all classes fluctuate during a time phase then converge towards the steady values $\mathbf{U}_2^\star = 381.4716$, $\mathbf{X}_2^\star = 2.1853$, $\mathbf{Y}_2^\star = 3.0000$ and $\mathbf{W}_2^\star = 18.7403$. By selecting certain values of σ, we observe that the solutions always reach the steady point $\mathbb{S}_2^\star = (\mathbf{U}_2^\star, \mathbf{X}_2^\star, \mathbf{Y}_2^\star, \mathbf{W}_2^\star)$. Thus, the viral infection becomes chronic with persistent humoral immune response.

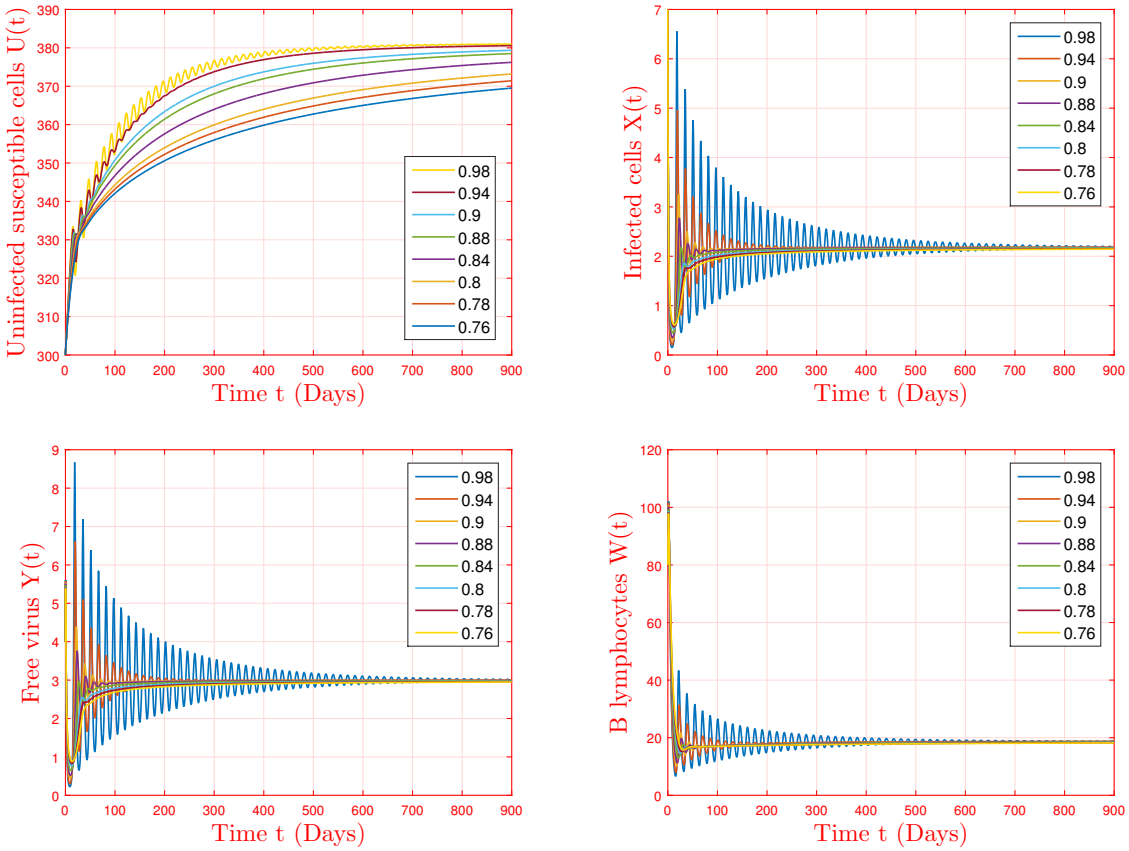

Figure 4. *Stability of the immunity-activated steady point with the humoral response* $\mathbb{S}_2^\star = (381.4716, 2.1853, 3.0000, 18.7403)$ *for different values of* $\sigma = 0.98; 0.94; 0.9; 0.88; 0.84; 0.8; 0.78; 0.76$.

5 Conclusion

This article investigated an improved four-compartment viral system that takes into consideration the effects of fractional derivatives. The central goal was to probe the long-term characteristics of the virus. For this reason, we have started by proved the well-posedness of the model, including existence, uniqueness, nonnegativity and boundedness of solutions. We have defined the steady points of the system and determining the associated critical thresholds, namely the basic reproduction number, $\mathcal{T}_\circ$, and the humoral immune response reproduction number, $\mathcal{T}_1$. Specifically, we have proved that our viral model admits three steady points, and under certain conditions on the thresholds, the asymptotic stability of all these points was examined. The obtained results of stability indicate that the infection level gets reduced to zero for $\mathcal{T}_\circ \leq 1$, whereas the infection persists in the host body for $\mathcal{T}_1 > 1$. From the theoretical and numerical point of view, we concluded that Caputo derivatives have no influence on the stability of the equilibria.

As a future study, we seek to extend our proposed model to the case of the fractal-fractional system with the use of Adams-Bashforth numerical scheme [45, 46]. This special derivative is widely introduced in physics to explain various phenomena and laws. Also, the proposed model in this study can be enhanced by considering the effect of randomness. By using the approaches presented in [47, 48, 49, 50], we can simultaneously probe the effect of both memory and stochasticity on the viral dynamics. We will deal with it in our next work.

Declarations

Consent for publication

Not applicable.

Conflicts of interest

The authors declare that they have no conflict of interests.

Funding

Not applicable.

Author's contributions

M.N.: Conceptualization, Methodology, Writing-Original draft. Y.S.: Data Curation, Writing-Original draft, Software, Validation. A.Z.: Visualization, Investigation, Writing-Reviewing and Editing.

References

[1] Wang, S., & Zou, D. Global stability of in-host viral models with humoral immunity and intracellular delays. *Applied Mathematical Modelling*, 36(3), 1313-1322, (2012). [CrossRef]
[2] Wang, T., Hu, Z., Liao, F., & Ma, W. Global stability analysis for delayed virus infection model with general incidence rate and humoral immunity. *Mathematics and Computers in Simulation*, 89, 13-22, (2013). [CrossRef]
[3] Elaiw, A. M. Global stability analysis of humoral immunity virus dynamics model including latently infected cells. *Journal of biological dynamics*, 9(1), 215-228, (2015). [CrossRef]
[4] Dhar, M., Samaddar, S., & Bhattacharya, P. Modeling the effect of non-cytolytic immune response on viral infection dynamics in the presence of humoral immunity. *Nonlinear Dynamics*, 98(1), 637-655, (2019). [CrossRef]
[5] Hattaf, K., & Yousfi, N. Dynamics of SARS-CoV-2 infection model with two modes of transmission and immune response. *Math. Biosci. Eng*, 17(5), 5326-5340, (2020). [CrossRef]
[6] Wodarz, D., Christensen, J.P., & Thomsen, A.R. The importance of lytic and nonlytic immune responses in viral infections. *Trends in Immunology*, 23(4), 194-200, (2002). [CrossRef]
[7] Hollenberg, M.D., & Epstein, M. The innate immune response, microenvironment proteinases, and the COVID-19 pandemic: pathophysiologic mechanisms and emerging therapeutic targets. *Kidney International Supplements*, 12(1), 48-62, (2022). [CrossRef]
[8] Prakasha, D.G., Malagi, N.S., Veeresha, P., & Prasannakumara, B.C. An efficient computational technique for time-fractional Kaup-Kupershmidt equation. *Numerical Methods for Partial Differential Equations*, 37(2), 1299-1316, (2021). [CrossRef]
[9] Prakasha, D.G., Malagi, N.S., & Veeresha, P. New approach for fractional Schrödinger-Boussinesq equations with Mittag-Leffler kernel. *Mathematical Methods in the Applied Sciences*, 43(17), 9654-9670, (2020). [CrossRef]
[10] Baishya, C., & Veeresha, P. Laguerre polynomial-based operational matrix of integration for solving fractional differential equations with non-singular kernel. *Proceedings of the Royal Society A*, 477(2253), 20210438, (2021). [CrossRef]
[11] Fan, Y., Huang, X., Wang, Z., & Li, Y. Nonlinear dynamics and chaos in a simplified memristor-based fractional-order neural network with discontinuous memductance function. *Nonlinear Dynamics*, 93(2), 611-627, (2018). [CrossRef]
[12] Fan, Y., Huang, X., Wang, Z., & Li, Y. Global dissipativity and quasi-synchronization of asynchronous updating fractional-order memristor-based neural networks via interval matrix method. *Journal of the Franklin Institute*, 355(13), 5998-6025, (2018). [CrossRef]
[13] Agarwal, P., Baleanu, D., Chen, Y., Momani, S., & Machado, J. A. T. (Eds.). Fractional Calculus: ICFDA 2018, Amman, Jordan, July 16-18. Berlin, Germany: Springer, vol.303, (2019).
[14] Agarwal, P., Deniz, S., Jain, S., Alderremy, A.A., & Aly, S. A new analysis of a partial differential equation arising in biology and population genetics via semi analytical techniques. *Physica A: Statistical Mechanics and its Applications*, 542, 122769, (2020). [CrossRef]
[15] Song, L., Xu, S., & Yang, J. Dynamical models of happiness with fractional order. *Communications in Nonlinear Science and Numerical Simulation*, 15(3), 616-628, (2010). [CrossRef]
[16] Magin, L.R. Fractional calculus in Bioengineering, Part 1. *Critical Reviews in Biomedical Engineering*, 32(1), 1–104, (2004).
[17] Sadek, O., Sadek, L., Touhtouh, S., & Hajjaji, A. The mathematical fractional modeling of TiO-2 nanopowder synthesis by sol–gel method at low temperature, *Mathematical Modeling and Computing*, 9(3), 616–626, (2022). [CrossRef]
[18] Naik, P.A., Yavuz, M., Qureshi, S., Zu, J., & Townley, S. Modeling and analysis of COVID-19 epidemics with treatment in fractional derivatives using real data from Pakistan. *The European Physical Journal Plus*, 135(10), 1-42, (2020). [CrossRef]
[19] Özköse, F., Şenel, M.T., & Habbireeh, R. Fractional-order mathematical modelling of cancer cells-cancer stem cells-immune system interaction with chemotherapy. *Mathematical Modelling and Numerical Simulation with Applications*, 1(2), 67-83, (2021). [CrossRef]
[20] Özköse, F., Yavuz, M., Şenel, M.T., & Habbireeh, R. Fractional order modelling of omicron SARS-CoV-2 variant containing heart attack effect using real data from the United Kingdom. *Chaos, Solitons & Fractals*, 157, 111954, (2022). [CrossRef]
[21] Din, A., & Abidin, M.Z. Analysis of fractional-order vaccinated Hepatitis-B epidemic model with Mittag-Leffler kernels. *Mathematical Modelling and Numerical Simulation with Applications*, 2(2), 59-72, (2022). [CrossRef]

[22] Fatmawati, M.A.K., Bonyah, E., Hammouch, Z., & Shaiful, E.M. A mathematical model of tuberculosis (TB) transmission with children and adults groups: A fractional model. *AIMS Mathematics*, 5(4), 2813-2842, (2020). [CrossRef]
[23] M. Naim, F. Lahmidi, and A. Namir. *Global stability of a fractional order SIR epidemic model with double epidemic hypothesis and nonlinear incidence rate*. Communications in Mathematical Biology and Neuroscience, vol. 2020, Art. ID 38, 2020.
[24] Naim, M., Lahmidi, F., Namir, A., & Kouidere, A. Dynamics of an fractional SEIR epidemic model with infectivity in latent period and general nonlinear incidence rate. *Chaos, Solitons & Fractals*, 152, 111456, (2021). [CrossRef]
[25] Gholami, M., Ghaziani, R.K., & Eskandari, Z. Three-dimensional fractional system with the stability condition and chaos control. *Mathematical Modelling and Numerical Simulation with Applications*, 2(1), 41-47, (2022). [CrossRef]
[26] Zahid, A., Masood, S., Mubarik, S., & Din, A. An efficient application of scrambled response approach to estimate the population mean of the sensitive variables. *Mathematical Modelling and Numerical Simulation with Applications*, 2(3), 127-146, (2022). [CrossRef]
[27] Din, A., & Abidin, M.Z. Analysis of fractional-order vaccinated Hepatitis-B epidemic model with Mittag-Leffler kernels. *Mathematical Modelling and Numerical Simulation with Applications*, 2(2), 59-72, (2022). [CrossRef]
[28] Sene, N. Second-grade fluid with Newtonian heating under Caputo fractional derivative: Analytical investigations via Laplace transforms. *Mathematical Modelling and Numerical Simulation with Applications*, 2(1), 13-25, (2022). [CrossRef]
[29] Kumar, P., & Erturk, V.S. Dynamics of cholera disease by using two recent fractional numerical methods. *Mathematical Modelling and Numerical Simulation with Applications*, 1(2), 102-111, (2021). [CrossRef]
[30] Hammouch, Z., Yavuz, M., & Özdemir, N. Numerical solutions and synchronization of a variable-order fractional chaotic system. *Mathematical Modelling and Numerical Simulation with Applications*, 1(1), 11-23, (2021). [CrossRef]
[31] Daşbaşı, B. Stability analysis of an incommensurate fractional-order SIR model. *Mathematical Modelling and Numerical Simulation with Applications*, 1(1), (2021). [CrossRef]
[32] Carvalho, A.R., Pinto, C., & Baleanu, D. HIV/HCV coinfection model: a fractional-order perspective for the effect of the HIV viral load. *Advances in Difference Equations*, 2018(1), 1-22, (2018). [CrossRef]
[33] Naik, P.A., Zu, J., & Owolabi, K.M. Modeling the mechanics of viral kinetics under immune control during primary infection of HIV-1 with treatment in fractional order. *Physica A: Statistical Mechanics and its Applications*, 545, 123816, (2020). [CrossRef]
[34] Oustaloup, A., Levron, F., Victor, S., & Dugard, L. Non-integer (or fractional) power model to represent the complexity of a viral spreading: Application to the COVID-19. *Annual Reviews in Control*, 52, 523-542, (2021). [CrossRef]
[35] Podlubny. I. Fractional Differential Equations. *Academic Press, San Diego*, 1999.
[36] Odibat, Z.M., & Shawagfeh, N.T. Generalized Taylor's formula. *Applied Mathematics and Computation*, 186(1), 286-293, (2007). [CrossRef]
[37] Lin, W. Global existence theory and chaos control of fractional differential equations. *Journal of Mathematical Analysis and Applications*, 332(1), 709-726, (2007). [CrossRef]
[38] Li, H.L., Zhang, L., Hu, C., Jiang, Y.L., & Teng, Z. Dynamical analysis of a fractional-order predator-prey model incorporating a prey refuge. *Journal of Applied Mathematics and Computing*, 54(1), 435-449, (2017). [CrossRef]
[39] K. Diethelm. Analysis of Fractional Differential Equations: An Application-Oriented Exposition Using Differential Operators of Caputo Type. *Lecture Notes in Mathematics*, Springer-Verlag, Berlin, Germany, (2010, January).
[40] Ali, A., Ullah, S., & Khan, M.A. The impact of vaccination on the modeling of COVID-19 dynamics: a fractional order model. *Nonlinear Dynamics*, 1-20, (2022). [CrossRef]
[41] I. Petras. *Fractional-order Nonlinear Systems: Modeling Anlysis and Simulation*. Higher Education Press, Beijing, 2011.
[42] Vargas-De-León, C. Volterra-type Lyapunov functions for fractional-order epidemic systems. *Communications in Nonlinear Science and Numerical Simulation*, 24(1-3), 75-85, (2015). [CrossRef]
[43] Aguila-Camacho, N., Duarte-Mermoud, M.A., & Gallegos, J.A. Lyapunov functions for fractional order systems. *Communications in Nonlinear Science and Numerical Simulation*, 19(9), 2951-2957, (2014). [CrossRef]
[44] Huo, J., Zhao, H., & Zhu, L. The effect of vaccines on backward bifurcation in a fractional order HIV model. *Nonlinear Analysis: Real World Applications*, 26, 289-305, (2015). [CrossRef]
[45] Veeresha, P. A numerical approach to the coupled atmospheric ocean model using a fractional operator. *Mathematical Modelling and Numerical Simulation with Applications*, 1(1), 1-10, (2021). [CrossRef]
[46] Veeresha, P., Baskonus, H.M., & Gao, W. Strong interacting internal waves in rotating ocean: novel fractional approach. *Axioms*, 10(2), 123, (2021). [CrossRef]
[47] Kiouach, D., & Sabbar, Y. The long-time behavior of a stochastic SIR epidemic model with distributed delay and multidimensional Lévy jumps. *International Journal of Biomathematics*, 15(03), 2250004, (2022). [CrossRef]
[48] Kiouach, D., & Sabbar, Y. Threshold analysis of the stochastic Hepatitis B epidemic model with successful vaccination and Levy jumps. *In 2019 4th World Conference on Complex Systems (WCCS) (pp. 1-6)*, IEEE, (2019, April). [CrossRef]
[49] Sabbar, Y., Kiouach, D., Rajasekar, S.P., & El-Idrissi, S.E.A. The influence of quadratic Lévy noise on the dynamic of an SIC contagious illness model: New framework, critical comparison and an application to COVID-19 (SARS-CoV-2) case. *Chaos, Solitons & Fractals*, 159, 112110, (2022). [CrossRef]
[50] Kiouach, D., & Sabbar, Y. Modeling the impact of media intervention on controlling the diseases with stochastic perturbations. *AIP Conference Proceedings (Vol. 2074, No. 1, p. 020026)*, AIP Publishing LLC, (2019, February). [CrossRef]

Mathematical Modelling and Numerical Simulation with Applications, 2022, 2(3), 177–186

https://www.mmnsa.org
ISSN Online: 2791-8564 / Open Access
https://doi.org/10.53391/mmnsa.2022.014

RESEARCH PAPER

Laplace transform collocation method for telegraph equations defined by Caputo derivative

Mahmut Modanlı [1,†] and Mehmet Emir Koksal [2,3,†,*]

[1]Department of Mathematics, Harran University, 63300 Sanliurfa, Türkiye, [2]Department of Mathematics, Ondokuz Mayis University, 55139 Samsun, Türkiye, [3]Department of Applied Mathematics, University of Twente, 7500 AE Enschede, The Netherlands

*Corresponding Author
† mmodanli@harran.edu.tr (Mahmut Modanlı); mekoksal@omu.edu.tr (Mehmet Emir Koksal)

Abstract

The purpose of this paper is to find approximate solutions to the fractional telegraph differential equation (FTDE) using Laplace transform collocation method (LTCM). The equation is defined by Caputo fractional derivative. A new form of the trial function from the original equation is presented and unknown coefficients in the trial function are computed by using LTCM. Two different initial-boundary value problems are considered as the test problems and approximate solutions are compared with analytical solutions. Numerical results are presented by graphs and tables. From the obtained results, we observe that the method is accurate, effective, and useful.

Key words: Caputo fractional derivative; collocation method; telegraph equation; approximation solution; error analysis
AMS 2020 Classification: 26A33; 35R11; 44A10; 65G99; 65N99

1 Introduction

Differential equations are a powerful tool for modeling, analyzing, and considering many physical and engineering problems and are an important branch of applied mathematics. In particular, they occur in network design, fluid dynamics, wave motion, telecommunications, electromagnetic, wave distribution, and electronic dynamics (see [1], [2] and the references therein). They are used not only in engineering and physical systems, but also in economics, risk theory, and many other social sciences. On the other hand, telegraph equation, a special kind of hyperbolic equations, is a partial differential equation that frequently appears in electrical engineering. In particular, power transmission lines are defined and designed using telegraph equations [3], [4], [5]. Many different problems in electric, electronics and communication engineering can be modeled by telegraph equations (see [4], [6] and the references therein). Mathematical modelling of problems in communication systems and transmission lines and their solvability (analytic or most of the time approximate) have great importance in today's world in which technology and communication tools regarding them have developed and spread with and increasing velocity. Depending on whether the terminations are short or open circuits and whether they are fed by current or voltage sources, there are many forms of this equation, including local or nonlocal boundary conditions.

Many of physical systems exhibit intrinsic behavior of fractional order. Therefore, fractional calculus provides more accurate models for such systems than classical calculus [7], [8], [9], [10], [11]. A significant advantage of fractional modeling is seen in systems where inheritance and memory behavior play a role, since the fractional derivative also accounts for the past. Another advantage arises in the analysis of porous and/or self-similar structures, where the theory of fractals plays a role. A great number of papers has been studied on the numerical solution methods of different types of telegraph partial differential equations. Finite

➤ **Received:** 18.08.2022 ➤ **Revised:** 23.09.2022 ➤ **Accepted:** 26.09.2022 ➤ **Published:** 28.09.2022

difference methods [1], [4], [12], [13], [14], [15] are used mostly in the literature. Less frequently, there variation methods using differential quadrature algorithm [16], Radial basis function [17], Chebyshev cardinal function [18], interpolation scaling functions [19], Chebyshev Tau method [20], Galerkin method [21].

In 2014, weighted residuals method was applied to numerical solutions of hyperbolic telegraph equations [22]. Then, LTCM was firstly implemented for the same equation in [23] in 2017 and the results were compared by weighted residuals method. From the numerical results published in the literature, it was observed that LTCM method is more convenient and effective comparing to weighted residuals method. In [6], LTCM was successfully applied to some nonlinear fractional differential equations.

This paper examines numerical solutions of the following fractional differential equation:

$$\begin{cases} \frac{\partial^{2\alpha} y(t,x)}{\partial t^{2\alpha}} + \frac{\partial^{\alpha} y(t,x)}{\partial t^{\alpha}} + y(t,x) = \frac{\partial^{2\alpha} y(t,x)}{\partial x^{2\alpha}} + f(t,x), \\ \text{where } x \in (0,L),\ t \in (0,T),\ \alpha \in (0,1], \\ y(0,x) = \phi(x),\ y_t(0,x) = \psi(x),\ \text{where } x \in [0,L], \\ y(t,0) = y(t,L) = 0,\ \text{where } t \in [0,T]. \end{cases} \tag{1}$$

Here, ϕ, ψ, f and y are known and unknown continuous functions, respectively. The term ${}_0^C D_t^{\alpha} y(t,x) = \frac{\partial^{\alpha} y(t,x)}{\partial t^{\alpha}}$ is Caputo fractional derivative. If $\alpha = 1$, then, the main equation in (1) is called a telegraph partial differential equation. LTCM method is used for finding numerical solutions of problem (1). Approximate solutions are compared to the exact solution found by LT method. Then, numerical solutions are shown by both graph and table and errors in numerical solutions are analysed.

2 LTCM for fractional-order telegraph equation

To clarify the essential mathematical details of LTCM, we consider a FTDE using a similar method in [6].

Taking the LT of problem (1), we get

$$s^{2\alpha} y(s,x) - s^{2\alpha-1} y(0,x) - s^{2\alpha-2} y_t(0,x) = -L\left[\frac{\partial^{\alpha} y(t,x)}{\partial t^{\alpha}}\right] + L\left[\frac{\partial^{2\alpha} y(t,x)}{\partial x^{2\alpha}}\right] - L\left[y(t,x)\right] + L\left[f(t,x)\right]. \tag{2}$$

After simple algebraic simplification and using initial conditions in (2), we have

$$y(s,x) = \frac{1}{s^{2\alpha}}\left\{ s^{2\alpha-1}\phi(x) + s^{2\alpha-2}\psi(x) - L\left[\frac{\partial^{\alpha} y(t,x)}{\partial t^{\alpha}}\right] + L\left[\frac{\partial^{2\alpha} y(t,x)}{\partial x^{2\alpha}}\right] - L\left[y(t,x)\right] + L\left[f(t,x)\right] \right\}. \tag{3}$$

The function $y(t,x)$ and its derivative in (3) are replaced with a trial function of the form

$$y = y_0 + \sum_{j=1}^{n} c_j y_j. \tag{4}$$

In the above equation, c_j is the constant coefficient and it is determined to satisfy initial conditions given in (1). Then, $y(s,x)$ is found as follows:

$$\begin{aligned} y(s,x) \quad = \quad & \frac{1}{s^{2\alpha}}\left\{ s^{2\alpha-1}\left(y_0(0,x) + \sum_{j=1}^{n} c_j y_j(0,x)\right) + \frac{\partial}{\partial t}\left[s^{2\alpha-2}\left(y_0(0,x) + \sum_{j=1}^{n} c_j y_j(0,x)\right)\right]\right. \\ & \left. -L\left[\frac{\partial^{\alpha}}{\partial t^{\alpha}}\left(y_0(t,x) + \sum_{j=1}^{n} c_j y_j(t,x)\right)\right] + L\left[\frac{\partial^{2\alpha}}{\partial x^{2\alpha}}\left(y_0(t,x) + \sum_{j=1}^{n} c_j y_j(t,x)\right)\right] - L\left[y(t,x)\right] + L\left[f(t,x)\right] \right\}. \end{aligned} \tag{5}$$

Taking the inverse LT of Eq. (5), we get

$$\begin{aligned} y_{new}(t,x) \quad = \quad & L^{-1}\left\{ \frac{1}{s^{2\alpha}}\left[s^{2\alpha-1}\left(y_0(0,x) + \sum_{j=1}^{n} c_j y_j(0,x)\right)\right.\right. \\ & + \frac{\partial}{\partial t}\left(s^{2\alpha-2} y_0(0,x) + \sum_{j=1}^{n} c_j y_j(0,x)\right) - L\left[\frac{\partial^{\alpha}}{\partial t^{\alpha}}\left(y_0(t,x) + \sum_{j=1}^{n} c_j y_j(t,x)\right)\right] \\ & \left.\left. + L\left[\frac{\partial^{2\alpha}}{\partial x^{2\alpha}}\left(y_0(t,x) + \sum_{j=1}^{n} c_j y_j(t,x)\right)\right] - L\left(y_0(t,x) + \sum_{j=1}^{n} c_j y_j(t,x)\right) + L\left[f(t,x)\right]\right] \right\}. \end{aligned} \tag{6}$$

Substituting Eq. (6) into Eq. (1), we obtain new collocating at points $x = x_k$ as follows:

$$\frac{\partial^{2\alpha} y_{new}(t,x_k)}{\partial t^{2\alpha}} + \frac{\partial^{\alpha} y_{new}(t,x_k)}{\partial t^{\alpha}} + y(t,x) - \frac{\partial^{2\alpha} y_{new}(t,x_k)}{\partial x^{2\alpha}} = f(t,x_k),\ \text{where } x_k = \frac{L-0}{n+1}, k = 1,2,\cdots,n. \tag{7}$$

Then, we can define the residual function by the following formula

$$R_n(t,x) = L[y_{new}(t,x)] - f(t,x), \tag{8}$$

where $y_n(t,x)$ and $y(t,x)$ demonstrate approximate and exact solutions, respectively and

$$L[y_n(t,x)] = \frac{\partial^{2\alpha} y_{new}(t,x)}{\partial t^{2\alpha}} + y(t,x) + \frac{\partial^{\alpha} y_{new}(t,x)}{\partial t^{\alpha}} - \frac{\partial^{2\alpha} y_{new}(t,x)}{\partial x^{2\alpha}}. \tag{9}$$

From the above formula, we can write

$$\frac{\partial^{2\alpha} y_{new}(t,x)}{\partial t^{2\alpha}} + \frac{\partial^{\alpha} y_{new}(t,x)}{\partial t^{\alpha}} + y(t,x) - \frac{\partial^{2\alpha} y_{new}(t,x)}{\partial x^{2\alpha}} = f(t,x) + R_n(t,x). \tag{10}$$

3 Numerical implementations

For the application of LTCM, we consider two different test problems in this section and compare approximate solutions with exact solutions.

Example 1 *As the first example, consider the following initial-boundary value problem for FTDE*

$$\begin{cases} \frac{\partial^{2\alpha} y(t,x)}{\partial t^{2\alpha}} + \frac{\partial^{\alpha} y(t,x)}{\partial t^{\alpha}} + y(t,x) - \frac{\partial^{2\alpha} y(t,x)}{\partial x^{2\alpha}} \\ = 6\left[\frac{t^{3-2\alpha}}{\Gamma(4-2\alpha)} + \frac{t^{3-\alpha}}{\Gamma(4-\alpha)}\right] x^3 + t^3\left[x^2 - x^3 + 6\frac{x^{3-2\alpha}}{\Gamma(4-2\alpha)} - 2t^3\frac{x^{2-2\alpha}}{\Gamma(3-2\alpha)}\right], \\ \text{where } x,t \in (0,1),\ \alpha \in (0,1], \\ y(0,x) = y_t(0,x) = 0, \text{ where } x \in [0,1], \\ y(t,0) = y(t,1) = 0, \text{ where } t \in [0,1]. \end{cases} \tag{11}$$

First, we calculate (11) by LTCM.

From the formula of the trial function (Eq. (4)), approximate solution can be written as:

$$y_{app}(t,x) = c_1 x^2(x-1)t^3 + c_2 x(x-1)^2 t^3. \tag{12}$$

Taking the LT of the main equation of (11) and using Eq. (5), we get

$$\begin{aligned} s^{2\alpha}y(s,x) - s^{2\alpha-1}y(0,x) - s^{2\alpha-2}y_t(0,x) &= -L\left[\frac{\partial^{\alpha} y(t,x)}{\partial t^{\alpha}}\right] - L\left[y(t,x)\right] + L\left[\frac{\partial^{2\alpha} y(t,x)}{\partial x^{2\alpha}}\right] \\ &\quad + L\left\{6\left[\frac{t^{3-2\alpha}}{\Gamma(4-2\alpha)} + \frac{t^{3-\alpha}}{\Gamma(4-\alpha)}\right] x^3 + t^3(x^2 - x^3) + \frac{6x^{3-2\alpha}}{\Gamma(4-2\alpha)} - \frac{2x^{2-2\alpha}}{\Gamma(3-2\alpha)}\right\}. \end{aligned} \tag{13}$$

Then, using zero initial conditions, the above formula can be simplified and written as:

$$\begin{aligned} y(s,x) &= \frac{1}{s^{2\alpha}}\left\{-L\left[\frac{\partial^{\alpha} y(t,x)}{\partial t^{\alpha}}\right] - L\left[y(t,x)\right] + L\left[\frac{\partial^{2\alpha} y(t,x)}{\partial x^{2\alpha}}\right]\right. \\ &\quad \left. + L\left[\left[\frac{6t^{3-2\alpha}}{\Gamma(4-2\alpha)} + \frac{6t^{3-\alpha}}{\Gamma(4-\alpha)}\right] x^3 + t^3\left(x^2 - x^3\right) + \frac{6x^{3-2\alpha}}{\Gamma(4-2\alpha)} - \frac{2x^{2-2\alpha}}{\Gamma(3-2\alpha)}\right]\right\}. \end{aligned} \tag{14}$$

From the formulas (12) and (14), we have

$$\begin{aligned} y(s,x) &= \frac{1}{s^{2\alpha}} L\left\{\left[-\frac{6(x^3 - x^2)t^{3-\alpha}}{\Gamma(4-\alpha)} + \left(-x^3 + x^2 + \frac{6x^{3-2\alpha}}{\Gamma(4-2\alpha)} - \frac{2x^{2-2\alpha}}{\Gamma(3-2\alpha)}\right) t^3\right] c_1\right. \\ &\quad -6\left[\frac{x(x-1)^2 t^{3-\alpha}}{\Gamma(4-\alpha)} + \left(-x(x-1)^2 + \frac{6x^{3-2\alpha}}{\Gamma(4-2\alpha)} - \frac{4x^{2-2\alpha}}{\Gamma(3-2\alpha)} + \frac{x^{1-2\alpha}}{\Gamma(2-2\alpha)}\right) t^3\right] c_2 \\ &\quad \left. + 6\left(\frac{t^{3-2\alpha}}{\Gamma(4-2\alpha)} + \frac{t^{3-\alpha}}{\Gamma(4-\alpha)}\right) x^3 + t^3(x^2 - x^3) + \frac{6x^{3-2\alpha}}{\Gamma(4-2\alpha)} - \frac{2x^{2-2\alpha}}{\Gamma(3-2\alpha)}\right\}. \end{aligned} \tag{15}$$

From the formula (15), $y(s,x)$ is found as follows:

$$y(s,x) = \left\{-\frac{6\left(x^3 - x^2\right)}{s^{4+\alpha}} + \frac{6}{s^{4+2\alpha}}\left[-\left(x^3 - x^2\right) + \frac{6x^{3-\alpha}}{\Gamma(4-\alpha)} - \frac{2x^{2-\alpha}}{\Gamma(3-\alpha)}\right]\right\} c_1 \tag{16}$$

$$+\left\{-\frac{6\left(x^3-2x^2+x\right)}{s^{4+\alpha}}+\frac{6}{s^{4+2\alpha}}\left[-x^3+2x^2-x+\frac{6x^{3-2\alpha}}{\Gamma(4-2\alpha)}-\frac{4x^{2-2\alpha}}{\Gamma(3-2\alpha)}+\frac{x^{1-2\alpha}}{\Gamma(2-2\alpha)}\right]\right\}c_2$$
$$+\left(\frac{6}{s^{4+\alpha}}+\frac{6}{s^4}\right)x^3+\frac{6}{s^{4+2\alpha}}\left[x^2-x^3+\frac{6x^{3-2\alpha}}{\Gamma(4-2\alpha)}-\frac{2x^{2-2\alpha}}{\Gamma(3-2\alpha)}\right].$$

Taking the inverse LT of (16), we obtain the following trial solution:

$$\begin{aligned} y_{new}(t,x) &= \left\{-6\left[\frac{t^{3+\alpha}}{\Gamma(4+\alpha)}+\frac{t^{3+2\alpha}}{\Gamma(4+2\alpha)}\right](c_1+c_2)+t^3+\frac{6t^{3+\alpha}}{\Gamma(4+\alpha)}-\frac{6t^{3+2\alpha}}{\Gamma(4+2\alpha)}\right\}x^3 \\ &+\left\{6\left[\frac{t^{3+\alpha}}{\Gamma(4+\alpha)}+\frac{t^{3+2\alpha}}{\Gamma(4+2\alpha)}\right](c_1+2c_2)+\frac{t^{3+2\alpha}}{\Gamma(4+2\alpha)}\right\}x^2+\left\{-6\left[\frac{t^{3+\alpha}}{\Gamma(4+\alpha)}+\frac{t^{3+2\alpha}}{\Gamma(4+2\alpha)}\right]c_2\right\}x \\ &+6\left[\frac{x^{3-\alpha}}{\Gamma(4-\alpha)}-2\frac{x^{2-\alpha}}{\Gamma(3-\alpha)}\right]c_1+\frac{6t^{3+2\alpha}}{\Gamma(4+2\alpha)}\left[\frac{6x^{3-2\alpha}}{\Gamma(4-2\alpha)}-\frac{4x^{2-2\alpha}}{\Gamma(3-2\alpha)}+\frac{x^{1-2\alpha}}{\Gamma(2-2\alpha)}\right]c_2 \\ &+\frac{6t^{3+2\alpha}}{\Gamma(4+2\alpha)}\left[\frac{x^{3-2\alpha}}{\Gamma(4-2\alpha)}-\frac{2x^{2-2\alpha}}{\Gamma(3-2\alpha)}\right]. \end{aligned} \tag{17}$$

Substituting (17) into Eq. (11), we have the following residual formula:

$$\begin{aligned} R(t,x,c_1,c_2) &= \frac{\partial^{2\alpha}y_{new}(t,x)}{\partial t^{2\alpha}}+\frac{\partial^{\alpha}y_{new}(t,x)}{\partial t^{\alpha}}+y(t,x)-\frac{\partial^{2\alpha}y_{new}(t,x)}{\partial x^{2\alpha}} \\ &-6\left[\frac{t^{3-2\alpha}}{\Gamma(4-2\alpha)}+\frac{t^{3-\alpha}}{\Gamma(4-\alpha)}\right]x^3-t^3\left[x^2-x^3+\frac{6x^{3-2\alpha}}{\Gamma(4-2\alpha)}-\frac{2x^{2-2\alpha}}{\Gamma(3-2\alpha)}\right]. \end{aligned} \tag{18}$$

Taking the derivatives of Eq. (17) with respect to x and t, and writing in (18), we obtain

$$\begin{aligned} R(t,x,c_1,c_2) &= (Ax^3-Ax^2+Bx^3-Bx^2+C+D)c_1+\left(Ax^3-2Ax^2+Ax+Bx^3-2Bx^2+Bx+E+F+C+G-\frac{G}{4x}+R\right)c_2 \\ &+K+L+M+N+S=0, \end{aligned} \tag{19}$$

where

$$A=-t^3-\frac{6}{\Gamma(4-\alpha)}t^{3-\alpha},\ B=-t^3-\frac{6}{\Gamma(4+\alpha)}t^{3+\alpha},$$

$$C=36\left[\frac{1}{\Gamma(4+\alpha)}t^{3+\alpha}+\frac{1}{\Gamma(4+2\alpha)}t^{3+2\alpha}\right]\frac{1}{\Gamma(4-2\alpha)}x^{3-2\alpha},\ D=-\frac{6}{\Gamma(4-3\alpha)}x^{3-3\alpha}-\frac{2}{\Gamma(3-2\alpha)}x^{2-2\alpha},$$

$$E=t^3\left[\frac{6}{\Gamma(4-3\alpha)}x^{3-3\alpha}-\frac{4}{\Gamma(3-2\alpha)}x^{2-2\alpha}+\frac{1}{\Gamma(2-2\alpha)}x^{1-2\alpha}\right],$$

$$F=\frac{6}{\Gamma(4+\alpha)}t^{3+\alpha}\left[\frac{6}{\Gamma(4-2\alpha)}x^{3-2\alpha}-\frac{4}{\Gamma(3-2\alpha)}x^{2-2\alpha}+\frac{1}{\Gamma(2-2\alpha)}x^{1-2\alpha}\right],$$

$$G=-24\left[\frac{1}{\Gamma(4+\alpha)}t^{3+\alpha}+\frac{1}{\Gamma(4+2\alpha)}t^{3+2\alpha}\right]\frac{1}{\Gamma(3-2\alpha)}x^{2-2\alpha},$$

$$R=-\frac{6}{\Gamma(4+2\alpha)}t^{3+2\alpha}\left[\frac{6}{\Gamma(4-4\alpha)}x^{3-4\alpha}-\frac{4}{\Gamma(3-4\alpha)}x^{2-4\alpha}+\frac{1}{\Gamma(2-4\alpha)}x^{1-4\alpha}\right],$$

$$K=x^3\left[t^3+\frac{12}{\Gamma(4-2\alpha)}t^{3-2\alpha}+\frac{18}{\Gamma(4-\alpha)}t^{3-\alpha}-\frac{6}{\Gamma(4+\alpha)}t^{3+\alpha}\right],$$

$$L=x^2\left[\frac{6}{\Gamma(4+\alpha)}t^{3+\alpha}-\frac{6}{\Gamma(4-\alpha)}t^{3-\alpha}-\frac{6}{\Gamma(4-2\alpha)}t^{3-2\alpha}\right],\ M=-\frac{6}{\Gamma(3-2\alpha)}x^{2-2\alpha}t^3,$$

$$N=\frac{6t^{3+\alpha}}{\Gamma(4+\alpha)}\left[-\frac{2}{\Gamma(3-2\alpha)}x^{2-2\alpha}-\frac{30}{\Gamma(4-2\alpha)}x^{3-2\alpha}\right],$$

$$S = \frac{1}{\Gamma(4+2\alpha)}t^{3+2\alpha}\left[\frac{36}{\Gamma(4-2\alpha)}x^{3-2\alpha} - \frac{12}{\Gamma(3-2\alpha)}x^{2-2\alpha} + \frac{12}{\Gamma(3-4\alpha)}x^{2-4\alpha} - \frac{36}{\Gamma(4-4\alpha)}x^{3-4\alpha}\right].$$

Then, from (19), we obtain

$$c_1 = -\frac{K+L+M}{Ax^3 - Ax^2 + Bx^3 - Bx^2 + C + D},$$

$$c_2 = \frac{N+S}{Ax^3 - 2Ax^2 + Ax + Bx^3 - 2Bx^2 + Bx + E + F + C + G - \frac{G}{4x} + R}.$$

Example 2 *As the second example, we consider the following initial-boundary value problem for FTDE*

$$\begin{cases} \frac{\partial^{2\alpha}y(t,x)}{\partial t^{2\alpha}} + 6\frac{\partial^{\alpha}y(t,x)}{\partial t^{\alpha}} + 2y(t,x) - \frac{\partial^{2\alpha}y(t,x)}{\partial x^{2\alpha}} = \left[-\frac{t^{1-2\alpha}}{\Gamma(2-2\alpha)} - 6\frac{t^{1-\alpha}}{\Gamma(2-\alpha)} + 2e^{-t}\right]\sin x - e^{-t}\frac{x^{1-2\alpha}}{\Gamma(2-2\alpha)}, \\ \text{where } x \in (0,\pi),\ t \in (0,1),\ \alpha \in (0,1], \\ y(0,x) = \sin x,\ y_t(0,x) = -\sin x,\ \text{where } x \in [0,\pi], \\ y(t,0) = y(t,\pi) = 0,\ \text{where } t \in [0,1]. \end{cases} \tag{20}$$

By following the similar manner of the previous example, we now calculate (20) by LTCM.

From Eq. (4), approximate solution can be written as:

$$y_{app}(t,x) = (1-t)\sin x + c_1x^2(x-\pi)t^2 + c_2x(x-\pi)^2t^2. \tag{21}$$

Taking the LT of Eq. (20) and using the formula (5), we obtain

$$\begin{aligned} s^{2\alpha}y(s,x) - s^{2\alpha-1}y(0,x) - s^{2\alpha-2}y_t(0,x) &= -6L\left[\frac{\partial^{\alpha}y(t,x)}{\partial t^{\alpha}}\right] - 2L\left[y(t,x)\right] + L\left[\frac{\partial^{2\alpha}y(t,x)}{\partial x^{2\alpha}}\right] \\ &\quad + L\left\{\left[-\frac{t^{1-2\alpha}}{\Gamma(2-2\alpha)} - 6\frac{t^{1-\alpha}}{\Gamma(2-\alpha)} + 2e^{-t}\right]\sin x - e^{-t}\frac{x^{1-2\alpha}}{\Gamma(2-2\alpha)}\right\}. \end{aligned} \tag{22}$$

Using initial condition of (20), $y(s,x)$ is obtained as:

$$\begin{aligned} y(s,x) &= \left(\frac{1}{s} - \frac{1}{s^2}\right)\sin x + \frac{1}{s^{2\alpha}}\left\{-6L\left[\frac{\partial^{\alpha}y(t,x)}{\partial t^{\alpha}}\right] - 2L\left[y(t,x)\right] + L\left[\frac{\partial^{2\alpha}y(t,x)}{\partial x^{2\alpha}}\right]\right. \\ &\quad \left. + L\left\{\left[-\frac{t^{1-2\alpha}}{\Gamma(2-2\alpha)} - 6\frac{t^{1-\alpha}}{\Gamma(2-\alpha)} + 2e^{-t}\right]\sin x - e^{-t}\frac{x^{1-2\alpha}}{\Gamma(2-2\alpha)}\right\}\right\}. \end{aligned} \tag{23}$$

From the formulas (20) and (23), we have

$$\begin{aligned} y(s,x) &= \left[\frac{1}{s} - \frac{2}{s^2} - \frac{2}{s^{2\alpha+1}} + \frac{2}{s^{2+2\alpha}} + \frac{2}{s^{2\alpha}(s+1)}\right]\sin x \\ &\quad + \left\{\left(-\frac{12}{s^{3+\alpha}} - \frac{4}{s^{3+2\alpha}}\right)x^2(x-\pi) + \frac{2}{s^{3+2\alpha}}\left[\frac{6x^{3-2\alpha}}{\Gamma(4-2\alpha)} - \frac{2\pi x^{2-2\alpha}}{\Gamma(3-2\alpha)}\right]\right\}c_1 \\ &\quad + \left\{\left(-\frac{12}{s^{3+\alpha}} - \frac{4}{s^{3+\alpha}}\right)x^2(x-\pi) + \frac{2}{s^{3+2\alpha}}\left[\frac{6x^{3-2\alpha}}{\Gamma(4-2\alpha)} - \frac{4\pi x^{2-2\alpha}}{\Gamma(3-2\alpha)} + \frac{\pi^2x^{1-2\alpha}}{\Gamma(2-2\alpha)}\right]\right\}c_2 \\ &\quad + \left(\frac{1}{s^{2\alpha+1}} - \frac{1}{s^{2\alpha+2}} - \frac{1}{s^{2\alpha}(s+1)}\right)\frac{x^{1-2\alpha}}{\Gamma(2-2\alpha)}. \end{aligned} \tag{24}$$

Taking the inverse LT of (24), the following new trial solution is obtained:

$$\begin{aligned} y_{new}(t,x) &= \left[-\frac{12t^{2+\alpha}}{\Gamma(3+\alpha)} - \frac{4t^{2+2\alpha}}{\Gamma(3+2\alpha)}\right](c_1+c_2)x^3 + \left[\pi\left(\frac{12t^{2+\alpha}}{\Gamma(3+\alpha)} + \frac{4t^{2+2\alpha}}{\Gamma(3+2\alpha)}\right)(c_1+2c_2)\right]x^2 \\ &\quad + \left[-\pi^2\left(\frac{12t^{2+\alpha}}{\Gamma(3+\alpha)} + \frac{4t^{2+2\alpha}}{\Gamma(3+2\alpha)}\right)c_2\right]x + \frac{t^{2+2\alpha}}{\Gamma(3+2\alpha)}\left[\frac{12x^{3-2\alpha}}{\Gamma(4-2\alpha)} - \frac{4\pi x^{2-2\alpha}}{\Gamma(3-2\alpha)}\right]c_1 \\ &\quad + \left[1 - 2t - \frac{2t^{2\alpha}}{\Gamma(1+2\alpha)} + \frac{2t^{1+2\alpha}}{\Gamma(2+2\alpha)} + \frac{2e^{-t}t^{2\alpha-1}}{\Gamma(2\alpha)}\right]\sin x \\ &\quad + \frac{t^{2+2\alpha}}{\Gamma(3+2\alpha)}\left[\frac{12x^{3-2\alpha}}{\Gamma(4-2\alpha)} - \frac{8\pi x^{2-2\alpha}}{\Gamma(3-2\alpha)} + \frac{2\pi^2x^{1-2\alpha}}{\Gamma(2-2\alpha)}\right]c_2 \end{aligned} \tag{25}$$

$$+\frac{x^{1-2\alpha}}{\Gamma(2-2\alpha)}\left[\frac{t^{2\alpha}}{\Gamma(1+2\alpha)}-\frac{t^{1+2\alpha}}{\Gamma(2+2\alpha)}-\frac{e^{-t}t^{2\alpha-1}}{\Gamma(2\alpha)}\right].$$

Substituting (25) into Eq. (20), we have the following residual formula:

$$\begin{aligned} R(t,x,c_1,c_2) &= \frac{\partial^{2\alpha}y(t,x)}{\partial t^{2\alpha}}+6\frac{\partial^{\alpha}y(t,x)}{\partial t^{\alpha}}+2y(t,x)-\frac{\partial^{2\alpha}y(t,x)}{\partial x^{2\alpha}} \\ &\quad -\left[-\frac{t^{1-2\alpha}}{\Gamma(2-2\alpha)}-\frac{6t^{1-\alpha}}{\Gamma(2-\alpha)}+2e^{-t}\right]\sin x+\frac{e^{-t}x^{1-2\alpha}}{\Gamma(2-2\alpha)}. \end{aligned} \tag{26}$$

Taking the derivatives of Eq. (25) with respect to x and t, and writing in Eq. (26), we obtain the formula of $R(t,x,c_1,c_2)$ as

$$\begin{aligned} R(t,x,c_1,c_2) &= \left[-9ax^3+9a\pi x^2+\frac{6ax^{3-2\alpha}}{\Gamma(4-2\alpha)}-\frac{2a\pi x^{2-2\alpha}}{\Gamma(3-2\alpha)}-\frac{dt^{2+2\alpha}}{\Gamma(3+2\alpha)}+bk\right]c_1 \\ &\quad +\left[-9ax^3+18a\pi x^2+\frac{4a\pi x^{2-2\alpha}}{\Gamma(3-2\alpha)}+\frac{6ax^{3-2\alpha}}{\Gamma(4-2\alpha)}-\frac{4a\pi x^{2-2\alpha}}{\Gamma(3-2\alpha)}-9a\pi^2x+\frac{a\pi^2x^{1-2\alpha}}{\Gamma(2-2\alpha)}+ck-\frac{et^{2+2\alpha}}{\Gamma(3+2\alpha)}\right]c_2 \\ &\quad +f\sin x+\frac{hx^{1-2\alpha}}{\Gamma(2-2\alpha)}-\frac{gx^{1-4\alpha}}{\Gamma(2-4\alpha)}=0, \end{aligned} \tag{27}$$

where,

$$a=-\frac{12\left(t^{2-\alpha}-4t^2\right)}{\Gamma(3-\alpha)},\quad b=\frac{12x^{3-2\alpha}}{\Gamma(4-2\alpha)}-\frac{4\pi x^{2-2\alpha}}{\Gamma(3-2\alpha)},\quad c=\frac{12x^{3-2\alpha}}{\Gamma(4-2\alpha)}-\frac{8\pi x^{2-2\alpha}}{\Gamma(3-2\alpha)}+\frac{2\pi^2x^{1-2\alpha}}{\Gamma(2-2\alpha)},$$

$$d=\frac{12x^{3-4\alpha}}{\Gamma(4-4\alpha)}-\frac{4\pi x^{2-4\alpha}}{\Gamma(3-4\alpha)},\quad e=\frac{12x^{3-4\alpha}}{\Gamma(4-4\alpha)}-\frac{8\pi x^{2-4\alpha}}{\Gamma(3-4\alpha)}+\frac{2\pi^2x^{1-4\alpha}}{\Gamma(2-4\alpha)},$$

$$f=-2t-\frac{8t^{1-\alpha}}{\Gamma(2-\alpha)}-\frac{12t^{\alpha}}{\Gamma(\alpha+1)}-\frac{t^{1-2\alpha}t^{2\alpha-1}}{\Gamma(2-2\alpha)\Gamma(2\alpha)}+\frac{12t^{\alpha+1}}{\Gamma(\alpha+2)}-\frac{12t^{1-\alpha}t^{2\alpha-1}}{\Gamma(2-\alpha)\Gamma(2\alpha)}-\frac{4t^{2\alpha}}{\Gamma(2\alpha+1)}+\frac{4t^{2\alpha+1}}{\Gamma(2\alpha+2)}+e^{-t}\left[\frac{2}{t}+\frac{12t^{\alpha-1}}{\Gamma(\alpha)}+\frac{4t^{2\alpha-1}}{\Gamma(2\alpha)}-2\right],$$

$$h=t+\frac{t^{1-2\alpha}t^{2\alpha-1}}{\Gamma(2-2\alpha)\Gamma(2\alpha)}+\frac{6t^{\alpha}}{\Gamma(\alpha+1)}-\frac{6t^{\alpha+1}}{\Gamma(\alpha+2)}+\frac{6t^{1-\alpha}t^{2\alpha-1}}{\Gamma(2-\alpha)\Gamma(2\alpha)}+\frac{4t^{2\alpha}}{\Gamma(2\alpha+1)}-\frac{4t^{2\alpha+1}}{\Gamma(2\alpha+2)}+e^{-t}\left[-\frac{1}{t}-\frac{6t^{\alpha-1}}{\Gamma(\alpha)}-\frac{4t^{2\alpha-1}}{\Gamma(2\alpha)}-2\right],$$

$$g=\frac{t^{2\alpha}}{\Gamma(2\alpha+1)}-\frac{t^{2\alpha+1}}{\Gamma(2\alpha+2)}-\frac{e^{-t}t^{2\alpha-1}}{\Gamma(2\alpha)},k=t^2+\frac{6t^{2+\alpha}}{\Gamma(3+\alpha)}+\frac{2t^{2+2\alpha}}{\Gamma 2\alpha+3)}.$$

From (27), we obtain

$$c_1=-\left[f\sin x+\frac{hx^{1-2\alpha}}{\Gamma(2-2\alpha)}\right]\left[-9ax^3+9a\pi x^2-\frac{2a\pi x^{2-2\alpha}}{\Gamma(3-2\alpha)}+\frac{6ax^{3-2\alpha}}{\Gamma(4-2\alpha)}+bk-\frac{dt^{2+2\alpha}}{\Gamma(3+2\alpha)}\right]^{-1},$$

$$c_2=\frac{gx^{1-4\alpha}}{\Gamma(2-4\alpha)}\left[-9ax^3+18a\pi x^2-\frac{4a\pi x^{2-2\alpha}}{\Gamma(3-2\alpha)}+\frac{6ax^{3-2\alpha}}{\Gamma(4-2\alpha)}+\frac{a\pi^2x^{1-2\alpha}}{\Gamma(2-2\alpha)}-9\pi^2ax+ck-\frac{et^{2+2\alpha}}{\Gamma(3+2\alpha)}\right]^{-1}.$$

4 Error analysis

Errors in numerical solutions are computed by the following error formula

$$Error = \max\left|y_{exact}-y_{app}\right|,$$

where $y_{exact}(t,x)$ represents the exact solution and $y_{app}(t,x)$ represents the approximate solution obtained by using LTCM. Exact solutions of the first and second examples are $t^3(x^2-x^3)$ and $e^{-t}\sin x$ respectively. Approximate solution for the first example is $c_1x^2(x-1)t^3+c_2x(x-1)^2t^3$. For Example 2, it is equal to $(1-t)\sin x+c_1x^2(x-\pi)t^2+c_2x(x-\pi)^2t^2$.

As seen from the yellow and greenish region of Figs. 1 and 2, when t changes between 0.2 and 0.8, and x approaches to 1 for $\alpha=0.5$, the difference between exact solution and approximate solution increases. For the other values, the difference between exact and approximate solution is not obvious. Moreover, when $t=0.6$ and $x=1$, exact solution is almost 3 times greater than approximate solution. When t changes between 0.2 and 0.8, and x approaches to 1 for 0.99, the difference between exact solution and approximate solution increases as a similar result for $\alpha=0.5$, but when $t=0.6$ and $x=1$, exact solution is almost 10 times greater than approximate solution as shown in Figs. 3 and 4. For the other values, the difference between exact and approximate

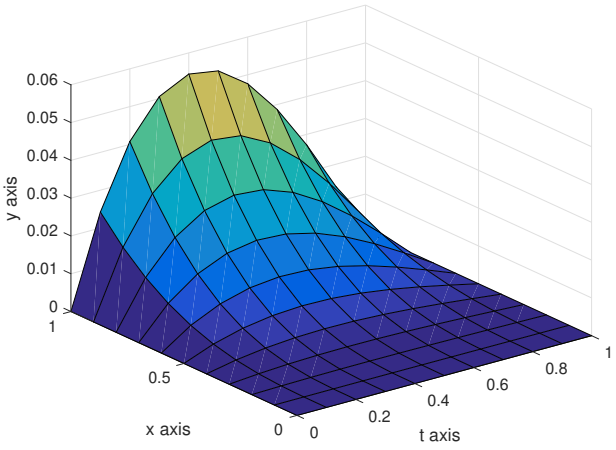

Figure 1. Approximate solution of Example 1 for $\alpha = 0.5$.

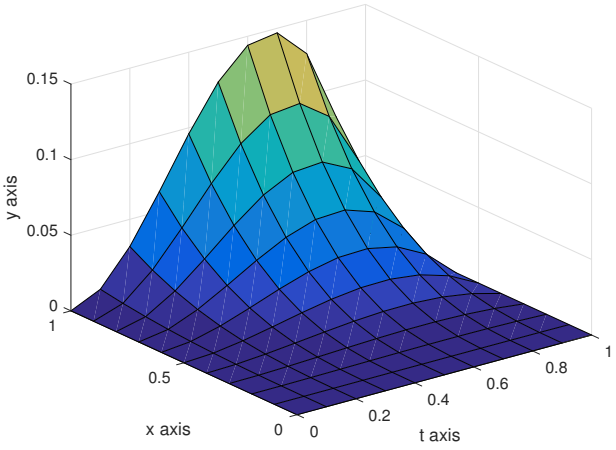

Figure 2. Exact solution of Example 1 for $\alpha = 0.5$.

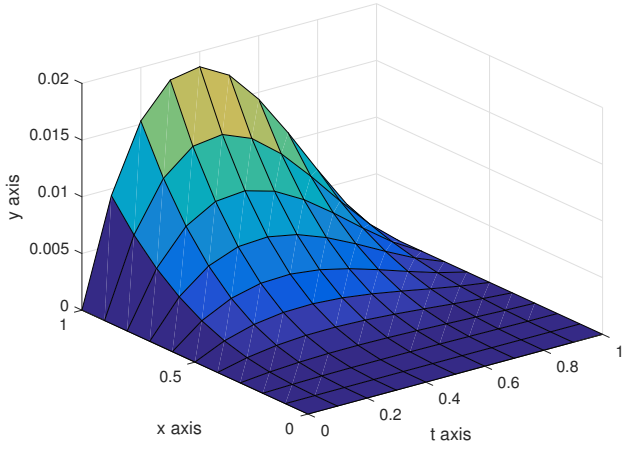

Figure 3. Approximate solution of Example 1 for $\alpha = 0.99$.

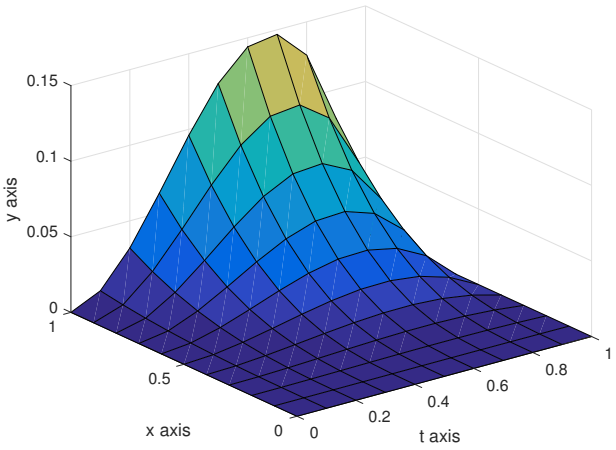

Figure 4. Exact solution of Example 1 for $\alpha = 0.99$.

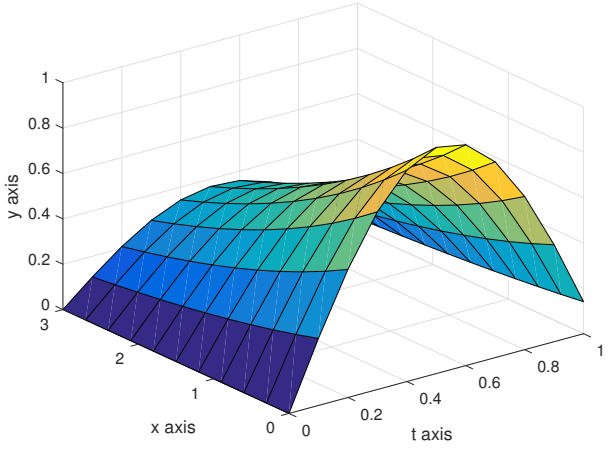

Figure 5. Exact solution of Example 2 for $\alpha = 1$.

solution is not obvious.
For Example 2, when t changes between 0.2 and 0.8, there is a great difference between the exact solution and approximate solution at the boundary point $x = 3$ as shown in Figs. 5 and 6. For the other values, the difference between exact and approximate solution is not obvious. For the better comparison of exact solution and approximate solution, we need to present results by Tables. Errors in the numerical solutions for different values of x, t, α for Examples 1 and 2 are presented in Tables 1 and 2, respectively.

Table 1. Error values for Example 1

x	t	α	**Errors**
0.01	0.01	0.01	9.9000×10^{-7}
0.01	0.01	0.5	9.9000×10^{-7}
0.01	0.01	0.99	1.7161×10^{-10}
0.1	0.591	0.01	0.00125
0.1	0.591	0.5	0.00183
0.1	0.591	0.99	8.1658×10^{-5}
0.248	0.9	0.01	0.03256
0.248	0.9	0.5	9.1222×10^{-6}
0.248	0.9	0.99	0.10107

When $x, t = 0.01$ and α changes from 0.01 to 0.5 for Example 1 in Table 1, there is no difference in the error but when α changes from 0.5 to 0.99, the error in the numerical solution decreases about 1000 times. When $x = 0.1, t = 0.591$ and α changes from 0.01 to 0.5, there is not much difference in the error but when α changes from 0.5 to 0.99, the error in the numerical solution decreases about 22 times. Lastly, when $x = 0.248, t = 0.9$ and α changes from 0.01 to 0.5, the error in the numerical solution decreases about 3570 times, but α changes from 0.01 to 0.99, the error increases about 7 times.

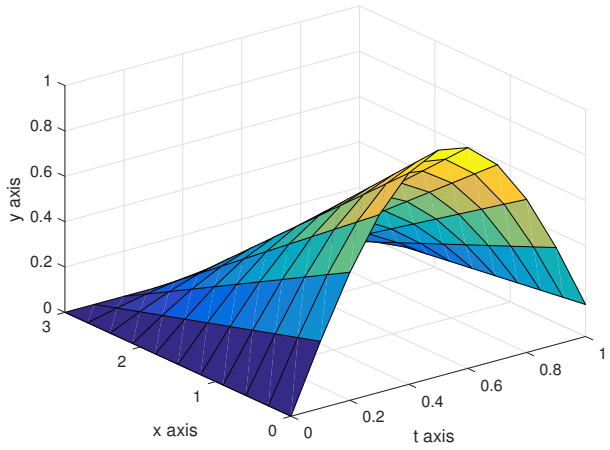

Figure 6. Approximate solution of Example 2 for $\alpha = 1$.

Table 2. Error values for Example 2

x	t	α	**Errors**
0	0.01	1	0
11/7	0.01	1	0.017
22/7	0.01	1	2.7494×10^{-7}
π	0.01	1	6.1029×10^{-21}
0.1	0.1	0.01	0.0043
0.1	0.1	0.5	0.0062
0.01	0.1	0.01	4.4652×10^{-4}
0.01	0.1	0.5	8.6324×10^{-5}

When $t = 0.01$ and $\alpha = 1$, x changes from 0 to 11/7 for Example 2, the error increases to 0.017 from 0, but when x changes from 11/7 to π, the error decreases to 6.1029×10^{-21} from 0.017. When $x, t = 0.1$ and α changes from 0.01 to 0.5, the error increases about 1.5 times, but when $x = 0.01, t = 0.1$ and α changes from 0.01 to 0.5, the error decreases about 5 times.

5 Conclusion

A combination of LTCM to develop approximate methods for fractional order telegraph partial differential equation has been adopted in this paper. The exact solution has been compared with approximate solutions in two different test problems. Error analysis has been done and it has been seen that the results were effective. However, due to the solution method for the approximate solution, when $x \to 1$, the solution goes to zero, causing the simulations to look far from each other. This deficiency due to the comparison of the simulations has been eliminated by giving the exact and approximate solutions in Table 1. As a future problem for the further developments of the present work, higher dimensional FTDEs can be studied. Moreover, this method can be also applied to nonlinear FTDEs by developing an algorithm due to the difficulty of processing.

Declarations

Consent for publication

Not applicable.

Conflicts of interest

The authors declare that they have no conflict of interests.

Funding

Not applicable.

Author's contributions

M.M.: Conceptualization, Methodology, Software, Data Curation, Writing-Original draft preparation. M.E.K.: Visualization, Investigation, Supervision, Validation, Writing-Reviewing and Editing. All authors discussed the results and contributed to the final manuscript.

References

[1] Koksal, M.E. Time and frequency responses of non-integer order RLC circuits. *AIMS Mathematics*, 4(1), 61-74, (2019). [CrossRef]

[2] Misra, D.K. Radio-frequency and microwave communication circuits: analysis and design. *Wiley-Interscience*, (2004).

[3] Palusinski, O.A., & Lee, A. Analysis of transients in nonuniform and uniform multiconductor transmission lines. *IEEE Transactions on Microwave Theory and Techniques*, 37(1), 127-138, (1989). [CrossRef]

[4] Koksal, M.E., Senol, M., & Unver, A.K. Numerical simulation of power transmission lines. *Chinese Journal of Physics*, 59, 507-524, (2019). [CrossRef]

[5] Liu, F., Schutt-Aine, J.E., & Chen, J. Full-wave analysis and modeling of multiconductor transmission lines via 2-D-FDTD and signal-processing techniques. *IEEE Transactions on Microwave Theory and Techniques*, 50(2), 570-577, (2002). [CrossRef]

[6] Modanli, M. Laplace transform collocation and Daftar-Gejii-Jafaris method for fractional order time varying linear dynamical systems. *Physica Scripta*, 96(9), 094003, (2021). [CrossRef]

[7] Ashyralyev, A, & Modanli, M. Nonlocal boundary value problem for telegraph equations. In Proceedings, *AIP Conference Proceedings*, 1676, 1-4, 020078, (2015). [CrossRef]

[8] Ashyralyev, A., Turkcan, K.T., & Koksal, M.E. Numerical solutions of telegraph equations with the Dirichlet boundary condition. In Proceedings, *AIP Conference Proceedings*, 1759, 1-6, 020055, (2016). [CrossRef]

[9] Metzler, R., & Klafter, J. The restaurant at the end of the random walk: recent developments in the description of anomalous transport by fractional dynamics. *Journal of Physics A: Mathematical and General*, 37(31), 161-208, (2004). [CrossRef]

[10] Sun, Q., Xiao, M., Tao, B., Jiang, G., Cao, J., Zhang, F., & Huang, C. Hopf bifurcation analysis in a fractional-order survival red blood cells model and PD^{α} control. *Advances in Difference Equations*, 10(2018), 1-12, (2018). [CrossRef]

[11] Koksal, M.E. Stability analysis of fractional differential equations with unknown parameters. *Nonlinear Analysis: Modeling and Control*, 24(2), 224-240, (2019). [CrossRef]

[12] Ashyralyev, A, & Modanli, M. A numerical solution for a telegraph equation. In Proceedings, *AIP Conference Proceedings*, 1611(1), 300-304, (2014). [CrossRef]

[13] Ashyralyev, A, & Modanli, M. An operator method for telegraph partial differential and difference equations. *Boundary Value Problems*, 41(2015), 1-17, (2015). [CrossRef]

[14] Ding, H.F., Zhang, Y.X., Cao, J.X., & Tian, J.H. A class of difference scheme for solving telegraph equation by new non-polynomial spline methods. *Applied Mathematics and Computation*, 218(9), 4671-4683, (2012). [CrossRef]

[15] Pandit, S., Kumar, M., & Tiawri, S. Numerical simulation of second-order hyperbolic telegraph type equations with variable coefficients. *Computer Physics Communications*, 187, 83-90, (2015). [CrossRef]

[16] Jiwari, R., Pandit, S., & Mittal, R.C. A differential quadrature algorithm to solve the two dimensional linear hyperbolic telegraph equation with Dirichlet and Neumann boundary conditions. *Applied Mathematics and Computation*, 218(13), 7279-7294, (2012). [CrossRef]

[17] Dehghan, M., & Shokri, A. A numerical method for solving the hyperbolic telegraph equation. *Numerical Methods for Partial Differential Equations: An International Journal*, 24(4), 1080-1093, (2008). [CrossRef]

[18] Dehghan, M., & Lakestani, M. The use of Chebyshev cardinal functions for solution of the second-order one-dimensional telegraph equation. *Numerical Methods for Partial Differential Equations*, 25(4), 931-938, (2009). [CrossRef]

[19] Lakestani, M., & Saray, B.N. Numerical solution of telegraph equation using interpolating scaling functions. *Computers & Mathematics with Applications*, 60(7), 1964-1972, (2010). [CrossRef]

[20] Saadatmandi, A., & Dehghan, M. Numerical solution of hyperbolic telegraph equation using the Chebyshev tau method. *Numerical Methods for Partial Differential Equations: An International Journal*, 26(1), 239-252, (2010). [CrossRef]

[21] Yousefi, S.A. Legendre multiwavelet Galerkin method for solving the hyperbolic telegraph equation. *Numerical Methods for Partial Differential Equations: An International Journal*, 26(3), 535-543, (2010). [CrossRef]

[22] Odejide, S.A., & Binuyo, A.O. Numerical solution of hyperbolic telegraph equation using method of weighted residuals. *International Journal of Nonlinear Science*, 18, 65-70, (2014).

[23] Adewumi, A.O., Akindeinde, S.O., Aderogba, A.A., & Ogundare, B.S. Laplace transform collocation method for solving hyperbolic telegraph equation. *International Journal of Engineering Mathematics*, 2017, 1-9, (2017). [CrossRef]

Mathematical Modelling and Numerical Simulation with Applications, 2022, 2(3), 187–196

https://www.mmnsa.org
ISSN Online: 2791-8564 / Open Access
https://doi.org/10.53391/mmnsa.2022.015

RESEARCH PAPER

Set-valued analysis of anti-angiogenic therapy and radiotherapy

Amine Moustafid [1,*,†]

[1]University Hassan II, Faculty of Sciences, Ain Chock Department of Mathematics and Informatics, 20000 Cassablanca, Morocco

[*]Corresponding Author
[†]a.moustafid@gmail.com (Amine Moustafid)

Abstract

The aim of the paper is to study a cancer model based on anti-angiogenic therapy and radiotherapy. A set-valued analysis is carried out to control the tumor and carrying capacity of the vasculature, so in order to reverse tumor growth and augment tumor repair. The viability technique is used on an augmented model to solve the control problem. Obtained control is a selection of set-valued map of regulation and reduces tumor volume to around zero. A numerical simulation scheme with graphical representations and biological interpretations are given.

Key words: Anti-angiogenic therapy; radiotherapy; viability theory; set-valued analysis
AMS 2020 Classification: 93C10; 93C95; 93D15; 93D23

1 Introduction

Mathematical modelling of treatments is essential for diseases controlling. [1] Considers a mathematical model of chemotherapy for cancer treatment, in fractional order form with Caputo sense, and discusses the local stability of the equilibrium point. [2] Analyses the bifurcation of a fractional-order SEIR epidemic model of HIV and HBV diseases. [3] Studies the stability of a novel model of COVID-19 epidemics, by considering the Lyapunov function. [4] Considers a fractional-order HIV epidemic model, and determines the positivity and boundedness of the solution and the stability conditions of the model, and discusses the global dynamics of the endemic equilibrium point, by using Lyapunov functional approach. [5] Employs the feedback control on a chaotic system with fractional-order. [6] Proposes a Caputo HIV-1 model incorporating AIDS-infected cancer cells, and investigates the existence and uniqueness of its solutions via fixed point theory, and performs the stability analysis of the model. [7] Investigates the bifurcation of a two-dimensional discrete-time chemical model. [8] Develops a three-dimensional fractional-order cancer model, and details analysis of the equilibrium points, and investigates the existence and uniqueness of the solution. [9] Models COVID-19 epidemics with treatment in fractional derivatives using real data from Pakistan, and discusses the stability conditions of the equilibrium points, and analysis the global dynamics equilibria by using the Lyapunov function. [10] Develops a Hilfer fractional model related to Parkinson's disease, and obtains a closed form solution in the terms of Wright function and Mittag-Leffler function, by using Sumudu transform technique. [11] Uses the Laplace transform and exponential Fourier transform of Atangana-Baleanu-Caputo (ABC) derivative, to obtain the approximate analytical solutions of a reaction-diffusion model for calcium dynamics in neurons, in terms of generalized Mittag-Leffler function. [12] Presents a two-dimensional fractional-order reaction-diffusion model to develop a control mechanism of Calcium in nerve cells, and uses the integral transform technique of arbitrary order to find the solution of the model. [13] Analyses a mathematical model for cancer chemotherapy which includes anti-angiogenic effects of the cytotoxic agent, to optimally control the tumor volume by administering the total dose in a single maximum dose session. [14] Analyses a mathematical model for the combination of chemotherapy with anti-angiogenic treatment as a multi-input optimal

➤ **Received:** 25.06.2022 ➤ **Revised:** 23.09.2022 ➤ **Accepted:** 27.09.2022 ➤ **Published:** 29.09.2022

control problem, and considers the problem to minimize a weighted average of tumor volume and the carrying capacity of the tumor vasculature. [15] Considers a mathematical model for tumor radiotherapy and chemotherapy as an optimal solution for a local tumor control.

The combinations of anti-angiogenics with each other or with other cancer therapies increase treatment efficacy [16, 17], notably with radiotherapy [18, 19, 20, 21, 22] which is unable to completely eradicate some tumors alone [23]. Mathematical modelling allows to develop methodologies of analysis and control for an appropriate polytherapy. We are interested in this paper to mathematical modelling of anti-angiogenic therapy with radiotherapy. We propose to take advantage of the Set-Valued Analysis (SVA) methodology applied in [24, 25] for models involving mono immunotherapy and chemotherapy, and in [26, 27] for combined modalities of cancer therapy, including immunotherapy and anti-angiogenic therapy with chemotherapy, to combine anti-angiogenic therapy and radiotherapy.

The rest of this paper is organized as follows : Section 2 describes a model of anti-angiogenic therapy and radiotherapy combination. Section 3 formulates the corresponding problem of control, and augments the considered model to translate the control problem into a viability one. Section 4 solves the viability problem by a single-valued selection of the set-valued map of regulation. Section 5 approaches the problem by the numerical methods of Euler and Uzawa.

2 Model presentation

The following complementary coupled dynamics between the tumor volume $p \in (0, \infty)$, and the time-varying carrying capacity $q \in (0, \infty)$, are considered from [28].

$$\dot{p} = -\xi p \ln\left(\frac{p}{q}\right) - (\alpha + \beta r)pw, \; p(0) = p_0 \in (0, \infty); \tag{1a}$$

$$\dot{q} = \kappa\left(bq^{\frac{2}{3}} - dq^{\frac{4}{3}}\right) + (1-\kappa)\left(bp - dp^{\frac{2}{3}}q\right) - \gamma qu - (\eta + \delta r)qw, \; q(0) = q_0 \in (0, \infty); \tag{1b}$$

where the third variable r was introduced by the ordinary differential equation

$$\dot{r} = -\rho r + w, \tag{1c}$$

and initiated by

$$r(0) = r_0 = 0, \tag{1d}$$

to model the temporal effects of tumor repair, and simplify the linear-quadratic damages quantification from Wein [29] on the tumor : $-(\alpha + \beta r)pw$, and on the carrying capacity : $-(\eta + \delta r)qw$, caused by the radiation control w, which takes values in $[0, w^{\max}]$. The control u represents the dose of the anti-angiogenic medicine, and takes values in $[0, u^{\max}]$, with carrying capacity elimination : $-\gamma qu$. The rest of uncontrolled expressions are summarized in the following table.

Expression	Description
$bq^{\frac{2}{3}}$ and bp	Carrying capacity stimulations
$-dq^{\frac{4}{3}}$ and $-dp^{\frac{2}{3}}q$	Carrying capacity inhibitions
$-\xi p \ln\left(\frac{p}{q}\right)$	Tumor proliferation

The parameter κ takes values in $[0, 1]$, and for the particular values $\kappa = 0$ and $\kappa = 1$, the meta-model (1) corresponds to Hahnfeldt [30, 31, 32] and Ergun [33, 34, 35] models, respectively. The model presentation is completed by describing parameters in table 1. Numerous studies related to the model (1) have been carried out :

- [31] Employs Pontryagin Minimum Principle (PMP), to minimize tumor volume subject to Hahnfeldt's sub-model, for an optimal cancer combination therapy from anti-angiogenic and radiation therapy.
- [32] Uses State-Dependent Riccati Equations (SDRE) as an optimal control methodology framework on Hahnfeldt's sub-model, and designs optimal rules to reduce the tumor growth by an appropriate administration of anti-angiogenic and radio-therapeutic doses.
- [33] Applies (PMP) on Ergun's sub-model, to determine the temporal scheduling of radiotherapy and angiogenic inhibitors that maximizes the control of a primary tumor.
- [36] Considers Ergun's sub-model as as optimal control problem with the objective of minimizing the tumor volume subject to isoperimetric constraints, that limit the total radiation dose and the overall amount of anti-angiogenic agents to be given.
- [37] Optimally controls Hahnfeldt's sub-model, by solving nonlinear programming problem via A Mathematical Programming Language (AMPL) and the Interior Point OPTimizer (IPOPT) method.
- [38] Executes (PMP) on Ergun's sub-model, to minimize tumor volume while limiting the total amount of administered anti-angiogenic agents, and also the total damage caused by the radiation treatment to the healthy tissue, so expressed in terms of its Biologically Equivalent Dose (BED).
- [39] Operates (PMP) to optimally control Hahnfeldt's sub-model, with the objective function of minimizing the size of cancer.
- [28] Proposes of the model (1), a Sequential Quadratic Hamiltonian (SQH) method to choose the optimisation weights, in order to obtain treatment functions that successfully reduce the tumor volume to zero.

- [40] Formulates more generalized model than (1), and adopts optimal control methodology, to minimize multi-functional objective.

3 Problem statement

We state the problem of control the tumor volume p by a coupled protocol (u, w) from Cartesian product constraint $[0, u^{\max}] \times [0, w^{\max}]$

$$\forall t \in [0, \infty), (u(t), w(t)) \in [0, u^{\max}] \times [0, w^{\max}], \tag{2a}$$

so in order that p strictly decreases on $[0, \infty)$

$$\forall t \in [0, \infty), \dot{p}(t) < 0, \tag{2b}$$

and admits zero as limit at infinity

$$\lim_{t \to \infty} p(t) = 0, \tag{2c}$$

subject to the model (1).
Before beginning any analysis, we augment the model (1) by the ordinary differential equation

$$\dot{w} = -w + v, \ w(0) = w_0 \in [0, w^{\max}], \tag{3}$$

to turn on the control w into a variable state, and control tumor volume dynamics (1b) indirectly via the parameter control $v \in [0, w^{\max}]$, subject to the objectives (2b) and (2c), however, we can still have the explicit expression for w

$$w(t) = e^{-t} \left(w_0 + \int_0^t e^{\tau} v(\tau) \, \mathrm{d}\tau \right). \tag{4}$$

The resolution of problem (2), can be done by finding (u, v)

$$\forall t \in [0, \infty), (u(t), v(t)) \in [0, u^{\max}] \times [0, w^{\max}], \tag{5a}$$

by which (p, q, r, w) is globally viable in D_θ

$$\forall t \in [0, \infty), (p(t), q(t), r(t), w(t)) \in D_\theta, \tag{5b}$$

where domain

$$D_\theta = \{(p, q, r, w) \in \mathbb{R}_+^* \times \mathbb{R}_+^* \times \mathbb{R}_+ \times [0, w^{\max}] \mid \psi_\theta(p, q, r, w) \leq 0\}, \tag{5c}$$

with function

$$\psi_\theta(p, q, r, w) = -\xi p \ln\left(\frac{p}{q}\right) - (\alpha + \beta r) p w + \theta p,$$

and parameter

$$\theta \in \mathbb{R}_+^*.$$

Proposition 1 *Assume that there exists* $\theta \in \mathbb{R}_+^*$ *such that* $(p_0, q_0, r_0, w_0) \in D_\theta$, *and* (u, v) *solution to the viability problem* (5), *then* (u, w) *solves the control problem* (2).

Proof Let $t \geq 0$, and let (p, q, r, w) be the globally viable trajectory in D_θ, leading by the control (u, v).
According to (1a) and (5b) we have the differential inequality

$$\dot{p}(t) = -\xi p \ln\left(\frac{p}{q}\right) - (\alpha + \beta r) p w \leq -\theta p(t),$$

by integrating we get the exponential estimate

$$0 \leq p(t) \leq p_0 e^{-\theta t},$$

then in the limit ∞, the tumor is deleted $\lim_{t \to \infty} p(t) = 0$, with the average speed of therapy θ. ■

4 Set-valued resolution

On the viability constraint D_θ by (5c), we define the set-valued map of regulation F_θ in the following way

$$F_\theta(p,q,r,w) = \Big\{(u,v) \in [0,u^{\max}] \times [0,w^{\max}] \mid \Big(-\xi p \ln\Big(\frac{p}{q}\Big) - (\alpha+\beta r)pw, \\ \kappa\Big(bq^{\frac{2}{3}} - dq^{\frac{4}{3}}\Big) + (1-\kappa)\Big(bp - dp^{\frac{2}{3}}q\Big) - \gamma qu - (\eta+\delta r)qw, -\rho r + w, -w + v\Big)^\top \in T_{D_\theta}(p,q,r,w)\Big\}, \tag{6a}$$

where

$$T_{D_\theta}(p,q,r,w) = \Big\{(\hat p,\hat q,\hat r,\hat w) \in \mathbb{R}^4 \;\Big|\; \liminf_{h \downarrow 0} \frac{d((p+h\hat p, q+h\hat q, r+h\hat r, w+h\hat w), D_\theta)}{h} = 0\Big\}, \tag{6b}$$

stands for the tangent cone to D_θ at point (p,q,r,w).

Lemma 1 *Let be $\theta \in \mathbb{R}_+^*$ such that $(p_0,q_0,r_0,w_0) \in D_\theta$. If for all $(p,q,r,w) \in D_\theta$, we have $F_\theta(p,q,r,w) \neq \emptyset$, then any single-valued selection (u,v) of the set-valued map of regulation F_θ solves (5).*

Proof The set-valued map of regulation F_θ admits a selection $(u,v) : D_\theta \to [0,u^{\max}]\times[0,w^{\max}]$ by which the system (1)–(3) admits a locally viable solution $(p(\cdot),q(\cdot),r(\cdot),w(\cdot))$ in D_θ, defined over a maximal interval $[0,t^{\max})$. We have to prove that $t^{\max} \to \infty$. Indeed, assume that $t^{\max}$ is finite.

- The non-negative function $p(\cdot)$ decreases on $[0,t^{\max})$, then it admits a limit $\bar p$, when $t \to t^{\max}$.
- Thanks to (1b), we have the differential inequality

$$\dot q \le b(q^{\frac{2}{3}} + p_0),$$

and by integrating

$$3\sqrt[2]{p_0}\left(\frac{\sqrt[3]{q}}{\sqrt[2]{p_0}} - \arctan\left(\frac{\sqrt[3]{q}}{\sqrt[2]{p_0}}\right)\right) \le bt + 3\sqrt[2]{p_0}\left(\frac{\sqrt[3]{q_0}}{\sqrt[2]{p_0}} - \arctan\left(\frac{\sqrt[3]{q_0}}{\sqrt[2]{p_0}}\right)\right),$$

then by maximizing

$$q \le \left(\frac{b}{3}t^{\max} + \sqrt[2]{p_0}\left(\frac{\sqrt[3]{q_0}}{\sqrt[2]{p_0}} - \arctan\left(\frac{\sqrt[3]{q_0}}{\sqrt[2]{p_0}}\right)\right) + \sqrt[2]{p_0}\frac{\pi}{2}\right)^3,$$

which proves that the function $q(\cdot)$ admits an upper limit $\bar q$, when $t \to t^{\max}$.

- According to (1c) the function $r(\cdot)$ admits a limit $\bar r = e^{-\rho t^{\max}}\displaystyle\int_0^{t^{\max}} e^{\rho\tau}w(\tau)\,\mathrm{d}\tau$, when $t \to t^{\max}$.
- By (4) the function $w(\cdot)$ admits a limit $\bar w = e^{-t^{\max}}\left(w_0 + \displaystyle\int_0^{t^{\max}} e^{\tau}v(\tau)\,\mathrm{d}\tau\right)$, when $t \to t^{\max}$.

Therefore $(p(\cdot),q(\cdot),r(\cdot),w(\cdot)) \to (\bar p,\bar q,\bar r,\bar w)$ when $t \to t^{\max}$, and $(\bar p,\bar q,\bar r,\bar w)$ belongs to D_θ because it is closed. Now, by considering $(\bar p,\bar q,\bar r,\bar w)$ as an initial state it follows that $(p(\cdot),q(\cdot),r(\cdot),w(\cdot))$ may be prolonged to a viable solution $(\tilde p(\cdot),\tilde q(\cdot),\tilde r(\cdot),\tilde w(\cdot))$ in D_θ, starting at $(\bar p,\bar q,\bar r,\bar w)$ on some interval $[t^{\max},t^{\sup})$ where $t^{\sup} > t^{\max}$, which is in contradiction with the maximality of $t^{\max}$, then the solution $(p(\cdot),q(\cdot),r(\cdot),w(\cdot))$ becomes globally viable in D_θ. ■

Motivated by the preceding Lemma 1, we are interested in an explicit expression of the set-valued map of regulation F_θ, so for that we give the following Lemma from [27], characterizing the tangent directions of the tangent cone T_{D_θ} by (6b).

Lemma 2 ([27]) *For each $(p,q,r,w) \in D_\theta$ the tangent directions $(\hat p,\hat q,\hat r,\hat w)$ of $T_{D_\theta}(p,q,r,w)$ are characterized by*

$$\begin{cases} \hat r \ge 0 & \text{if} \quad r = 0, \\ \hat w \ge 0 & \text{if} \quad w = 0, \\ \hat w \le 0 & \text{if} \quad w = w^{\max}, \\ \dot\psi_\theta(p,q,r,w)(\hat p,\hat q,\hat r,\hat w) \le 0 & \text{if} \quad \psi_\theta(p,q,r,w) = 0. \end{cases}$$

Proof See [27]. ■

Lemma 3 ([27]) *The set-valued map of regulation F_θ may be expressed explicitly on the viability constraint D_θ as*

$$F_\theta(p,q,r,w) = \begin{cases} [0,u^{\max}]\times[0,w^{\max}] & \text{if} \quad \psi_\theta(p,q,r,w) < 0, \\ C_\theta(p,q,r,w) & \text{if} \quad \psi_\theta(p,q,r,w) = 0, \end{cases} \tag{7a}$$

where

$$C_\theta(p,q,r,w) = \Big\{(u,v) \in [0,u^{\max}]\times[0,w^{\max}] \mid \ell_\theta(p,q,r,w) + \langle h(p,q,r,w),(u,v)\rangle \le 0\Big\}, \tag{7b}$$

with

$$\ell_\theta(p,q,r,w) = \Big\langle \nabla\psi_\theta(p,q,r,w), \Big(-\xi p \ln\Big(\frac{p}{q}\Big) - (\alpha+\beta r)pw, \kappa\Big(bq^{\frac{2}{3}} - dq^{\frac{4}{3}}\Big) + (1-\kappa)\Big(bp - dp^{\frac{2}{3}}q\Big) - (\eta+\delta r)qw, -\rho r + w, -w\Big)^\top \Big\rangle, \tag{8a}$$

and

$$h(p,q,r,w) = \Big(-\gamma q \frac{\partial\psi_\theta}{\partial q}(p,q,r,w), \frac{\partial\psi_\theta}{\partial w}(p,q,r,w)\Big)^\top. \tag{8b}$$

Proof Thanks to Eqs. (1c) and (3)

- If $r = 0$, then

$$-\rho r + w = w \geq 0.$$

- If $w = 0$, then

$$-w + v = v \geq 0.$$

- If $w = w_i^{\max}$, then

$$-w + v = -w^{\max} + v \leq -w^{\max} + w^{\max} \leq 0.$$

- For all $(p,q,r,w) \in D_\theta$, we have

$$\dot\psi_\theta(p,q,r,w)\Big(-\xi p\ln\Big(\frac{p}{q}\Big) - (\alpha+\beta r)pw, \kappa\Big(bq^{\frac{2}{3}} - dq^{\frac{4}{3}}\Big) + (1-\kappa)\Big(bp - dp^{\frac{2}{3}}q\Big) - \gamma qu - (\eta+\delta r)qw, -\rho r + w, -w + v\Big)^\top =$$

$$\Big\langle \nabla\psi_\theta(p,q,r,w), \Big(-\xi p\ln\Big(\frac{p}{q}\Big) - (\alpha+\beta r)pw, \kappa\Big(bq^{\frac{2}{3}} - dq^{\frac{4}{3}}\Big) + (1-\kappa)\Big(bp - dp^{\frac{2}{3}}q\Big) - \gamma qu - (\eta+\delta r)qw, -\rho r + w, -w + v\Big)^\top \Big\rangle =$$

$$\Big\langle \nabla\psi_\theta(p,q,r,w), \Big(-\xi p\ln\Big(\frac{p}{q}\Big) - (\alpha+\beta r)pw, \kappa\Big(bq^{\frac{2}{3}} - dq^{\frac{4}{3}}\Big) + (1-\kappa)\Big(bp - dp^{\frac{2}{3}}q\Big) - (\eta+\delta r)qw, -\rho r + w, -w\Big)^\top \Big\rangle + \Big\langle \nabla_{(q,w)}\psi_\theta(p,q,r,w), (-\gamma qu, v)^\top \Big\rangle.$$

■

Lemma 4 *A single-valued selection of the set-valued map of regulation F_θ may be given on the viability constraint D_θ by the expression*

$$c_\theta(p,q,r,w) = \pi_{C_\theta(p,q,r,w)}(0), \tag{9}$$

where $\pi_{C_\theta(p,q,r,w)}(0)$ denotes the projection of $0_{\mathbb{R}^2}$ onto the closed convex set $C_\theta(p,q,r,w)$.

Proof See [27]. ■

5 Numerical resolution

This section is devoted to numerically analysis the following model by combining the numerical methods of Euler by step h and Uzawa of parameter λ.

$$\dot p = -\xi p\ln\Big(\frac{p}{q}\Big) - (\alpha+\beta r)pw, \tag{10a}$$

$$\dot q = \kappa\Big(bq^{\frac{2}{3}} - dq^{\frac{4}{3}}\Big) + (1-\kappa)\Big(bp - dp^{\frac{2}{3}}q\Big) - \gamma qu - (\eta+\delta r)qw, \tag{10b}$$

$$\dot r = -\rho r + w, \tag{10c}$$

$$\dot w = -w + v, \tag{10d}$$

$$u = c_\theta^1(p,q,r,w), \tag{10e}$$

$$v = c_\theta^2(p,q,r,w). \tag{10f}$$

The used algorithm is as follows

i. Initialization

a) $t_0 \in \mathbb{R}_+$,
b) $(p_0, q_0, r_0, w_0) \in D_\theta$,
c) $\lambda^0 \in \mathbb{R}_+^5$,

ii. Iteration

a) $t_{n+1} = t_n + h$,
b)

$$\begin{cases} p_{n+1} &= p_n + h\left(-\xi p_n \ln\left(\frac{p_n}{q_n}\right) - (\alpha + \beta r_n) p_n w_n\right), \\ q_{n+1} &= q_n + h\left(\kappa\left(b q_n^{\frac{2}{3}} - d q_n^{\frac{4}{3}}\right) + (1-\kappa)\left(b p_n - d p^{\frac{2}{3}} q_n\right) - \gamma q_n u_n - (\eta + \delta r_n) q_n w_n\right), \\ r_{n+1} &= r_n + h(-\rho r_n + w_n), \\ w_{n+1} &= w_n + h(-w_n + v_n), \end{cases} \tag{11}$$

c)

$$\begin{cases} u_n = -\lambda_5^n h(p_n, q_n, r_n, w_n) + \lambda_3^n - \lambda_1^n, \\ v_n = -\lambda_5^n h(p_n, q_n, r_n, w_n) + \lambda_4^n - \lambda_2^n, \end{cases}$$

d)

$$\begin{cases} \lambda_1^{n+1} = \max(\lambda_1^n + \sigma(u_n - u^{\max}), 0), \\ \lambda_2^{n+1} = \max(\lambda_2^n + \sigma(v_n - v^{\max}), 0), \\ \lambda_3^{n+1} = \max(\lambda_3^n - \sigma u_n, 0), \\ \lambda_4^{n+1} = \max(\lambda_4^n - \sigma v_n, 0), \\ \lambda_5^{n+1} = \max(\lambda_5^n + \sigma(h_1(p_n, q_n, r_n, w_n)u_n + h_2(p_n, q_n, r_n, w_n)v_n + \ell_\theta(p_n, q_n, r_n, w_n), 0), \text{ with } 0 < \sigma < \dfrac{2}{\|h(p,q,r,w)\|}. \end{cases}$$

- For the absence of therapy we choose $(p_0, q_0, r_0, w_0) = (15000, 12000, 0, 0)$ as an initial state, the tumor volume p stimulates the carrying capacity q to increase by the dynamics (10b), and to proliferate by the dynamics (10a), as we see in Figure 1.
- In the presence of therapy we choose $(p_0, q_0, r_0, w_0) = (15000, 12000, 0, 2)$ as an initial state, with the parameter $\theta = \xi \ln(\frac{p_0}{q_0}) + \alpha w_0 \simeq 1.4$, in order that $(p_0, q_0, r_0, w_0) \in D_\theta$, the protocols $u(t) = c_\theta^1(p(t), q(t), r(t), w(t))$ and $w(t) = e^{-t}(w_0 + \int_0^t e^\tau c_\theta^2(p(\tau), q(\tau), r(\tau), w(\tau))\,d\tau)$ limits the stimulation of the tumor volume p on the carrying capacity q in the dynamics (10b), and reverses the proliferation of p in the dynamics (10a), as we see in Figure 2.

As in (1d) we have $r_0 = 0$ for the initial value of the tumor repair r, and we consider $v_0 = 0$ as the initial value of the parameter control v, for the parameter κ of the dynamics (10b) we propose $\kappa = 0.5$, as in [28] to combine Hahnfeldt and Ergun dynamics, while the following table 1 gives the numerical values of the model (10) parameters.

Table 1. Parameters description.

Parameter	Description	Value	Unit
ξ	Parameter for tumor growth	0.084	$[\text{day}^{-1}]$
b	Tumor-induced stimulation parameter	5.85	$[\text{day}^{-1}]$
d	Tumor-induced inhibition parameter	0.00873	$[\text{mm}^{-2} \cdot \text{day}^{-1}]$
γ	Anti-angiogenic elimination parameter	0.15	$\left[\frac{\text{kg}}{\text{mg(doses)}}\right] \cdot \text{day}^{-1}$
α	Radiosensitive parameter for tumor	0.7	$[\text{Gy}^{-1}]$
β	Radiosensitive parameter for tumor	0.14	$[\text{Gy}^{-2}]$
η	Radiosensitive parameter for healthy tissue	0.136	$[\text{Gy}^{-1}]$
δ	Radiosensitive parameter for healthy tissue	0.086	$[\text{Gy}^{-2}]$
ρ	Tumor repair rate	$\frac{\ln 2}{0.02}$	$[\text{day}^{-1}]$

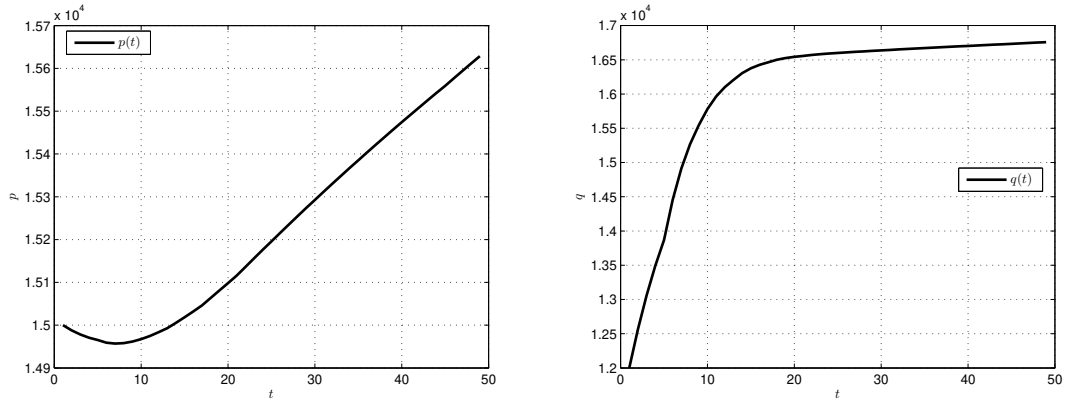

Figure 1. Tumor volume p begins to decrease from the initial value $p_0 = 15000$, but p stimulates the carrying capacity q to increase from the initial value $q_0 = 12000$, until they have approximate values $p = 14957$ and $q = 14912$ ($p \simeq q$) , then p starts to increase.

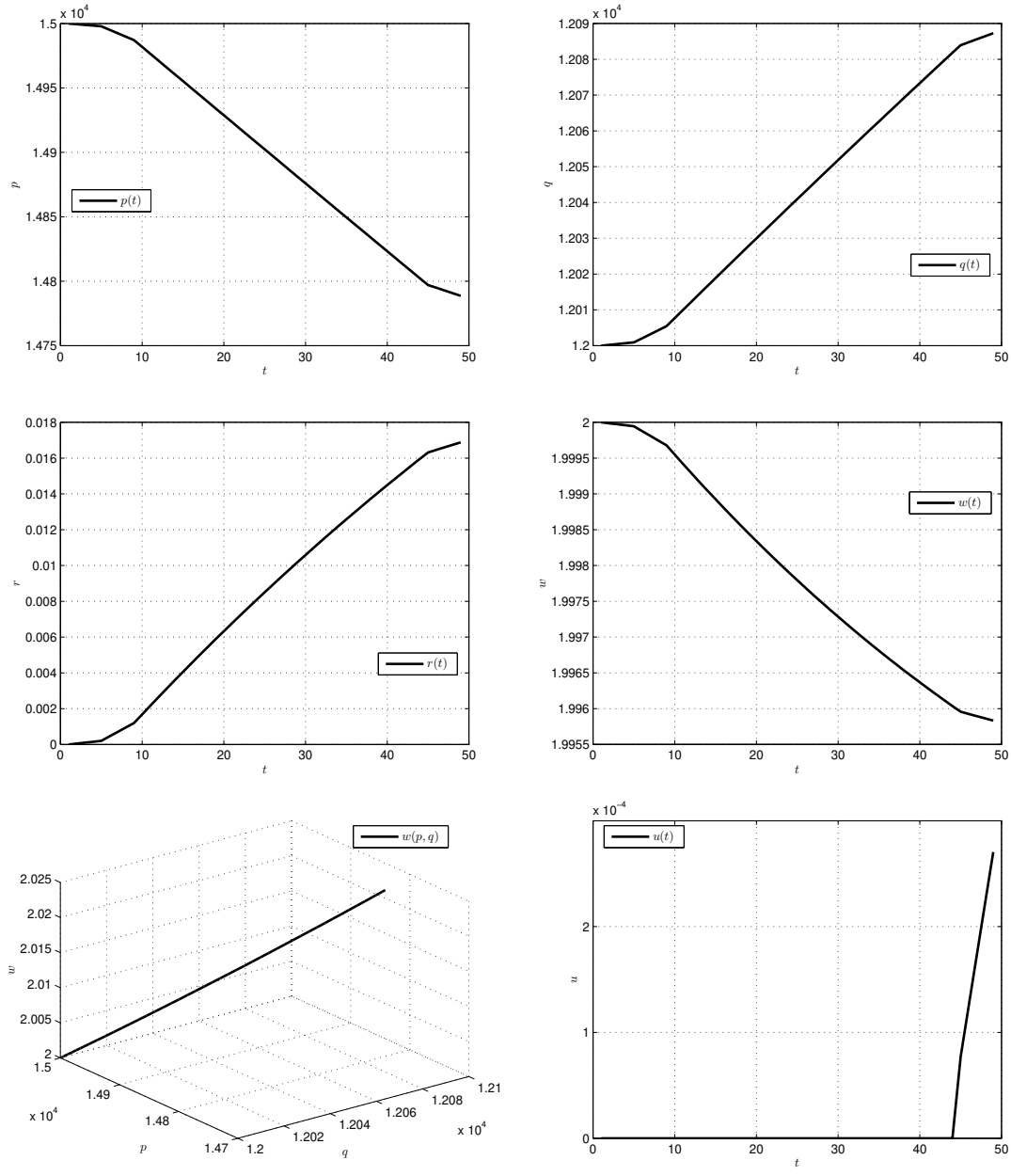

Figure 2. Tumor volume p begins from the same initial value $p_0 = 15000$ as in Figure 1, but kept on decreasing state all over time therapy in accordance with (2b) and (2c), caused by growth limitation of the carrying capacity q due to combined anti-angiogenic therapy and radiotherapy (u, w), and by direct effect of the radiotherapy $w(p, q)$ on the tumor volume p, while the tumor repair r is augmented.

6 Conclusion

The problem control (2) to the class of mathematical models (1) is achieved by combining anti-angiogenic therapy with radiotherapy. The set-valued analysis gives the feedback protocols $u(t) = c_\theta^1(f(t))$, and $w(t) = e^{-t}(w_0 + \int_0^t e^\tau c_\theta^2(f(\tau))\,d\tau)$, where $f(.) = (p(.), q(.), r(.), w(.))$ to administrate the temporal doses of anti-angiogenic medicine and radiation, in order to dynamically limit the stimulation of the tumor volume $p_{(u,w)}(t)$ on the time carrying capacity $q_{(u,w)}(t)$, and force $p_{(u,w)}(t)$ to decrease : $\forall t \in [0,\infty), \dot{p}_{(u,w)}(t) < 0$, under the exponential estimate : $0 \leq p_{(u,w)}(t) \leq p_0 e^{-\theta t}$, and converge to the null limit : $\lim_{t\to\infty} p_{(u,w)}(t) = 0$. The obtained protocols u and w, provide from the single-valued selection c_θ by (9) to the set-valued map of regulation F_θ by (6a), which should be strict on the subset D_θ by (5c) : $\forall (p,q,r,w) \in D_\theta, F_\theta(p,q,r,w) \neq \emptyset$, and they rend the model (1) globally viable on the subset D_θ, as it is demonstrated in the Proof 4 of the Lemma 1. The linear dynamics (1c) and (3) of the tumor repair r and the radiation control w respectively, allow to get the useful expression (7a) of the set-valued map of regulation F_θ, as it is proved in the Proof 4 of the Lemma 3, and the single-valued selection c_θ is a solution to the following problem of minimization : $\min ||(u,v)||$ such that $(u,v) \in [0,u^{\max}] \times [0,w^{\max}]$ by (5a), and $\ell_\theta(p,q,r,w) + \langle h(p,q,r,w),(u,v)\rangle \leq 0$ by (8), which is numerically approached by the method of Uzawa in the last Section 5, and implemented into the discretized model (11) by the method of Euler, to get the numerical simulations of Figure 2, which are in perfect conformity with the theoretical results of the preceding Section 4.

Declarations

List of abbreviations

- Atangana–Baleanu–Caputo (ABC) derivative
- A Mathematical Programming Language (AMPL)
- Biologically Equivalent Dose (BED)
- Interior Point OPTimizer (IPOPT)
- Pontryagin Minimum Principle (PMP)
- State-Dependent Riccati Equations (SDRE)
- Sequential Quadratic Hamiltonian (SQH)
- Set-Valued Analysis (SVA)

Consent for publication

Not applicable.

Conflicts of interest

The author declares that she has no conflict of interests.

Funding

The author declares that there is no funding source for the reported research.

Author's contributions

The research was carried out by the author and she accepts that the contributions and responsibilities belong to the author.

Acknowledgements

Not applicable.

References

[1] Özköse, F., Şenel, M.T., & Habbireeh, R. Fractional-order mathematical modelling of cancer cells-cancer stem cells-immune system interaction with chemotherapy. *Mathematical Modelling and Numerical Simulation with Applications*, 1(2), 67-83, (2021). [CrossRef]

[2] Ghori, M.B., Naik, P.A., Zu, J., Eskandari, Z., & Naik, M.U.D. Global dynamics and bifurcation analysis of a fractional-order SEIR epidemic model with saturation incidence rate. *Mathematical Methods in the Applied Sciences*, 45(7), 3665-3688, (2022). [CrossRef]

[3] Sinan, M., Leng, J., Anjum, M., & Fiaz, M. Asymptotic behavior and semi-analytic solution of a novel compartmental biological model. *Mathematical Modelling and Numerical Simulation with Applications*, 2(2), 88-107, (2022). [CrossRef]

[4] Naik, P.A., Yavuz, M. & Zu, J. The role of prostitution on HIV transmission with memory: A modeling approach. *Alexandria Engineering Journal*, 59(4), 2513-2531, (2020). [CrossRef]

[5] Gholami, M., Ghaziani, R.K., & Eskandari, Z. Three-dimensional fractional system with the stability condition and chaos control. *Mathematical Modelling and Numerical Simulation with Applications*, 2(1), 41-47, (2022). [CrossRef]

[6] Naik, P.A., Owolabi, K.M., Yavuz, M., & Zu, J. Chaotic dynamics of a fractional order HIV-1 model involving AIDS-related cancer cells. *Chaos, Solitons & Fractals*, 140, 110272, (2020). [CrossRef]
[7] Naik, P.A., Eskandari, Z., & Shahraki, H.E. Flip and generalized flip bifurcations of a two-dimensional discrete-time chemical model. *Mathematical Modelling and Numerical Simulation with Applications*, 1(2), 95-101, (2021). [CrossRef]
[8] Naik, P.A., Zu, J., & Naik, M.U.D. Stability analysis of a fractional-order cancer model with chaotic dynamics. *International Journal of Biomathematics*, 14(06), 2150046, (2021). [CrossRef]
[9] Naik, P.A., Yavuz, M., Qureshi, S., Zu, J., & Townley, S. Modeling and analysis of COVID-19 epidemics with treatment in fractional derivatives using real data from Pakistan. *The European Physical Journal Plus*, 135(10), 1-42, (2020). [CrossRef]
[10] Joshi, H., & Jha, B.K. Chaos of calcium diffusion in Parkinson's infectious disease model and treatment mechanism via Hilfer fractional derivative. *Mathematical Modelling and Numerical Simulation with Applications*, 1(2), 84-94, (2021). [CrossRef]
[11] Joshi, H., & Jha, B.K. On a reaction–diffusion model for calcium dynamics in neurons with Mittag–Leffler memory. *The European Physical Journal Plus*, 136(6), 1-15, (2021). [CrossRef]
[12] Joshi, H., & Jha, B.K. Generalized Diffusion Characteristics of Calcium Model with Concentration and Memory of Cells: A Spatiotemporal Approach. *Iranian Journal of Science And Technology, Transactions A: Science*, 46(1), 309-322, (2022). [CrossRef]
[13] Ledzewicz, U., & Schättler, H. The structure of optimal protocols for a mathematical model of chemotherapy with antiangiogenic effects. *SIAM Journal on Control and Optimization*, 60(2), 1092-1116, (2022). [CrossRef]
[14] Ledzewicz, U., & Schättler, H. Combination of antiangiogenic treatment with chemotherapy as a multi-input optimal control problem. *Mathematical Methods in the Applied Sciences*, 45(5), 3058-3082, (2022). [CrossRef]
[15] Ghita, M., Ghita, M., Copot, D., Birs, I.R., Muresan, C., & Ionescu, C.M. Optimizing radiotherapy with chemotherapy using PKPD modeling for lung cancer. *2022 IEEE 20th Jubilee World Symposium on Applied Machine Intelligence and Informatics (SAMI)*, 000299-000304, (2022). [CrossRef]
[16] O'Reilly, M.S. The combination of antiangiogenic therapy with other modalities. *Cancer Journal (Sudbury, Mass.)*, 8, S89-99, (2002). [CrossRef]
[17] Gasparini, G., Longo, R., Fanelli, M., & Teicher, B.A. Combination of antiangiogenic therapy with other anticancer therapies: results, challenges, and open questions. *Journal Of Clinical Oncology*, 23(6), 1295-1311, (2005). [CrossRef]
[18] Shannon, A.M., & Williams, K.J. Antiangiogenics and radiotherapy. *Journal of Pharmacy and Pharmacology*, 60(8), 1029-1036, (2008). [CrossRef]
[19] Senan, S., & Smit, E.F. Design of clinical trials of radiation combined with antiangiogenic therapy. *The Oncologist*, 12(4), 465-477, (2007). [CrossRef]
[20] O'Reilly, M.S. The interaction of radiation therapy and antiangiogenic therapy. *The Cancer Journal*, 14(4), 207-213, (2008). [CrossRef]
[21] O'Reilly, M.S. Radiation combined with antiangiogenic and antivascular agents. *Seminars In Radiation Oncology*, 16(1), 45-50, (2006). [CrossRef]
[22] Mazeron, R., Azria, D., & Deutsch, E. Angiogenesis inhibitors and radiation therapy: from biology to clinical practice. *Cancer Radiotherapie: Journal de la Societe Francaise de Radiotherapie Oncologique*, 13(6-7), 568-573, (2009). [CrossRef]
[23] Mortezaee, K., Parwaie, W., Motevaseli, E., Mirtavoos-Mahyari, H., Musa, A., Shabeeb, D., Esmaely, F., Najafi, M., & Farhood, B. Targets for improving tumor response to radiotherapy. *International Immunopharmacology*, 76, 105847, (2019). [CrossRef]
[24] Moustafid, A. General chemotherapy protocols. *Journal of Applied Dynamic Systems and Control*, 4(2), 18-25, (2021). [CrossRef]
[25] Kassara, K., & Moustafid, A. Feedback protocol laws for immunotherapy. *PAMM: Proceedings in Applied Mathematics and Mechanics*, 7(1), 2120033-2120034, (2007). [CrossRef]
[26] Moustafid, A. General anti-angiogenic therapy protocols with chemotherapy. *International Journal of Mathematical Modelling & Computations*, 11(3), (2021). [CrossRef]
[27] Kassara, K., & Moustafid, A. Angiogenesis inhibition and tumor-immune interactions with chemotherapy by a control set-valued method. *Mathematical Biosciences*, 231(2), 135-143, (2011). [CrossRef]
[28] Kienle-Garrido, M.L., Breitenbach, T., Chudej, K., & Borzì, A. Modeling and numerical solution of a cancer therapy optimal control problem. *Applied Mathematics*, 9(8), (2018). [CrossRef]
[29] Wein, L.M., Cohen, J.E., & Wu, J.T. Dynamic optimization of a linear–quadratic model with incomplete repair and volume-dependent sensitivity and repopulation. *International Journal of Radiation Oncology, Biology, Physics*, 47(4), 1073-1083, (2000). [CrossRef]
[30] Ledzewicz, U., D'Onofrio, A., & Schättler, H. Tumor development under combination treatments with anti-angiogenic therapies. *In Mathematical Methods and Models in Biomedicine, Springer*, 311-337, (2013). [CrossRef]
[31] Chudej, K., Huebner, D., & Pesch, H.J. Numerische Lösung eines mathematischen Modells für eine optimale Krebskombinationstherapie aus Anti-Angiogenese und Strahlentherapie. *Tagungsband ASIM 2016-23 Symposium Simulationstechnik, Dresden*, 52, 169-176, (2016).
[32] Mellal, L., Folio, D., Belharet, K., & Ferreira, A. Modeling of optimal targeted therapies using drug-loaded magnetic nanoparticles for liver cancer. *IEEE Transactions On Nanobioscience*, 15(3), 265-274, (2016). [CrossRef]
[33] Ergun, A., Camphausen, K., & Wein, L.M. Optimal scheduling of radiotherapy and angiogenic inhibitors. *Bulletin Of Mathematical Biology*, 65(3), 407-424, (2003). [CrossRef]
[34] Ledzewicz, U., & Schättler, H. Multi-input optimal control problems for combined tumor anti-angiogenic and radiotherapy treatments. *Journal of Optimization Theory And Applications*, 153, 195-224, (2012). [CrossRef]
[35] Jarrett, A.M., Faghihi, D., Hormuth, D.A., Lima, E.A., Virostko, J., Biros, G., Patt, D., & Yankeelov, T. Optimal control theory for personalized therapeutic regimens in oncology: Background, history, challenges, and opportunities. *Journal of Clinical Medicine*, 9(5), 1314, (2020). [CrossRef]
[36] Ledzewicz, U., Maurer, H., & Schättler, H. Optimal combined radio-and anti-angiogenic cancer therapy. *Journal of Optimization Theory And Applications*, 180(1), 321-340, (2019). [CrossRef]
[37] Chudej, K., Wagner, L., & Pesch, H. Numerical solution of an optimal control problem in cancer treatment: Combined radio and anti-angiogenic therapy. *IFAC-PapersOnLine*, 48(1), 665-666, (2015). [CrossRef]
[38] Schättler, H., & Ledzewicz, U. Optimal control for mathematical models of cancer therapies: An application of geometric

methods. *New York: Springer*, Vol. 42, (2015).
[39] Nastitie, N., & Arif, D.K. Analysis and optimal control in the cancer treatment model with combining radio and anti-angiogenic therapy. *IJCSAM (International Journal Of Computing Science And Applied Mathematics)*, 3(2), 55-60, (2017). [CrossRef]
[40] Ledzewicz, U., & Schättler, H. On the role of the objective in the optimization of compartmental models for biomedical therapies. *Journal Of Optimization Theory And Applications*, 187(2), 305-335, (2020). [CrossRef]

Mathematical Modelling and Numerical Simulation with Applications (MMNSA) (https://www.mmnsa.org)